#7632—REVISION #2—03 August 2020—submitted to *American Mineralogist*

An evolutionary system of mineralogy, Part IV: Planetesimal differentiation and impact mineralization (4566 to 4560 Ma)

SHAUNNA M. MORRISON[1] AND ROBERT M. HAZEN[1,*]

[1]Earth and Planets Laboratory, Carnegie Institution for Science,

5251 Broad Branch Road NW, Washington D.C. 20015, U. S. A.

ABSTRACT

The fourth installment of the evolutionary system of mineralogy considers two stages of planetesimal mineralogy that occurred early in the history of the solar nebula, commencing by 4.566 Ga and lasting for at least 5 million years: (1) primary igneous minerals derived from planetesimal melting and differentiation into core, mantle, and basaltic components; and (2) impact mineralization resulting in shock-induced deformation, brecciation, melting, and high-pressure phase transformations.

We tabulate 90 igneous differentiated asteroidal minerals, including the earliest known occurrences of minerals with Ba, Cl, Cu, F, and V as essential elements, as well as the first appearances of numerous phosphates, quartz, zircon, and amphibole group minerals. We also record 40 minerals formed through high-pressure impact alteration, commencing with the period of asteroid accretion and differentiation. These stages of mineral evolution thus mark the first time that high pressures, both static and dynamic, played a significant role in mineral paragenesis.

Keywords: classification; mineral evolution; planetesimals; non-chondrite meteorites; iron meteorites; stony-iron meteorites; achondrites; differentiation; shock minerals

***E-mail:** rhazen@carnegiescience.edu

INTRODUCTION

The evolutionary system of mineralogy amplifies the well-established International Mineralogical Association (IMA) classification system, which is based on mineral species that display unique combinations of idealized chemical composition and crystal structure (e.g., Burke 2006; Mills et al. 2009; Schertl et al. 2018). We expand on IMA protocols by incorporating time and parageneses as central aspects of mineral classification. The emphasis is thus on the historical sequence of physical, chemical, and ultimately biological processes that led to the observed diversity and distribution of minerals on Earth, as well as on other planets and moons (Hazen et al. 2008; Hazen 2019). Previous contributions in this series considered stellar minerals that predate our solar nebula, prior to 4.567 Ga (Part I; Hazen and Morrison 2020); primary interstellar and nebular condensates commencing ~4.567 Ga (Part II; Morrison and Hazen 2020); and the primary mineralogy of chondrules from ~4.567 to ~4.563 Ga (Part III; Hazen et al. 2021).

In this contribution we consider the primary mineralogy of planetesimals and their shattered asteroidal remnants, as preserved in diverse suites of non-chondritic meteorites (Mittlefehldt et al. 1998; Krot et al. 2014; Mittlefehldt 2014). All of these meteorites reflect large-scale igneous processing within more than 100 presumed parental asteroidal objects (Keil et al. 1994; Grady and Wright 2006), which ranged in sizes from tens to hundreds of kilometers in diameter, coupled in many cases with evidence for transformative impact events. Each non-chondritic meteorite thus tells a story of the time when gravity and high pressures first began to play central roles in mineral evolution.

Asteroids are thought to have formed within the first few million years of the solar nebula and thus experienced thermal processing, and in larger bodies melting and differentiation, associated

with heating by short-lived radionuclides, as well as melting and other forms of alteration by high-energy impact processes. Accordingly, this contribution features minerals formed in two broad paragenetic categories. First, in Part IVA we examine the primary igneous mineralogy of differentiated asteroids, encompassing a diversity of iron, stony-iron, and achondrite meteorites. In Part IVB we consider meteoritic shock minerals that formed through various impact processes at a range of scales and intensities.

PART IVA: PRIMARY MINERALOGY OF NON-CHONDRITIC METEORITES

The first rocks of the solar system were components of chondrite meteorites, whose minerals formed at high temperatures (> 600ºC) and low pressures (< 10^{-2} atm) prior to 4.56 Ga. Chondrites are sedimentary accumulations of four principal components (Kerridge and Matthews 1988; Hewins et al. 1996; Brearley and Jones 1998; Scott and Krot 2014; Rubin and Ma 2017, 2020; Russell et al. 2018; Morrison and Hazen 2020; Hazen et al. 2021): (1) inclusions, including refractory calcium-aluminum inclusions and amoeboid olivine aggregates, that formed primarily through condensation from an incandescent vapor phase near the protosun; (2) chondrules, which are igneous droplets ranging from tens of micrometers to several centimeters in diameter that formed in rapid heating and cooling environments; (3) assemblages of Fe-Ni metal alloys and other opaque phases; and (4) a fine-grained matrix (to be considered in Part V of this series). In addition, chondrite meteorites often incorporate a small fraction of presolar stardust grains with a suite of refractory minerals that formed in the expanding, cooling atmospheres of earlier generations of stars (Clayton and Nittler 2004; Lodders and Amari 2005; Lugaro 2005; Davis 2011, 2014; Zinner 2014; Nittler and Ciesla 2016; Hazen and Morrison 2020).

The earliest stages of clumping in the solar nebula have been ascribed primarily to electrostatic forces, by which presolar dust grains and refractory inclusions coalsced into fluffy accumulations, not unlike nebular "dust bunnies." Subsequent flash heating events generated droplet-like chondrules, some of which stuck together and formed objects referred to as "pebbles," with diameters from a few millimeters to a few centimeters. Current models suggest that vast numbers of pebbles collected in small volumes through interactions with nebular gas – a mechanism that leads to a collective gravitational instability and coalescence into a single body (e.g., Youdin and Goodman 2005), perhaps enhanced by contributions from the magnetic coattraction of ferromagnetic minerals (Hubbard 2016). Self-gravity becomes dominant in such incipient planetesimals at sizes between about 100 meters and 1 kilometer in diameter (Benz and Asphaug 1999). Numerical simulations (Johansen et al. 2007) and experimentally determined cooling rates from iron meteorite textures (Randich and Goldstein 1978; Yang and Goldstein 2005, 2006; Yang et al. 2008; Goldstein et al. 2009) suggest that the resulting solid bodies grew to sizes from tens to many hundreds of kilometers in diameter, i.e., large enough for internal heating by short-lived radioisotopes to melt Fe-Ni metal components and initiate core formation, while beginning evolution of a silicate mantle (Woolum and Cassen 1999).

Thousands of such objects must have formed in the early solar system, each competing for gravitational doiminance over a volume of nebular real estate. Superimposed on these melting events were large impacts, which are likely to have caused significant shock melting episodes during the first few million years of the solar nebula, as well as throughout the subsequent history of the solar system (Tonks and Melosh 1992).

The formation of myriad asteroidal bodies had profound mineralogical consequences. At the coarsest scale, melting and differentiation led to separation of metal and silicate fractions –

endmembers preserved as the least altered iron versus achondrite meteorites. However, incomplete core/mantle separation within smaller bodies, mixed core-mantle boundary regions, and especially massive disruptions and jumblings of mineralogies through large impacts, led to the complex diversity of non-chondritic meteorites, which reflect a continuum of formative processes on asteroidal bodies large and small.

Non-chondritic meteorites and their mineralogies have been reviewed by a number of authors (Mittlefehldt et al. 1998; Benedix et al. 2014; Krot et al. 2014; Mittlefehldt 2014; Rubin and Ma 2017, 2020). These objects represent fragments of diverse pre-planetary objects, ranging in size from less than 10 to greater than 400 kilometers in diameter (Rasmussen 1989; Yang et al. 1997a; Mittlefehldt et al. 1998). Non-chondritic meteorites are thought to have derived from chondritic precursors by melting and differentiation, as well as by impact processing. However, they differ from chondrites to varying degrees in texture, composition, and mineralogy. In contrast to chondrite meteorites, which are initially sedimentary rocks that often were modified by varying degrees of aqueous, hydrothermal, and thermal metamorphic processes (Brearley and Jones 1998; Krot et al. 2014; Russell et al. 2018), the non-chondritic meteorites initially derive from partially to completely molten material and are thus igneous rocks (Mittlefehldt et al. 1998; Benedix et al. 2014; Mittlefehldt 2014). Note, however, that continuous gradations exist in aqueous alteration, thermal metamorphism, partial melting, and shock effects, so that classifications of intermediate mineralogical states are somewhat subjective.

Three broad (and overlapping) groups of non-chondritic meteorites, based on their dominant mineralogies and textures, are summarized below.

Iron Meteorites

Many meteorites dominated by metallic Fe-Ni-alloys, collectively referred to as iron meteorites, represent the cores of differentiated planetesimals that have subsequently experienced catastrophic fragmentation through one or more large impacts (Benedix et al. 2014; Krot et al. 2014). Therefore, these objects display features associated with orderly fractional crystallization and cooling from a melt, as well as the subsequent disruptive effects of impact phenomena. Iron meteorites account for fewer than 100 documented falls – only about 1 in 20 occurrences (Krot et al. 2014). Nevertheless, the more than 1000 iron meteorite falls and finds represent most of the mass of meteorite collections owing to their durability, large average size, and distinctive appearance.

Iron meteorites typically incorporate 5 to 20 weight percent nickel, in addition to usually minor amounts of other siderophile transition elements (notably Co, Cr, Cu, Mn, and Zn) and alkali and alkaline earth elements (Na, K, Mg, and Ca), as well as C, N, O, P, S, and Si. More than 40 mineral species containing these essential elements have been reported from iron meteorites (Mittlefehldt et al. 1998, Table 2; Rubin and Ma 2020; see Table 1).

Fe-Ni alloys constitute greater than 99 weight percent of some iron meteorites, which prior to the 1970s were primarily divided into three types – hexahedrites, octahedrites, and ataxites (e.g., Buchwald 1975). Examples with less than ~6 weight percent nickel consist almost entirely of a single alloy phase – body-centered cubic (*Im*3*m*) α-iron, universally referred to as "kamacite" in the meteoritics literature, though officially termed "iron" by the IMA. These meteorites, which may be nearly mono-mineralic, have been called "hexahedrites" in the literature owing to the cubic (i.e., hexahedral) cleavage of α-iron crystals.

More commonly, iron alloys incorporate greater than ~6 weight percent Ni. These compositions initially crystallize from the melt in a single-phase region with the face-centered

cubic γ-iron structure of taenite. However, below ~800ºC a miscibility gap results in the exsolution of the more Ni-rich taenite phase from kamacite, which incorporates only about 6 weight percent Ni. This distinctive exsolution behavior, which is vividly revealed in the so-called Widmanstätten patterns of polished and etched meteoritic metal (Figure 1A), follows octahedral planes of the dominant cubic α-iron phase (e.g., McSween 1999; Yang and Goldstein 2005). Consequently, these iron meteorites have traditionally been called "octahedrites." Their Ni-enriched exsolution lamellae contain several alloy phases, including taenite, tetrataenite, "martensite", and awaruite (Reuter et al. 1988; Yang et al. 1996, 1997b; Mittlefehldt et al. 1998; Benedix et al. 2014; see below). In the less common circumstances of meteorites with greater than 15 weight percent Ni, exsolution may occur at lower temperature and at a much finer scale in a group of meteorites called "ataxites."

Several schemes beyond the hexahedrite/octahedrite/ataxite division have been used to classify iron meteorites. For example, octahedrites have been subdivided into seven textural groups on the basis of the average width of exsolution features, which depend primarily on the Ni content and cooling history of the alloy (Buchwald 1975; Hutchison 2004; McCoy et al. 2006; Goldstein et al. 2009; Rubin and Ma 2020). A complementary approach focuses on the development of subsequent alteration textures in hexahedrites and octahedrites, for example mechanical twinning, fracturing, and/or phase transitions in the metal alloys by impacts (Buchwald 1975).

The modern classification of iron meteorites is based on pioneering research by John T. Wasson and colleagues at UCLA (e.g., Wasson 1967, 1970, 1971, 1974; Scott and Wasson 1975; Wasson et al. 1989, 1998), who discovered striking systematic variations in the distribution of Ni and several trace elements, notably Ga, Ge, and Ir (Wasson 1974, 1990; Willis 1980; Mittlefehldt

et al. 1998), but also P, Co, Cu, As, Sb, Au, and W (e.g., Moore et al. 1969; Wasson and Choe 2009). This compositional scheme is widely employed to recognize more than a dozen different major groups of iron meteorites, each with at least five representative examples and each given a designation with a Roman numeral followed by one or more letters (e.g., IIAB or IIICD), as well as several "grouplets" with 2 to 4 members and additional unique iron meteorites (Benedix et al. 2014; Krot et al. 2014; Rubin and Ma 2020). In this scheme, the Roman numerals from I to IV are assigned based on decreasing Ge and Ga contents, while letter designations (A to G) refer to systematic differences in Ir and other trace elements that point to different parent bodies. As a consequence, iron meteorite classification schemes have led to the recognition of many discrete types of iron meteorites, each of which may represent a sample of the core from a different differentiated asteroid source (e.g., Scott 1979; Wasson 1990; Benedix et al. 2014).

Iron meteorite classification systems are not based on mineral species, per se; therefore, details of the current chemical classification system are beyond the scope of this mineralogical treatment. For additional information on iron meteorite classification see Mittlefehldt et al. (1998), Benedix et al. (2014), Rubin and Ma (2020), and references therein.

Several compositionally distinct groups of iron meteorites – the so-called "magmatic groups" – are primarily products of planetesimal differentiation and core separation and thus are essentially silicate free with a minor suite of associated phases, including graphite, carbides, schreibersite, carlsbergite, and sulfides (Benedix et al. 2014; Krot et al. 2014). These meteorites display trace element distributions that are unambiguously the consequence of fractional crystallization. Additional evidence for an origin in asteroidal cores comes from the relatively large sizes (perhaps to >10 meters maximum dimension) of some iron meteorites, a feature not consistent with dispersed masses of Fe-Ni alloy, as well as the occurrence of individual kamacite

187 crystals several meters in length – a sign of slow cooling (i.e., on the order of ~1 to 10 degrees
188 per million years) in the differentiated interior of an asteroid at least tens of kilometers in
189 diameter (Haack et al. 1990; McSween 1999; Goldstein et al. 2009).

190 Formation of a metal core and silicate mantle requires significant internal heating by sources
191 other than long-lived radionuclides or accretional heating (Benedix et al. 2014). Hypervelocity
192 impacts could have caused local heating to melting temperatures in some instances (Davison et
193 al. 2010). However, the most probable heat sources for melting of asteroids >20 kilometers in
194 diameter were short-lived radionuclides, notably ^{26}Al (Srinivasan et al. 1999; Keil 2000) and
195 ^{60}Fe (Shukolyukov and Lugmair 1992; Mostefaoui et al. 2005). However, given the 0.717 and
196 2.6 million year half-lives of ^{26}Al and ^{60}Fe (Wallner et al. 2015), respectively, such heating
197 must have been restricted to the first few million years of the solar nebula. Indeed, age
198 determinations of iron meteorites suggest core formation within a few million years of CAI
199 condensation, i.e., older than 4.56 Ga (Blichert-Toft et al. 2010).

200 By contrast, the "nonmagmatic" iron meteorite groups often have significant silicate
201 components, as well as minor and trace element distributions that are not consistent with
202 extensive fractional crystallization (Scott and Wasson 1975; Benedix et al. 2014). These groups
203 are thus thought to represent metal melt pooling, shock melting, breciation, and mixing of
204 lithologies. They commonly incorporate inclusions of other minerals, such as silicates, sulfides,
205 graphite, carbides, and phosphates (Wasson and Kallemeyn 2002). Silicate inclusions of
206 essentially chondritic composition are common in these nonmagmatic iron meteorites; they often
207 feature a reduced (i.e., low FeO content) assemblage with orthoenstatite, diopside, forsterite,
208 albite ($An_{\sim 10\text{-}20}$), troilite, graphite, phosphates, and minor minerals (Bunch et al. 1970;

Mittlefehldt et al. 1998), with varied inclusion morphologies (Bunch et al. 1970; Olsen and Jarosewich 1971; Bild and Wasson 1977; Wlotzka and Jarosewich 1977; Wasson et al. 1980; Takeda et al. 1994, 1997a; Choi et al. 1995; McCoy et al. 1996; Yugami et al. 1997; Benedix et al. 2000). Sulfide inclusions in iron meteorites are typically troilite-rich, with associated graphite and schreibersite (Buchwald 1975, 1977). Inclusions with up to 70 volume percent phosphates (McCoy et al. 1993), as well as silicate inclusions with abundant phosphate minerals, are also common features of iron meteorites.

The origin of these varied inclusion-bearing iron meteorites has been ascribed to partial melting and melt migration (Kelly and Larimer 1977; McCoy et al. 1993; Yugami et al. 1997); to impact heating and segregation on a porous iron body (Wasson and Kallemeyn 2002); or to catastrophic disruption of a partially melted body, which mixed and reassembled asteroidal materials (Benedix et al. 2000). Models that invoke post-asteroidal formation mechanisms of silicate inclusions through shock events are supported by radiometric age determinations, most of which fall within the range 4.50 +/- 0.03 Ga, or significantly after estimated ages of asteroid formation, but mostly well within the first 100 million years of the solar system (Bogard et al. 1967; Niemeyer 1979a, 1979b; Stewart et al. 1996), though meteorite ages for some silicate-bearing irons are as young as 3.5 Ga (Bogard et al. 1969; Göpel et al. 1985; Olsen et al. 1994).

Mineral Natural Kinds in Iron Meteorites

A reccurent question in the evolutionary system of mineralogy, as in most classification systems, relates to the “lumping” versus “splitting” of objects into natural kinds (Dupré 1981; Bailey 1994; Boyd 1999; Hawley and Bird 2011; Magnus 2012; Hazen 2019). Iron meteorites present a particularly relevant example. On the one hand, all iron meteorites incorporate kamacite as a major mineral – an Fe-Ni alloy with ~6 weight percent Ni and a suite of dozens of

minor and trace elements. All examples formed in asteroidal parent bodies in the early solar system. Furthermore, all parent bodies of iron meteorites experienced subsequent fragmentation through large impacts that produced the objects we study today. In this overview, we have chosen to lump all of these occurrences into a single natural kind: differentiated asteroidal iron, or "*DA iron*."

However, one might justifiably ask if further subdivision is warranted? For example, meteoritic iron could be split into two groups. On the one hand, "magmatic DA iron" derives from the initial melting and differentiation of an asteroidal body and is characterized by relatively unshocked kamacite with trace element distributions consistent with fractional crystallization (e.g., Benedix et al. 2014). These samples contrast with "nonmagmatic DA iron," which often display compelling textural and trace element evidence for formation via rapid impact melting (Scott 1972; Scott and Wasson 1975; Wasson et al. 1980; Wasson and Wang 1986). However, a number of iron meteorites display intermediate characteristics that possibly point to a combination of magmatic- and impact-related melting (Takeda et al. 1994; Benedix et al. 2000).

Evidence from Ni-, Mo-, and W-isotopic compositions suggests an additional division for iron meteorites between those that formed in planetesimals from isotope reservoirs that sample non-carbonaceous chondrite regions within Jupiter's orbit, versus planetesimals derived from carbonaceous chondrite precursors that formed beyond Jupiter's orbit (Trinquier et al. 2007, 2009; Burkhardt et al. 2011; Warren 2011; Kruijer et al. 2017). Carried to an extreme, each of the more than two dozen iron meteorite groups, grouplets, and unique examples holds a distinctive suite of compositional and textural attributes, which could be used to catalog a similar number of different natural kinds of meteoritic iron.

This is the peer-reviewed, final accepted version for American Mineralogist, published by the Mineralogical Society of America.
The published version is subject to change. Cite as Authors (Year) Title. American Mineralogist, in press.
DOI: https://doi.org/10.2138/am-2021-7632. http://www.minsocam.org/

A recurring feature of the effort to identify natural kinds through cluster analysis is a degree of subjectivity in how coarsely to lump, or finely to split, the objects of interest. In the evolutionary system of mineralogy in general, and in this study of non-chondritic meteorites in particular, we adopt a more conservative approach. We tend to lump minerals with similar paragenetic modes, such as meteoritic kamacite, whenever possible. However, in the future, experts in meteorite mineralogy may elect to apply the ideas of multi-dimensional cluster analysis to further subdivide meteoritic iron and other meteoritic phases into a number of additional catagories.

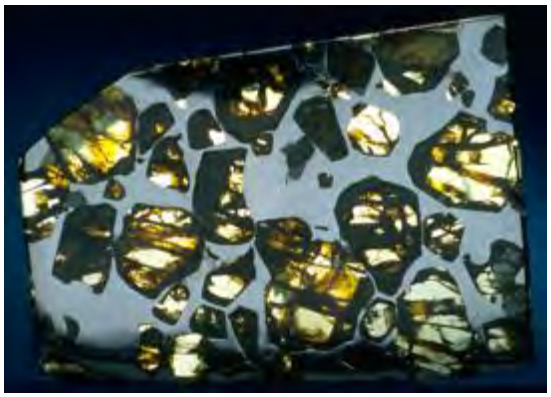

This is the peer-reviewed, final accepted version for American Mineralogist, published by the Mineralogical Society of America.
The published version is subject to change. Cite as Authors (Year) Title. American Mineralogist, in press.
DOI: https://doi.org/10.2138/am-2021-7632. http://www.minsocam.org/

Figure 1. Non-chondritic meteorites. (A) A polished and etched slab (1151 gm; 10 cm maximum diameter) from the Staunton iron meteorite with taenite exsolved from kamacite in a Widmanstätten pattern; (B) A polished slab of the Esquel pallasite (1091 gm; 8 cm maximum diameter), a stony-iron meteorite, with kamacite (silver in reflected light) and forsteritic olivine (yellow in transmitted light); (C) The Cumberland Falls aubrite (1227 gm; 11 cm maximum dimension), an achondrite meteorite observed to fall in Kentucky in 1919. This polymict breccia contains a rich variety of silicate-rich clasts of different lithologies derived primarily from ordinary chondrites. [Photos courtesy of the National Museum of Natural History, Smithsonian Institution]

Stony-Iron Meteorites

A few percent of meteorite falls, including the mesosiderite and pallasite groups, consist of subequal mixtures of Fe-Ni alloys and silicates (Figure 1B). These diverse "stony-iron meteorites," of which a few hundred are known, represent both transitional regions from the core-mantle boundaries of differentiated asteroids and violently shattered and mixed lithologies as a consequence of impacts.

Mesosiderites are impact breccias with 20 to 80 weight percent Fe-Ni alloys and troilite, typically in millimeter-scale grains. The balance comprises igneous lithic fragments, including predominantly basalt, gabbro, and pyroxenite, with minor dunite (Mittlefehldt et al. 1998; Krot et al. 2014; Mittlefehldt 2014). Mesosiderites have experienced varying degrees of metamorphism and remelting, which leads to corresponding variations in texture. However, the origin of these complex meteorites remains enigmatic (Hewins 1983; Wasson and Rubin 1985; Scott et al. 2001; Benedix et al. 2014).

Pallasites are a suite of ~100 distinctive stony-iron meteorites, perhaps derived from as many as 10 different parent bodies, with prominent silicate crystals (most typically olivine, $Fo_{\sim 88}$) in a metal matrix (Mittlefehldt et al. 1998; Benedix et al. 2014; Figure 1B). The mineralogy and textures of pallasites appear to be consistent with a deep mantle origin, from a cumulate zone

near the core-mantle boundary (however, for alternative origin hypotheses see Scott 1977a, 1977b; Ulff-Møller et al. 1997; Mittlefehldt et al. 1998; Boesenberg et al. 2012; Wasson 2016).

Note that meteorites with both metal and silicate components span the range from silicate-bearing iron meteorites with just a few silicate inclusions, to rocks that are near equal mixtures of metal and silicates, to silicate-dominant examples. Consequently, there are no sharp, unambiguous dividing criteria among iron, stony-iron, and achondrite meteorites. Nevertheless, many types of stony-iron meteorites have distinctive compositional and textural features that warrant their inclusion in a separate category.

Differentiated Achondrite Meteorites

Achondrite meteorites encompass a range of meteorites that lack chondrules or solar-like average compositions of chondrite meteorites. As such, they represent a range of igneous types, including melt-depleted ultramafic lithologies, mafic partial melts, and varied cumulates from felsic to ultramafic compositions that arose from crystal settling or flotation. Differentiated achondrites include the related HED meteorites (howardites, eucrites, and diogenites), the most abundant examples, as well as less common angrites, aubrites, and ureilites (Mittlefehldt 2014).

The HED meteorites, which are thought to derive from a single asteroidal parent body, probably 4 Vesta (McCord et al. 1970; Drake 2001; McSween et al. 2011), epitomize differentiated achondrites. Eucrites are by far the most abundant of the achondrites, with more than 600 finds and falls. When unaltered, eucrites represent either basalt or cumulate gabbro, with approximately equal amounts of calcic plagioclase and pigeonite (Takeda et al. 1997b; McSween et al. 2011; Krot et al. 2014). However, most eucrites have been altered by metamorphism and/or impacts.

315 The more than 200 known diogenites are igneous cumulate rocks, typically brecciated and
316 composed of igneous rock fragments. The majority of diogenites are 85 to 100 volume percent
317 (vol %) orthopyroxene, with minor olivine and chromite (McSween et al. 2011), though a few
318 examples are olivine-dominant, ranging to dunite cumulates with up to 95 vol % forsteritic
319 olivine (Beck et al. 2011).

320 Howardites are regolith breccias with mixtures of eucrites and diogenites, the consequence of
321 impact fracturing, jumbling, and welding (McSween et al. 2011). Relative proportions of the
322 brecciated components range continuously between the eucrite and diogenite endmembers;
323 consequently, the HED meteorites, in spite of significant differences among individual examples,
324 represent a unified collection of differentiated igneous rocks.

325 Other achondrites are presumed to have originated from varied differentiated asteroidal parent
326 bodies. Angrite meteorites are extremely alkali-depleted, silica-undersaturated (olivine-nepheline
327 normative) basalts, dominated by fassaite, olivine, and anorthite, which occur as both extrusive
328 volcanic and near-surface intrusive igneous rocks (Mittlefehldt and Lindstrom 1990; Clayton and
329 Mayeda 1996; Mikouchi et al. 1996; Mittlefehldt et al. 2002; Jambon et al. 2005; Mittlefehldt
330 2014). The accessory mineralogy of angrites includes Fe-Ni metal, troilite, kirschsteinite (the Ca-
331 Fe olivine), Ti-rich magnetite, hercynite, ulvöspinel, ilmenite, with rare celsian, rhönite, and
332 baddelyite (Keil 2012; Krot et al. 2014). Angrites are thus thought to represent partial melting of
333 primitive source material under relatively oxidizing conditions (Longhi 1999; Mittlefehldt et al.
334 2002).

335 Aubrites, also known as enstatite achondrites, are intriguing, highly-reduced, orthoenstatite-
336 dominant achondrites, with 75 to 95 vol % near endmember orthorhombic $MgSiO_3$, plus minor
337 albite, forsterite, and diopside (Watters and Prinz 1979; Keil 2010; Mittlefehldt 2014; Figure

This is the peer-reviewed, final accepted version for American Mineralogist, published by the Mineralogical Society of America.
The published version is subject to change. Cite as Authors (Year) Title. American Mineralogist, in press.
DOI: https://doi.org/10.2138/am-2021-7632. http://www.minsocam.org/

338 1C). Aubrites also incorporate some of the same rare sulfide minerals with Ca, Cr, Mn, Na, and
339 Ti that are found in enstatite chondrites, including alabandite (MnS), daubréelite ($FeCr_2S_4$),
340 heidite ($FeTi_2S_4$), and oldhamite (CaS). Many aubrites are brecciated.

341 Ureilites, once thought to represent ultramafic cumulates, are now recognized as mantle
342 restites formed by partial removal of basalt and metal components (Singletary and Grove 2006;
343 Weisberg et al. 2006; Goodrich et al. 2007, 2013; Warren 2012). They are predominantly olivine
344 with low-Ca pyroxene, though strongly depleted in a feldspathic component; ureilite mineralogy
345 is thus consistent with greater than 15 percent partial melting and melt segregation (Goodrich
346 1992; Goodrich et al. 2004, 2010; Mittlefehldt et al. 2014). Evidence from short-lived
347 radioisotopes suggest parent body formation within 1 million years of CAIs (van Kooten et al.
348 2017). A subset of ureilites are polymict breccias that incorporate ureilitic minerals and lithic
349 clasts – evidence for a major disruptive event early in the parent body's history (Cohen et al.
350 2004; Downes et al. 2008; Herrin et al. 2010).

351 A number of ungrouped achondrite meteorites are known in addition to the well-characterized
352 types reviewed above. For instance, the unique felsic achondrite GRA 06128/06129 is
353 mineralogically distinctive, with 70 to 90 vol % albitic plagioclase, with up to 25 vol % other
354 silicates (Fe-bearing olivine, orthopyroxene, and augite), and minor chlorapatite, merrillite,
355 troilite, pentlandite, chromite, and ilmenite (Day et al. 2009, 2012; Shearer et al. 2010). This
356 assemblage appears to be a flotation cumulate. Also of special note is the unique achondrite
357 NWA 11119 (Srinivasan et al. 2018), which is a silica-rich (i.e., andesitic) extrusive rock dated
358 by ^{26}Al-^{26}Mg methods to 4564.8 +/- 0.3 Ma (i.e., within ~ 3 Ma of CAIs), making this the oldest
359 known silica-rich basalt. Important features include numerous millimeter-diameter vesicles

This is the peer-reviewed, final accepted version for American Mineralogist, published by the Mineralogical Society of America.
The published version is subject to change. Cite as Authors (Year) Title. American Mineralogist, in press.
DOI: https://doi.org/10.2138/am-2021-7632. http://www.minsocam.org/

representing > 1 vol %, phenocrysts surrounded by quenched melt, and 30 vol % tridymite associated with an unusual mineralogical suite, including tranquillityite, zircon, fayalite, and tsangpoite.

An additional suite of "primitive achondrites," including winonaites, acapulcopites, lodranites, and perhaps brachinites, represent chondrites that have been subjected to high degrees of aqueous and thermal alteration – processes sometimes collectively referred to as "ultrametamorphism" (e.g., Krot et al. 2014; Mitlefehldt 2014). These meteorites lack chondrules, though they have not been extensively melted and thus retain some of the idiosyncratic compositional features of chondrites. The metamorphic mineralogy of primitive achondrites will be considered in Part V, along with secondary alteration mineralogy of chondrite meteorites. Note that, as with many stages of mineral evolution, there are no sharp dividing criteria between partially melted primitive achondrites and incompletely differentiated achondrites.

SYSTEMATIC PRIMARY MINERALOGY OF NON-CHONDRITIC METEORITES

The mineralogy of non-chondritic meteorites has been reviewed by Mittlefehldt et al. (1998) and Rubin and Ma (2017, 2020), as well as by Buchwald (1975, 1977) for iron meteorites and Ruzicka (2014) for silicate inclusions. Here we summarize the primary igneous mineralogy of differentiated asteroidal bodies, including 90 phases formed through melt crystallization, as well as by inversion, exsolution, and other solid-state reactions on cooling, as preserved in the relatively unaltered portions of iron, stony-iron, and achondrite meteorites (Table 1). Minerals formed through impact processes are summarized in Part IVB below, whereas minerals formed by secondary aqueous alteration and thermal metamorphism will appear in Part V of this series.

383 Distinguishing between primary and secondary minerals, especially in the many cases of rare,
384 sub-millimeter-scale phases, is often problematic. Here we cite phases for which petrologic and
385 mineralogic contexts strongly suggest a primary origin, defined for differentiated meteorites as
386 the result of igneous processes or through solid-state reactions upon initial cooling. Secondary
387 phases, by contrast, arise through subsequent aqueous, thermal, or shock processes. A significant
388 number of other phases of less than certain origins have been deferred to Part V, for example, the
389 enigmatic Al-bearing metal alloys from the unusual Khatyrka carbonaceous chondrite, including
390 hollisterite (Al_3Fe), kryachkoite $(Al,Cu)_6(Fe,Cu)$, stolperite (AlCu), decagonite ($Al_{71}Ni_{24}Fe_5$),
391 and icosahedrite ($Al_{63}Cu_{24}Fe_{13}$) (Bindi et al. 2011, 2012, 2016; Ma et al. 2017a; Rubin and Ma
392 2020). We also exclude the unusual carbides, andreyivanovite (FeCrP; Zolensky et al. 2008) and
393 florenskyite (FeTiP); Ivanov et al. 2000) from the complex brecciated Kaidun meteorite; these
394 minute grains may be primary but they occur embedded in secondary serpentine and their origins
395 are uncertain. Similarly, unique minor phases from acapulcoites, including melliniite $[(Ni,Fe)_4P$;
396 Pratesi et al. (2006)] and chopinite $[(Mg,Fe)_3\square(PO_4)_2$; Grew et al. 2010] appear in Part V.

397 In the following section we list 90 primary minerals formed by igneous processes in
398 differentiated asteroidal bodies, which incorporate 24 different essential elements, 17 of which
399 occur in multiple phases (Figure 2). These elements include the first appearances of Ba (celsian),
400 Cl (chlorapatite), Cu (copper), F (fluoro-richterite), and V (uakitite) as essential mineral-forming
401 elements.

This is the peer-reviewed, final accepted version for American Mineralogist, published by the Mineralogical Society of America.
The published version is subject to change. Cite as Authors (Year) Title. American Mineralogist, in press.
DOI: https://doi.org/10.2138/am-2021-7632. http://www.minsocam.org/

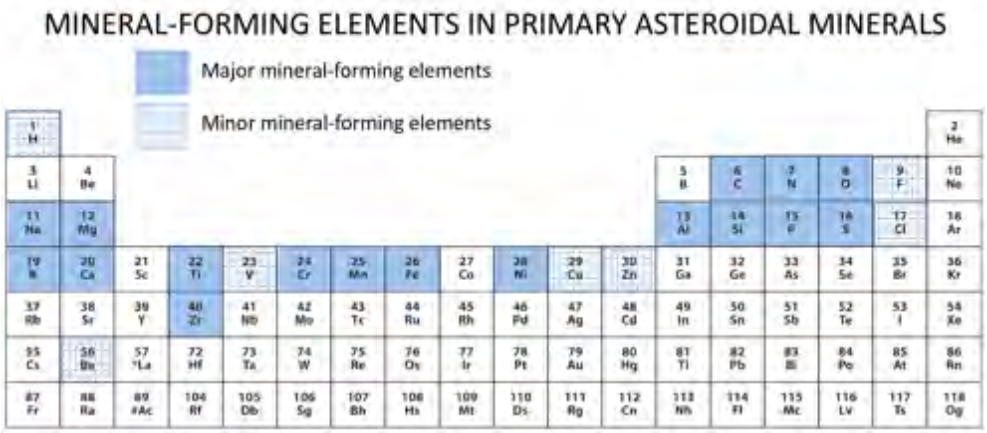

Figure 2. Essential mineral-forming elements in 90 primary asteroidal minerals.

We employ a binomial nomenclature: in most cases the official IMA-approved species name is preceded by "DA," for "differentiated asteroidal." Thus we list "*DA iron*," "*DA forsterite*," and so on. However, in a few instances we deviate from IMA nomenclature, as follows.

- The Fe-Ni phosphides schreibersite [$(Fe,Ni)_3P$] and nickelphosphide [$(Ni,Fe)_3P$] appear to form a continuous solid solution by identical paragenetic processes, with iron compositions predominant; therefore, we lump them together as *DA schreibersite*. Similarly, we lump barringerite [$(Fe,Ni)_2P$] and transjordanite [$(Ni,Fe)_2P$] as *DA barringerite.*
- We lump the NaCl-structured monosulfides, niningerite (MgS) and keilite (FeS), as *DA niningerite*, based on their continuous solid solution and similar mode of origin.
- Merrillite [$Ca_9NaMg(PO_4)_7$] and whitlockite [$Ca_9Mg(PO_3OH)(PO_4)_6$] form a continuous solid solution that we designate *DA merrillite*.

This is the peer-reviewed, final accepted version for American Mineralogist, published by the Mineralogical Society of America.
The published version is subject to change. Cite as Authors (Year) Title. American Mineralogist, in press.
DOI: https://doi.org/10.2138/am-2021-7632. http://www.minsocam.org/

- Analyses of meteoritic graftonite [$Fe^{2+}_3(PO_4)_3$] and beusite [$Mn^{2+}_3(PO_4)_2$] by Steele et al. (1991) revealed a continuous range of compositions, the majority of which fall within the Fe^{2+}-rich graftonite field. Therefore, we designate all occurrences as *DA graftonite*.

- We lump all Ca-poor clinopyroxenes into *DA pigeonite*.

NATIVE ELEMENTS AND ALLOYS

Several alloys of iron and nickel, as well as minor native copper and the carbon allotrope graphite, occur as primary igneous minerals in non-chondritic meteorites. Iron-nickel alloys are the commonest of these phases, representing more than 99 vol % of some examples. These alloys occur as the IMA-approved minerals iron (also commonly known as "kamacite"), taenite, tetrataenite, and awaruite, as well as the distinctive fine-grained exsolved mixture of kamacite and taenite known as "plessite" (Goldstein and Michael 2006). Fe-Ni alloys usually hold significant amounts of other elements; high C, P, or Si contents, for example, may lead to exsolution of new minerals, such as graphite, carbides, schreibersite, perryite, and/or silica glass (see below).

Iron [α-(Fe,Ni)]: The most abundant, defining phase in iron meteorites is body-centered cubic (*Im*3*m*) *DA iron*, commonly referred to as "kamacite" in the meteoritics literature (a name employed here when the term "iron" may be ambiguous) and as "ferrite" in metallurgy. Kamacite, the stable low-Ni iron alloy, typically contains up to ~6 weight percent (wt %) Ni, as well as minor Co (Buchwald 1977; Mittlefehldt et al. 1998; Rubin and Ma 2020). In meteorites with more than 6 wt % Ni, kamacite features exsolution of one or more Ni-enriched alloys, including taenite, tetrataenite, and awaruite. In hexahedrites with < 6 total wt % Ni, kamacite may compose >99 wt % of the total meteorite mass (Henderson 1941).

Kamacite is an important phase in stony-iron meteorites, both mesosiderites and pallasites (Powell 1969; Buseck 1977; Ulff-Møller et al. 1997). It is also a minor phase in achondrites, including aubrites (Watters and Prinz 1979) and HED group meteorites (Delany et al. 1984).

Taenite [γ-(Fe,Ni)]: The primitive cubic (*Pm*3*m*) alloy of iron and nickel, *DA taenite* (referred to as "austenite" in the metallurgical literature), typically has ~25 to 35 wt % Ni. Taenite is the solidus phase in the Fe-Ni phase diagram; however, at ~800ºC taenite transforms to a kamacite + taenite mixture. Taenite is thus typically the more Ni-rich major phase in iron and stony-iron meteorites with Widmanstätten patterns (Powell 1969; Buseck 1977; Buchwald 1977; Mittlefehldt et al. 1998). Note, however, Yang et al. (1997a, 1997b) suggest that at temperatures below ~400ºC "taenite" undergoes a solid-state reaction to a submicroscopic mixture of body-centered cubic (α_2-Fe,Ni), known as "martensite" in metallurgy, and the orthorhombic ordered phase tetrataenite. Taenite is also present in the minor metal phase of many achondrites, including aubrites, HED group meteorites, and the brachinite LEW 88763 (Delany et al. 1984; Okada et al. 1988; Swindle et al. 1998).

Tetrataenite (FeNi): *DA tetrataenite*, a low-temperature ordered Fe-Ni alloy (tetragonal, space group *P*4/*mmm*; Clarke and Scott 1980), typically forms a layer a few micrometers thick at the kamacite-taenite boundary in iron and stony-iron meteorites with Widmanstätten patterns. As such, it is a common, if volumetrically minor, phase in many iron and stony-iron meteorites. In addition, Okada et al. (1988) described minor tetrataenite in association with kamacite and taenite from the Norton County aubrite.

Awaruite (Ni_2Fe to Ni_3Fe): The Ni-dominant alloy *DA awaruite*, with face-centered cubic structure (space group *Fm*3*m*), was reported by Yang et al. (1997a, 1997b) as forming a thin

462 layer that separates tetrataenite from kamacite in the Widmanstätten patterns of some iron
463 meteorites.

464 **Copper (Cu):** *DA copper* is a rare accessory phase in enstatite achondrites (aubrites), where it
465 occurs in association with a suite of highly-reduced sulfides and other phases (Keil and
466 Fredricksson 1963; Ramdohr 1973; Watters and Prinz 1979). Native Cu is a common accessory
467 phase in troilite nodules from the Cape York (IIIAB) iron meteorite (Kracher et al. 1977). Near
468 endmember (~98 mol % Cu) copper occurs in the Bilanga diogenite (Domanik et al 2004).

469 **Graphite (C):** *DA graphite* is a common accessory phase in iron meteorites, likely formed
470 both by decomposition of cohenite and by exsolution from C-bearing metal (Mittlefehldt et al.
471 1998, and references therein). In some cases, graphite adopts a cube-shaped morphology (known
472 as "cliftonite") – a form imposed by the isometric symmetry of its metallic host. Other
473 occurrences of less well-ordered graphite in meteorites, as well as diamond and "lonsdaleite,"
474 have been ascribed to impact processes and are considered in the next section (Rubin 1997a;
475 Rubin and Scott 1997).

476 Graphite is an important component of carbon-rich ureilites, which are mantle restites
477 dominated by olivine and pigeonite. Graphite, at times in association with impact-generated
478 chaoite and organic molecules (kerogen), is most commonly fine-grained, but also occurs as
479 millimeter-diameter euhedral crystals and as intergrowths with metal and/or sulfide (Vdovykin
480 1970; Berkley and Jones 1982; Treiman and Berkley 1994).
481
482 **CARBIDES**

483 **Cohenite (Fe_3C):** *DA cohenite* is a common accessory mineral in iron meteorites (e.g.,
484 Buchwald 1975). In ureilites, cohenite occurs in association with graphite, troilite, and Fe-Ni
485 alloy (Goodrich and Berkley 1986).

This is the peer-reviewed, final accepted version for American Mineralogist, published by the Mineralogical Society of America.
The published version is subject to change. Cite as Authors (Year) Title. American Mineralogist, in press.
DOI: https://doi.org/10.2138/am-2021-7632. http://www.minsocam.org/

Haxonite [$(Fe,Ni)_{23}C_6$]: *DA haxonite* occurs in a variety of iron meteorites (e.g., Taylor et al. 1981), though it is significantly less common than cohenite in non-chondritic meteorites (Mittlefehldt et al. 1998).

Edscottite (Fe_5C_2): *DA edscottite* was formally described by Ma and Rubin (2019), following its reported occurrence decades earlier based on composition measurements by Scott and Agrell (1971). It occurs in slender crystal laths up to 40 micrometers in maximum dimension as inclusions in kamacite and in association with taenite, plessite, nickelphosphide, and cohenite in the Ni-rich Wedderburn (IAB) iron meteorite. The empirical formula found by Ma and Rubin (2019) is $[(Fe_{4.73}Ni_{0.23}Co_{0.04})C_{2.00}]$.

SILICIDES

Perryite [$(Ni,Fe)_8(Si,P)_3$]: *DA perryite* occurs as a minor accessory phase in the Norton County and Mt. Egerton enstatite achondrites (aubrites), in association with a suite of unusual highly reduced sulfides and other phases (Wasson and Wei 1970; Watters and Prinz 1979).

Carletonmooreite (Ni_3Si): *DA carletonmooreite* from the Norton County aubrite was approved as a new mineral based on characterization by Garvie et al. (2020). The mineral is cubic (space group *Pm*{bar3}*m*) and appears to be related to suessite (Fe_3Si), an impact-generated silicide that has a different cubic space group.

PHOSPHIDES

The phosphide schreibersite (and its Ni isomorph nickelphosphide) is an important primary phase in many iron-bearing meteorites. A number of other phosphides, including the barringerite-transjordanite solid solution included below, are rare in non-chondritic meteorites.

509 However, the origins of andreyivanovite (FeCrP; Zolensky et al. 2008), florenskyite (FeTiP);
510 Ivanov et al. 2000), and melliniite [$(Ni,Fe)_4P$; Pratesi et al. (2006)] are uncertain and will be
511 included in Part V.

512 **Schreibersite [$(Fe,Ni)_3P$] and Nickelphosphide [$(Ni,Fe)_3P$]:** *DA schreibersite* is the most
513 important P-bearing phase in iron meteorites (Mittlefehldt et al. 1998). It occurs in most iron
514 meteorites in several morphotypes (Buchwald 1977; Benedix et al. 2000) – as coarse masses, as
515 skeletal inclusions, and as small euhedral crystals (the latter sometimes called "rhabdites").
516 Schreibersite also occurs in the reduced suite of phases in enstatite achondrites (aubrites; Watters
517 and Prinz 1979), rarely in ureilites (Mittlefehldt et al. 1998), and as a minor phase in pallasites
518 (Buseck 1977).

519 Schreibersite usually contains significant Ni, in rare instances in amounts slightly exceeding
520 Fe in mol percent (mol %), which corresponds to the IMA-approved species nickelphosphide.
521 For example, Ma and Rubin (2019) report a composition of $[(Ni_{1.63}Fe_{1.37}Co_{0.01})P_{0.99}]$ for a
522 sample in association with edscottite in the Wedderburn (IAB) iron meteorite. Here we lump
523 nickelphosphide with schreibersite, with which it forms a continuous solid solution.

524 **Barringerite [$(Fe,Ni)_2P$] and Transjordanite [$(Ni,Fe)_2P$]:** *DA barringerite* from the
525 Ollague pallasite was characterized by Buseck (1969) for a sample with composition
526 $[(Fe_{1.11}Ni_{0.81})P]$. Britvin et al. (2020a) recently discovered Ni-dominant isomorphs with
527 maximum Ni content $[(Fe_{0.48}Ni_{1.52})P]$ in the ungrouped Cambria iron meteorite, which they
528 called transjordanite. Britvin and colleagues also described a range of intermediate compositions,

529 some with Fe~Ni, such as [$(Fe_{1.18}Ni_{0.81})P$]. Given the continuous solid solution and similar
530 paragenetic modes, we lump both species into *DA barringerite*.
531
532 **NITRIDES**
533 Osbornite, carlsbergite, and uakitite [(Ti,Cr,V)N] are cubic nitrides with the NaCl structure.
534 Solid solutions among these and other compositions may occur, but known meteoritic examples
535 lie close to their respective endmembers. Therefore, we recognize the following three natural
536 kinds, as well as the rare iron nitride roaldite and the silicon oxy-nitride sinoite.
537 **Osbornite (TiN):** Osbornite is best known as a common accessory phase in enstatite
538 chondrites (e.g., Hazen et al. 2020). However, *DA osbornite* also occurs in the Bishopville and
539 Bustee enstatite achondrites (aubrites) as a rare accessory phase in association with a suite of
540 unusual sulfides and other highly-reduced phases (Bannister 1941; Watters and Prinz 1979).
541 **Carlsbergite (CrN):** *DA carlsbergite* is a common minor constituent of iron meteorites
542 (Buchwald 1975). Published analyses of carlsbergite from the Cape York (IIIAB; Buchwald and
543 Scott 1971) and Sikhote-Alin (IIAB; Axon et al. 1981) iron meteorites are close to the
544 endmember composition.
545 **Uakitite (VN):** Sharygin et al. (2020) discovered the new vanadium nitride, *DA uakitite*, as
546 euhedral (cube-shaped) to rounded crystals less than 5-micrometers maximum dimension in the
547 Uakit (IIAB) iron meteorite. Uakitite occurs in troilite-daubréelite small inclusions (to 100-
548 micrometers diameter) and large nodules (to 1-centimeter diameter). Uakitite has an observed
549 composition of [$(V_{0.91}Cr_{0.07}Fe_{0.02})N$] and is the earliest known vanadium mineral.
550 **Roaldite [$(Fe,Ni)_4N$)]:** *DA roaldite* occurs sparsely in the Jerslev and Youndegin (IAB) iron
551 meteorites as exsolved platelets 1- to 2-micrometers thick and many millimeters in lateral extent

This is the peer-reviewed, final accepted version for American Mineralogist, published by the Mineralogical Society of America.
The published version is subject to change. Cite as Authors (Year) Title. American Mineralogist, in press.
DOI: https://doi.org/10.2138/am-2021-7632. http://www.minsocam.org/

552 in kamacite, as described by (Nielsen and Buchwald 1981). It contains ~6 mol % Ni substituted
553 for Fe.

554 **Sinoite (Si_2N_2O):** The silicon oxy-nitride *DA sinoite* occurs as a rare minor phase in the
555 Zakłodzie ungrouped enstatite achondrite, where it is associated with major enstatite, anorthite,
556 and troilite, and accessory silica polymorphs, schreibersite, keilite, buseckite, and other phases
557 (Ma et al. 2012a).
558
559 **SULFIDES**

560 The iron sulfide troilite is a common, and at times major, phase in non-chondritic meteorites
561 (Mittlefehldt et al. 1998: Tables 2 and 29). An additional suite of rare, highly-reduced sulfides
562 and associated phases occurs in enstatite achondrites (aubrites).

563 Some models of asteroidal differentiation suggest that predicted sulfide-rich meteorites may
564 be missing from collections, based on the assumption that asteroid core formation should also
565 result in late-stage sulfur-rich immiscible melts (Chabot and Drake 1999, 2000). However, the
566 corresponding S-rich meteorites have not yet been found. One possibility is that sulfide-
567 dominant meteors are selectively lost, as they will more easily decompose in space and fragment
568 upon atmospheric entry than iron- or silicate-rich meteors (Kracher and Wasson 1982).

569 **Troilite (FeS):** *DA troilite*, the hexagonal (space group $P6_3/mmc$) polymorph of FeS, is by far
570 the commonest sulfide mineral in non-chondritic meteorites, at times exceeding Fe-Ni metal in
571 volume (Mittlefehldt et al. 1998). In iron meteorites, troilite occurs in several forms, most
572 dramatically in nodules or veins in Fe-Ni alloys up to several centimeters in maximum
573 dimension, in which it may occur in association with graphite, cohenite, and schreibersite. Other
574 morphotypes in iron meteorites include oriented platelets up to a centimeter in maximum

575 dimension but only a few millimeters thick, suggesting exsolution from the host Fe-Ni alloy
576 (Buchwald 1975; Scott 1982; Casanova et al. 1995; Benedix et al. 2000).

577 Troilite is the dominant S-bearing phase in association with Fe-Ni alloys in stony-iron
578 meteorites, including both pallasites (Buseck 1977) and mesosiderites, in which it can account
579 for up to 14 vol % (Powell 1969; Floran 1978; Scott et al. 1996). Troilite occurs commonly as an
580 accessory phase in achondrites, for example, in brachinites (Nehru et al. 1992), in HED group
581 meteorites (Delany et al. 1984; Takeda and Mori 1985; Bowman et al. 1997), and in angrites
582 (Prinz et al. 1977, 1988, 1990; McKay et al. 1988, 1990). Troilite significantly enriched in Ti
583 (with 17 to 25 wt % Ti, equivalent to 29 to 39 mol % TiS) occurs commonly in aubrites in
584 association with a suite of highly reduced phases (Watters and Prinz 1979; McCoy 1998).
585
586 **NaCl-type Monosulfide Group [(Mg,Fe,Ca,Mn)S]:** Niningerite, keilite, oldhamite, and
587 alabandite are monosulfides with the cubic (space group *Fd*3*m*) NaCl structure. All are rare,
588 occurring with suites of unusual phases in enstatite chondrites and enstatite achondrites (also
589 known as aubrites). These phases may represent a continuous solid solution among the Mg-Fe-
590 Ca-Mn endmembers, as all analyzed examples incorporate these four elements. However, until
591 further data are available, we lump only niningerite-keilite (Fe-Mg-dominant) members.

592 **Niningerite (MgS) and Keilite (FeS):** *DA niningerite* was originally described from
593 enstatite chondrites by Keil and Snetsinger (1967) as a cubic monosulfide of Mg, with significant
594 Fe substitution, in some instances with Fe > Mg. McCoy (1998) subsequently described
595 niningerite with significant Mn and Fe (15 and 7 mol %, respectively) from the Bustee enstatite
596 achondrite in association with a suite of highly-reduced sulfides and other phases, while Shimizu
597 et al. (2002) reported Fe-dominant analogs of niningerite from five different enstatite chondrites
598 – a mineral species approved by the IMA as keilite. Ma et al. (2012a) then identified minor

599 keilite in the Zakłodzie ungrouped enstatite achondrite, where it is associated with major
600 enstatite, anorthite, and troilite, and accessory silica polymorphs, schreibersite, buseckite, and
601 other phases. Because these occurrences suggest a continuous solid solution between the Mg and
602 Fe endmembers, and they always occur in association with troilite in enstatite achondrites, we
603 lump these two species into DA niningerite with the general formula [(Mg,Fe,Mn)S].

604 **Oldhamite (CaS):** *DA oldhamite* occurs as a minor phase in enstatite achondrites (aubrites)
605 as grains ~100 micrometers in diameter, typically in association with a suite of highly-reduced
606 phases (Graham et al. 1977; Watters and Prinz 1979). In aubrites, which lack phosphates,
607 oldhamite is often the principal repository of rare-earth elements (Floss and Crozaz 1993;
608 Wheelock et al. 1994). Note that in some models of aubrite formation, which invoke partial
609 melting of an enstatite chondrite precursor, oldhamite is thought to be a relict phase of nebular
610 condensation processes rather than a product of asteroidal differentiation (Floss and Crozaz
611 1993; Lodders 1996). However, based on the very different trace element fractionation patterns
612 in different samples, a combination of both nebular and igneous origins seems likely for different
613 oldhamite occurrences (Wheelock et al. 1994; McCoy 1998).

614 **Alabandite (MnS):** *DA alabandite* with significant Fe^{2+} and Mg occurs as a minor phase in
615 enstatite achondrites (aubrites), in association with a suite of highly reduced phases (Keil and
616 Fredriksson 1963; Watters and Prinz 1979). For example, a specimen from the Mayo Belwa
617 aubrite has composition $[(Mn_{0.52}Fe_{0.35}Mg_{0.02}Ca_{0.02}Cr_{0.03})S_{0.99}]$ (Watters and Prinz 1979).
618
619 **Sphalerite Monosulfide Group [(Zn,Fe,Mn)S]:** The sphalerite group of cubic (space group
620 *F*{bar4}3*m*) monosulfides is represented in non-chondritic meteorites by two rare occurrences,
621 including sphalerite and browneite. Solid solution occurs among the Zn-Fe-Mn endmembers, but

622 the two reported examples are close to Zn and Mn endmembers. Therefore, we list them as
623 discrete natural kinds.

624 **Sphalerite (ZnS):** *DA sphalerite* has been recorded by Kracher et al. (1977) as rare grains
625 within troilite nodules, often in close association with Fe^{2+}-rich alabandite in the Cape York
626 (IIIAB) iron meteorite. The average composition is $[(Zn_{0.82}Fe_{0.14}Mn_{0.04})S]$. Kracher et al.
627 (1977) suggest that sphalerite may have exsolved from alabandite.

628 **Browneite (MnS):** *DA browneite* of approximate composition $[(Mn_{0.99}Fe_{0.01})S]$ was
629 reported by Ma et al. (2012b) from the Zakłodzie ungrouped enstatite achondrite, where it was
630 found as a single 16-micrometer-diameter crystal encased by plagioclase and in close association
631 with troilite and enstatite. Browneite is metastable with respect to alabandite at all temperatures
632 and pressures relevant to meteorite paragenesis; therefore, Ma et al. (2012b) speculated that
633 browneite formed metastably at T < 200ºC, though the mechanism of formation is uncertain.
634 Therefore, the possibility of a secondary origin through aqueous or weathering processes cannot
635 be ruled out.

636 **Buseckite [(Fe,Zn,Mn)S]:** *DA buseckite* is the Fe^{2+}-dominant, hexagonal wurtzite-structure
637 (space group $P6_3mc$) monosulfide. It was discovered by Ma et al. (2012a) in the Zakłodzie
638 ungrouped enstatite achondrite, where it occurs as subhedral grains to 20-micrometers diameter
639 in association with troilite, orthoenstatite, anorthite, and numerous other phases.
640
641 **Thiospinel Group [(Fe,Mn)Cr_2S_4]:** Daubréelite, joegoldsteinite, and kalininite, the Fe, Mn, and
642 Zn chromite members of the cubic (space group $Fd3m$) thiospinel group, are known exclusively
643 from meteorites. Extensive solid solution may occur among these and other endmembers;

644 however, reported compositions are sufficiently close to endmember compositions to warrant
645 three distinct natural kinds.

646 **Daubréelite ($FeCr_2S_4$):** *DA daubréelite* is found in numerous iron and achondrite meteorites
647 as a minor accessory phase. It was reported as an exsolved phase in troilite from the Bishop
648 Canyon (IVA) silicate-bearing iron meteorite (Scott et al. 1996) and as a minor component of
649 silicate inclusions in a variety of iron meteorites (Buchwald 1975). It also occurs as a minor
650 phase in aubrites with average composition [$(Fe_{0.89}Mg_{0.09}Mn_{0.07}Cr_{1.82})S_4$], in association with
651 a suite of highly-reduced phases (Graham et al. 1977; Watters and Prinz 1979).

652 **Joegoldsteinite ($MnCr_2S_4$):** *DA joegoldsteinite*, the Mn analog of daubréelite, was
653 discovered by Isa et al. (2016) in the Social Circle (IVA) magmatic iron meteorite. The
654 specimen, which occurs as two 13- to 15-micrometer maximum dimension inclusions in
655 kamacite, has an empirical formula of [$(Mn_{0.82}Fe_{0.23})Cr_{1.99}S_{3.95}$].

656 **Kalininite ($ZnCr_2S_4$):** Sharygin (2020) lists *DA kalininite* as a trace phase in the Uakit
657 (IIAB) iron meteorite in a preliminary report of its unusual accessory mineralogy, which also
658 contains uakitite and an as yet unapproved Cu-Cr sulfide associated with troilite-rich inclusions.
659
660 **Wilkmanite Group [$(Fe,Cr)(Fe,Cr,Ti)_2S_4$]:** Two new monoclinic (space group *I*2/*m*) sulfides
661 discovered in meteorites, brezinaite and heidite, are isomorphous with wilkmanite (Ni_3Se_4).

662 **Brezinaite (Cr_3S_4):** The presence of the rare mineral *DA brezinaite* in the ungrouped Tucson
663 iron meteorite is an indicator of its extremely reduced state, as revealed by coexisting Cr^{2+} and
664 Cr^{3+} in this thiospinel (Bunch and Fuchs 1969a; Nehru et al. 1982). Brezinaite has also been

reported from the anomalous Cr-rich ureilite LEW 88774 in association with chromite, eskolaite, a Cr-Fe carbide [~$(Fe,Cr)_2C$], and graphite (Prinz et al. 1994), as well as the Mt. Egerton aubrite (Casanova et al. 1993).

Heideite [$(Fe,Cr)_{1.15}(Ti,Fe)_2S_4$]: *DA heideite* was reported by Keil and Brett (1974) from the Bustee aubrite, in which it is associated with a suite of highly-reduced sulfides and other phases (Watters and Prinz 1979).

Other Sulfides

Pentlandite [$(Ni,Fe)_9S_8$]: *DA pentlandite* has been reported in brachinites, coexisting with Ni-rich troilite and taenite (Nehru et al. 1983, 1992).

Caswellsilverite ($NaCrS_2$): *DA caswellsilverite* occurs as inclusions in oldhamite in the Norton County enstatite achondrite in association with a suite of unusual highly-reduced sulfides and other phases (Watters and Prinz 1979). Okada and Keil (1982) measured a composition of $[(Na_{0.95}Cr_{1.00}Ti_{0.05})S_{1.95}]$.

Unnamed ($CuCrS_2$): Sharygin (2020) described an as yet unnamed sulfide, which we designate *DA* $CuCrS_2$, from the Uakit (IIAB) iron meteorite. Preliminary data, obtained on 10-micrometer maximum dimension crystals in phosphide-sulfide inclusions in kamacite and schreibersite, suggest that this phase may be a Cu^{1+} analog of caswellsilverite. The observed composition is $[(Cu_{0.94}Fe_{0.09}Cr_{0.97})S_2]$.

Djerfisherite [$K_6(Fe,Cu,Ni)_{25}S_{26}Cl$]: *DA djerfisherite*, originally described by Fuchs (1966) from enstatite chondrites, also occurs in the Pena Blanca Springs enstatite achondrite as a minor

686 mineral associated with a suite of highly-reduced sulfides and other phases (Ramdohr 1963;
687 Watters and Prinz 1979).
688
689 **PHOSPHATES**

690 A diversity of phosphate minerals, both in P-rich nodules and in more widely dispersed
691 grains, occur widely in non-chondritic meteorites (Fuchs 1969a; Mittlefehldt et al. 1998: Tables
692 2 and 16). Phosphate minerals, which may comprise as much as 70 vol % of some inclusions in
693 iron meteorites (McCoy et al. 1993), only occur in relatively oxidized iron meteorites (Olsen and
694 Fredriksson 1966; Olsen et al. 1999); otherwise schreibersite is the dominant P-bearing phase.
695 Note that phosphates are particularly important components of pallasite stony-iron meteorites
696 (Buseck 1977; Buseck and Holdsworth 1977).

697 **Chlorapatite [$Ca_5(PO_4)_3Cl$]:** *DA chlorapatite* is a significant phosphate mineral in several
698 types of non-chondritic meteorites, including in phosphate-rich inclusions in the Carlton (IIICD)
699 iron meteorite (McCoy et al. 1993); in brachinites (Nehru et al. 1992; Swindle et al. 1998); in
700 polymict ureilites (Mittlefehldt et al. 1998); and in HED group meteorites (Mittlefehldt et al.
701 1998). Chlorapatite constitutes ~8 vol % of silicate inclusions in the ungrouped Sombrerete
702 (IAB) iron meteorite (Prinz et al. 1982).

703 **Merrillite [$Ca_9NaMg(PO_4)_7$] and Whitlockite [$Ca_9Mg(PO_3OH)(PO_4)_6$]:** *DA merrillite*,
704 including continuous solid solution with whitlockite, is a common phase in non-chondritic
705 meteorites. It is an abundant phosphate mineral with brianite and panethite in the Dayton (IAB)
706 iron meteorite (McCoy et al. 1993, 1994). Merrillite has been reported from pallasites (Buseck
707 1977; Buseck and Holdsworth 1977; Davis and Olsen 1991; Boesenberg et al. 1995), as a minor
708 accessory mineral in mesosiderites (Floran et al. 1978; Rubin and Mittlefehldt 1992), and from

the unique Enon stony-iron (Bunch et al. 1970). In achondrites, merrillite occurs in brachinites in association with chlorapatite (Nehru et al. 1996; Swindle et al. 1998), in basaltic eucrites (Ikeda and Takeda 1985), and as a minor phase in angrites (McKay et al. 1990).

Matyhite [$Ca_9(Ca_{0.5}\square_{0.5})Fe(PO_4)_7$]: Hwang et al. (2019) characterized the new Ca-Fe phosphate mineral (presumed *DA*) *matyhite* from the D'Orbigny angrite, which is an analog of merrillite but with high Fe and low Na and Mg. Matyhite occurs as elongated crystallites up to ~10 micrometers maximum dimension in association with fayalite, kirchsteinite, and hedenbergite. It was previously reported from other angrites, including Angra do Reis (Prinz et al. 1977), LEW 86010 (McKay et al. 1988), Asuka 881371 (Prinz and Weisberg 1995), and NWA 1296 (Jambon et al. 2005). Hwang et al. (2019) suggest that matyhite formed as part of a residual melt assemblage that includes tsangpoite and kuratite. However, they could not rule out the possibility of formation by metasomatism.

Graftonite [$Fe^{2+}_3(PO_4)_3$] and Beusite [$Mn^{2+}_3(PO_4)_2$]: *DA graftonite* was reported by Olsen and Steele (1993, 1997) from troilite nodules in iron meteorites in association with sarcopside, galileiite, and chromite. Steele et al. (1991) reported an intermediate composition ~[$(Fe_{1.5}Mn_{1.5})(PO_4)_3$], which they designated beusite. Their survey of more than a dozen graftonite-beusite analyses from the El Sampal (IIIA), Grant (IIIB), and other iron meteorites, revealed a range of Ca-free compositions from near endmember graftonite to samples with 33 to 58 mol % beusite. Because these compositions represent a continuous solid solution and the majority of specimens lie well within the Fe^{2+}-rich graftonite field, we designate all of these occurrences as *DA graftonite*.

Farringtonite [$(Mg,Fe)_3(PO_4)_3$]: *DA farringtonite* is found in pallasites, occurring with fairfieldite and whitlockite (Buseck 1977; Buseck and Holdsworth 1977).

Sarcopside [$(Fe,Mn)_3(PO_4)_2$]: *DA sarcopside* was reported by Olsen and Steele (1997) from troilite nodules in iron meteorites in association with graftonite, galileiite, and chromite.

Stanfieldite [$Ca_4Mg_5(PO_4)_6$]: *DA stanfieldite* was described by Fuchs (1967) and has been reported from several pallasites (Buseck 1977; Buseck and Holdsworth 1977; Davis and Olsen 1991).

Buchwaldite ($NaCaPO_4$): *DA buchwaldite* is a rare Na-Ca-phosphate described from a 40-micrometer-diameter crystal by Olsen et al. (1977a). It occurs within troilite nodules associated with chromite and other phosphate minerals in the Cape York (IIIAB) iron meteorite (Kracher et al. 1977).

This is the peer-reviewed, final accepted version for American Mineralogist, published by the Mineralogical Society of America.
The published version is subject to change. Cite as Authors (Year) Title. American Mineralogist, in press.
DOI: https://doi.org/10.2138/am-2021-7632. http://www.minsocam.org/

741 **Marićite ($NaFePO_4$):** *DA marićite* was reported by Kracher et al. (1977) from the Cape York
742 (IIIAB) iron meteorite. This rare occurrence is in association with buchwaldite and two other
743 unidentified alkali phosphates.

744 **Moraskoite [$Na_2Mg(PO_4)F$]:** *DA moraskoite* was described by Karwowski et al. (2015) in
745 the Morasko (IAB) iron meteorite, in which it is associated with other primary phosphate
746 minerals.

747 **Xenophyllite [$Na_4Fe_7(PO_4)_6$]:** Britvin et al. (2020b) reported the new phosphate *DA*
748 *xenophyllite* from the Augustinovka (IIIAB) iron meteorite, associated with sarcopside,
749 schreibersite, chromite, and pentlandite.

750 **Brianite [$Na_2CaMg(PO_4)_2$]:** *DA brianite* was discovered by Fuchs et al. (1967) as a minor
751 phase in pockets up to 1.5-centimeters maximum dimensions with individual crystals up to 200-
752 micrometers across from the Dayton (IAB) hexahedrite, where it occurs in association with
753 whitlockite and panethite (McCoy et al. 1993, 1994). Scott and Bild (1974) reported brianite as
754 scattered veins throughout silicate inclusions, but also commonly in contact with metal, in the
755 San Cristobal (unique IAB) iron meteorite. Brianite has also been found in the Youndegin (IAB)
756 low-Ni iron meteorite (Fuchs 1969a).

757 **Panethite [$Na_2(Fe,Mn)_2(PO_4)_2$]:** *DA panethite* occurs with whitlockite and brianite in the
758 Dayton (IAB) iron meteorite in pockets up to 1.5-centimeters maximum dimensions, with
759 individual crystals up to 200-micrometers diameter (Fuchs et al. 1967; McCoy et al. 1993, 1994).
760
761 **Fillowite Group [$Na_2(Ca,Fe,Mg,Mn)_8(PO_4)_6$]:** Three closely-related members of the
762 hexagonal (space group $R\bar{3}$) fillowite group – johnsomervilleite, chladniite, and galileiite –

have been reported from troilite nodules in iron meteorites. We suspect that these three species may represent a single natural kind with a continuous solid solution and similar paragenetic mode. However, until more compositional data are available we list these species as distinct natural kinds.

Johnsomervilleite [$Na_2Ca(Fe,Mg,Mn)_7(PO_4)_6$]: *DA johnsomervilleite* was reported by Olsen and Steele (1993, 1997) as rare accessory phases from troilite nodules in the Carlton (IIICD), Chupaderos (IIIB), Grant (IIIB), El Sampal (IIIA), and Sandtown (IIIAB) iron meteorites in association with chromite plus graftonite and/or sarcopside.

Chladniite [$Na_2CaMg_7(PO_4)_6$]: *DA Chladniite* was identified and named by McCoy et al. (1994) based on a single crystal ~1-millimeter in maximum dimension, which was found in a silicate-bearing inclusion in the Carlton (IIICD) iron meteorite in association with dominant chlorapatite (70 vol %), forsterite, orthoenstatite, and albite. McCoy et al. (1994) measured the chemical formula as $[Na_{1.77}Ca_{0.98}(Mg_{6.96}Fe_{0.26}Mn_{0.04})(PO_4)_6]$.

Galileiite [$Na_2(Fe,Mn)_8(PO_4)_6$]: The Na-Fe-phosphate *DA galileiite* was described by Olsen and Steele (1997) from five different group III iron meteorites. It occurs as rare grains up to 30-micrometers in diameter in troilite nodules in association with graftonite, sarcopside, and chromite.

Tsangpoite [$Ca_5(PO_4)_2(SiO_4)$]: *DA tsangpoite* was characterized by Hwang et al. (2019) from the D'Orbigny angrite, where it occurs as numerous elongated hexagonal prismatic crystals to tens of micrometers maximum dimension in association with hedenbergite, iron sulfide, and magnetite. Earlier reports of this rare Ca-silico-phosphate in angrites include occurrences in

This is the peer-reviewed, final accepted version for American Mineralogist, published by the Mineralogical Society of America.
The published version is subject to change. Cite as Authors (Year) Title. American Mineralogist, in press.
DOI: https://doi.org/10.2138/am-2021-7632. http://www.minsocam.org/

Asuka 881371 (Prinz and Weisberg 1995), NWA 1296 and 1670 (Jambon et al. 2005, 2008), NWA 4590 (Mikouchi et al. 2011), and NWA 11119 (Srinivasan et al. 2018).

OXIDES

Oxides minerals are common, if usually minor, phases in non-chondritic meteorites (Mittlefehldt et al. 1998: Tables 17, 32, and 38). The oxide spinels and ilmenite account for most reported occurrences, while instances of perovskite group oxides, corundum, eskolaite, rutile, and baddeleyite are rare.

Oxide Spinel Group [$(Mg,Fe^{2+})(Al,Fe^{3+},Cr^{3+},Ti)_2O_4$]: The oxide spinel group, the most ubiquitous oxide phases in non-chondritic meteorites, encompass a complex range of solid solutions, representing at least eight major idealized endmembers: spinel ($MgAl_2O_4$), hercynite ($Fe^{2+}Al_2O_4$), magnesioferrite ($MgFe^{3+}{}_2O_4$), magnetite ($Fe^{2+}Fe^{3+}{}_2O_4$), magnesiochromite ($MgAl_2O_4$), chromite ($Fe^{2+}Cr^{3+}{}_2O_4$), qandilite ($Mg_2Ti^{4+}O_4$), and ulvöspinel ($Fe^{2+}{}_2Ti^{4+}O_4$). In addition, some spinels incorporate significant amounts of Ca, Mn^{2+}, Zn, V^{3+}, Ti^{3+}, and/or Si. Given the compositional diversity and extensive solid solution among natural meteoritic samples of oxide spinels, it is challenging to determine how many distinct natural kinds are represented. In some instances, as with the angrites (Mittlefehldt et al. 1998, Table 38), two distinct oxide spinel compositions – one hercynitic and the other Al-poor, either magnetite or ulvöspinel – commonly coexist. We therefore recognize *DA hercynite*, *DA magnetite*, and *DA ulvöspinel* as distinct natural kinds. In other meteorite groups, including pallasites, brachinites, ureilites, diogneites, and eucrites, a range of Cr-rich spinel compositions usually closest to the chromite endmember is observed; we lump all such examples into *DA chromite*.

This is the peer-reviewed, final accepted version for American Mineralogist, published by the Mineralogical Society of America.
The published version is subject to change. Cite as Authors (Year) Title. American Mineralogist, in press.
DOI: https://doi.org/10.2138/am-2021-7632. http://www.minsocam.org/

807 **Chromite ($Fe^{2+}Cr_2O_4$):** *DA chromite* is often the most abundant oxide mineral in non-
808 chondritic meteorites. It is an important Cr-bearing phase in many iron meteorites (Buchwald
809 1975; Ulff-Møller et al. 1995; Scott et al. 1996), at times occurring as oriented thin
810 "Reichenbach lamellae" encased by kamacite. Chromite is found in most pallasites (Buseck
811 1977), with modest substitution of Al for Cr^{3+} in some samples (Bunch and Keil 1971); as a
812 minor phase in brachinites (up to ~3 vol. %; Nehru et al. 1983); in ureilites (up to ~6 vol. %;
813 Mittlefehldt et al. 1998; Goodrich et al. 2014); as a common minor mineral up to 5 vol % in
814 diogenites (Mittlefehldt 1994; Bowman et al. 1997); and in eucrites (Lovering 1975).

815 **Magnetite (Fe_3O_4):** The Angra dos Reis angrite holds accessory Ti-rich *DA magnetite* of
816 average composition ($Fe^{2+}_{1.50}Mg_{0.06}Al_{0.15}Fe^{3+}_{0.51}Ti_{0.61}O_4$), which occurs in association with
817 fassaite, forsterite, hercynite, and troilite, as well as an unusual suite of accessory phases
818 including kirschsteinite, celsian, and baddeleyite (Prinz et al. 1977). A similar association was
819 observed by McKay et al. (1988) in the LEW 86010 angrite, in which Ti-rich magnetite of
820 average composition ($Fe^{2+}_{0.72}Mg_{0.06}Al_{0.19}Fe^{3+}_{1.01}Ti_{0.68}O_4$) occurs with hercynite.

821 **Hercynite ($Fe^{2+}Al_2O_4$):** *DA hercynite* is a minor phase in several angrite meteorites.
822 Hercynite of average composition [$(Fe^{2+}_{0.75}Mg_{0.25})(Al_{1.80}Fe^{3+}_{0.07}Cr^{3+}_{0.07})O_4$] occurs in the
823 Angra dos Reis angrite with fassaite, olivine, and troilite, as well as an unusual suite of accessory
824 phases including kirschsteinite, celsian, Ti-rich magnetite, and baddeleyite (McKay et al. 1988;
825 Prinz et al. 1977). In the Asuka 881371 angrite, hercynite of composition
826 [$(Fe^{2+}_{0.80}Mg_{0.32})(Al_{1.35}Cr^{3+}_{0.50}Ti_{0.03})O_4$] coexists with ulvöspinel (Mikouchi et al. 1996),
827 whereas in the LEW 86010 angrite hercynite of average composition

This is the peer-reviewed, final accepted version for American Mineralogist, published by the Mineralogical Society of America.
The published version is subject to change. Cite as Authors (Year) Title. American Mineralogist, in press.
DOI: https://doi.org/10.2138/am-2021-7632. http://www.minsocam.org/

828 [$(Fe^{2+}_{0.76}Mg_{0.25})(Al_{1.90}Fe^{3+}_{0.04}Cr^{3+}_{0.03}Ti_{0.02})O_4$] occurs with Ti-rich magnetite (McKay et
829 al. 1988). Thus, meteoritic hercynite is commonly found in association with a second, Al-poor
830 oxide spinel.

831 **Ulvöspinel ($Fe^{2+}_2Ti^{4+}O_4$):** Mikouchi et al. (1996) described *DA ulvöspinel* from the Asuka
832 881371 angrite, with reported average composition close to ($Fe^{2+}_{2.2}Al_{0.1}Ti_{0.8}O_4$). It co-occurs
833 with Cr-rich hercynite [$(Fe^{2+}_{0.80}Mg_{0.32})(Al_{1.35}Cr_{0.50}Ti_{0.03})O_4$]
834
835 **Other Oxides**

836 **Ilmenite ($FeTiO_3$):** *DA ilmenite* was reported by Mittlefehldt and Lindstrom (1993) from a
837 lithic clast in a diogenite. Ilmenite is a common accessory mineral in eucrites, where it occurs as
838 individual grains, as composite grains with chromite, and as an exsolved phase in chromite
839 grains (Bunch and Keil 1971; Delaney et al. 1984), as well as in a variety of iron meteorites
840 (Prinz et al. 1982; Ruzicka 2014).

841 **Corundum (Al_2O_3):** *DA corundum* was reported by Prinz et al. (1994) from the ureilite LEW
842 88774 as micrometer-scale grains with chromite and Cr-rich pyroxene.

843 **Eskolaite (Cr_2O_3):** *DA eskolaite* occurs in the LEW 88774 Cr-rich, anomalous ureilite in
844 association with a reduced assemblage with carbides, chromite, brezinaite, and graphite (Prinz et
845 al. 1994; Warren and Kallemeyn 1994).

846 **Rutile (TiO_2):** *DA rutile* is a minor phase in silicate inclusions in the Sombrerete (IAB) iron
847 meteorite, in which it is associated with albitic glass (the dominant phase), orthoenstatite,

This is the peer-reviewed, final accepted version for American Mineralogist, published by the Mineralogical Society of America.
The published version is subject to change. Cite as Authors (Year) Title. American Mineralogist, in press.
DOI: https://doi.org/10.2138/am-2021-7632. http://www.minsocam.org/

anorthite, chlorapatitie, and minor kaersutite, tridymite, and oxides (Prinz et al. 1982). Rutile was also reported in some mesosiderites (El Goresy 1971).

Baddeleyite (ZrO_2): *DA baddeleyite* occurs in the Angra dos Reis angrite as a minor mineral in association with major fassaite, forsterite, hercynite, and troilite, as well as an unusual suite of accessory phases including kirschsteinite, Ti-rich magnetite, and celsian (Prinz et al. 1977). It is also found in eucrites (Haba et al. 2014).

Perovskite ($CaTiO_3$): Rosenshein et al. (2006) reported a single occurrence of *DA perovskite* of composition $[(Ca_{0.94}Mg_{0.05}Fe_{0.02})Ti_{0.99}O_3]$ in an unusual oxide clast in the Allan Hills 84008 aubrite. Perovskite occurs in association with geikeilite as inclusions in troilite.

Geikeilite ($MgTiO_3$): One occurrence of *DA geikeilite* close to endmember composition was described by Rosenshein et al. (2006) from an unusual oxide clast in the Allan Hills 84008 aubrite.

Armalcolite [$(Mg,Fe^{2+})Ti_2O_5$]: *DA armalcolite* is a rare phase in the silicate inclusions of iron meteorites (Ruzicka 2014). It has been reported from several IIE iron meteorites, including Elga, Colomera, and Miles (Prinz et al. 1983a; Ebihara et al. 1997; Rubin and Ma 2020).

SILICATES

Forsteritic olivine, low- and high-Ca pyroxenes, and calcic plagioclase are major minerals in a wide range of achondrite, stony-iron, and silicate-bearing iron meteorites (Bunch et al. 1970; McCoy et al. 1993; Benedix et al. 1998, 2000; Mittlefehldt et al. 1998; Rubin and Ma 2020). These and other silicates in supposedly non-chondritic meteorites underscore the difficulty of distinguishing minerals formed through asteroidal differentiation, as opposed to earlier and later

events. For example, silicate inclusions in the Netschaëvo (IIE) iron meteorite appear to be relatively unaltered chondritic clasts, while those in Techado (IIE) are partially melted but undifferentiated. On the other hand, many non-chondritic meteorites display evidence for extensive impact alteration through brecciation and shock melting – processes that postdate asteroidal differentiation. In some instances, meteorites may represent a mixture of impact-induced metal melts surrounding fragmented and only partially melted silicates. Here we include all known phases from non-chondritic meteorites that appear to have formed by crystallization from a melt or vapor, or by subsequent solid-state reactions during cooling/annealing – i.e., minerals that were not formed directly by shock processes, aqueous alteration, or thermal metamorphism.

Silica Group (SiO_2): Silica group minerals, including tridymite and less frequently cristobalite, quartz, and silica glass, are minor/trace phases in mafic lithologies.

Tridymite (SiO_2): *DA tridymite* is the most common silica polymorph in meteorites. It has been reported from a variety of iron meteorites (Buchwald 1975; Prinz et al. 1982; Scott et al. 1996), notably from the Gibeon and Steinbach (IVA) irons (Reid et al. 1974). The former contains a tridymite grain exceeding 2 centimeters maximum dimension (Marvin et al. 1997). Tridymite is also a common phase in mafic meteorite lithologies: it accounts for 5 to 14 vol % in mesosiderite basaltic clasts (Nehru et al. 1980) and up to 8 vol % in basaltic eucrites (Delany et al. 1984; Ikeda and Takeda 1985; Mittlefehldt et al. 1998).

Cristobalite (SiO_2): *DA cristobalite* is a minor phase in several eucrites, where it occurs in association with other silica polymorphs (Aoudjehane and Jambon 2007), and as an accessory mineral in the troilite nodules of the Carbo (IID) iron meteorite (Marvin 1962). Ma et al. (2012a)

record cristobalite as a rare accessory phase in the Zakłodzie ungrouped enstatite achondrite, where it co-occurs with more abundant tridymite and quartz.

Quartz (SiO_2): *DA quartz* has been reported as a minor phase in basaltic eucrites (Mittlefehldt et al. 1998). Marvin et al. (1997) described quartz-rich regions 3 to 4 millimeters in diameter occurring in the cracked core of a large (> 2 centimeters maximum dimension) tridymite grain from the Gibeon (IVA) iron meteorite. Quartz also occurs with tridymite, rare cristobalite, and sinoite in the Zakłodzie ungrouped enstatite achondrite (Ma et al. 2012a).

Silica glass (SiO_2): Ruzicka (2014) summarizes silica-rich glass compositions, which are common in some silicate inclusions of iron meteorites. Of note are occurrences of *DA silica glass* with compositions exceeding 80 wt % SiO_2 in inclusions from Weekeroo Station and Miles (IIE) irons, in contrast to many glasses of more feldspathic compositions (see below).

Olivine Group [$(Mg,Fe,Ca)_2SiO_4$]: Olivine is a major mineral in many types of non-chondritic meteorites (Mittlefehldt et al. 1998: Tables 7, 11, 13, 20, 24, 28, 31, 36, 43, and Figures 17 and 58). Note that while forsterite and fayalite form a continuous solid solution, the great majority of non-chondritic olivine occurrences fall in the range Fo_{55-99}. An exception is the occurrence of more fayalitic olivine in some angrites (Fo_{32-86}; Mittlefehldt et al. 1998, Table 36); however, Prinz et al. (1990) and Mikouchi et al. (1996) reported that larger olivine grains are strongly zoned with magnesian cores (Fo_{73-90}) compared to more ferroan rims. Otherwise, the few outlier occurrences of fayalite are near endmember Fe_2SiO_4. For example, Yanai (1994, Figure 8) summarized a bimodal distribution of olivine compositions in angrites, with most analyses in the range Fo_{45-90}, but a few analyses clustered at Fo_{1-9}. Therefore, we recognize *DA forsterite* and *DA fayalite* as distinct natural kinds.

Forsterite (Mg_2SiO_4): *DA forsterite* is a major silicate phase in many non-chondritic meteorites. The most olivine-rich meteorites are brachinites with as much as 98 vol % olivine with average 30 to 35 mol % fayalitic component (Kring et al. 1991; Nehru et al. 1992). Ureilites are ultramafic cumulates with up to >90 vol. % olivine, typically with ~5 to 25 mol % Fe_2SiO_4 (Mittlefehldt et al. 1998, and references therein). Up to ~10 vol % of nearly pure endmember forsterite (typically $Fo_{99.99}$) is a common phase in highly reduced enstatite achondrites (aubrites), in which orthoenstatite is the dominant silicate phase (Watters and Prinz 1979).

Forsterite also occurs in pallasites with crystals of forsteritic olivine to > 1-centimeter diameter that are typically close to Fo_{90} associated with Fe-Ni alloys (Buseck and Goldstein 1969; Buseck 1977; Ulff-Møller et al. 1998; Figure 1B). In some instances, pallasite olivine incorporates P-rich zones, locally with up to 5 wt. % P_2O_5 (Buseck 1977).

Fayalite (Fe_2SiO_4): Olivine close to fayalite in composition occurs rarely in non-chondritic meteorites. Ikeda and Takeda (1985) describe *DA fayalite* (Fo_{10-14}) associated with augite ($\sim Wo_{40}Fs_{40}$), tridymite, and plagioclase ($An_{\sim 80}$) in unusual ferroan igneous clasts in howardites. Yanai (1994, Figure 8) reported olivine compositions in angrites, with most analyses in the range Fo_{45-90}, but a few analyses clustered at Fo_{1-9}. Olivine in angrites are often Ca-rich, with up to 20 mol % of the Ca end member in the most Fe-rich examples (Mittlefehldt et al. 2002). Fayalite was also reported by Srinivasan et al. (2018) as a minor phase in the unique silica-rich achondrite NWA 11119, which features millimeter-diameter vesicles comprising > 1 vol % and 30 vol %

tridymite associated with an unusual mineralogical suite, including tranquillityite, zircon, and tsangpoite.

Kirschsteinite ($CaFe^{2+}SiO_4$): The calcic olivine *DA kirschsteinite* with average composition $[(Ca_{0.94}Fe^{2+}_{0.06})(Fe^{2+}_{0.60}Mg_{0.40})SiO_4]$ is an accessory phase in the Angra dos Reis and other angrite achondrites, where it occurs as inclusions in low-Ca olivine in association with fassaite, hercynite, Ti-rich magnetite, and troilite (Prinz et al. 1977; McKay et al. 1988, 1990). In LEW 86010, kirschsteinite occurs as exsolution lamellae in Mg-Fe olivine (Mikouchi et al., 1995), while in D'Orbigny, it is observed as overgrowths on Mg-Fe olivine (Mittlefehldt et al., 2002).

Pyroxene Group $[(Ca,Mg,Fe,Ti,Al)_2(Al,Si)_2O_6]$: Pyroxene group minerals are principal constituents of most types of achondrite and stony-iron meteorites (Mittlefehldt et al. 1998: Tables 7, 11, 15, 20, 25, 28, 30, 37, 42, and Figure 42). The nomenclature of meteoritic pyroxene group minerals is potentially confusing and replete with archaic and discredited terminology, owing to both chemical and structural complexities (Morimoto et al. 1988; Deer et al. 1997; Wenk and Bulakh 2003). Most meteoritic examples fall close to the familiar Mg-Fe-Ca pyroxene quadrilateral, bounded by endmembers enstatite (En; $Mg_2Si_2O_6$), ferrosilite (Fs: $Fe_2Si_2O_6$), diopside (Di: $CaMgSi_2O_6$), and hedenbergite (Hd: $CaFeSi_2O_6$). Pyroxene compositions are also commonly reported in terms of the mol % of their pure calcium component, wollastonite (Wo: $Ca_2Si_2O_6$). Four different pyroxene phase regions occur for Mg-Fe-Ca compositions near liquidus temperatures (e.g., Deer et al. 1997). Above ~1200 ºC, a miscibility gap separates (1) Ca-rich augites (all compositions with $>Wo_{\sim 30}$) and (2) Ca-poorer pigeonites ($<Wo_{\sim 15}$), both of which are monoclinic (space group *C*2/*c*). A second gap occurs between pigeonites ($Wo_{>10}$) and

957 compositions close to the $MgSiO_3$-$FeSiO_3$ join ($Wo_{<05}$), for which the high-temperature
958 pyroxene phases are (3) protoenstatite (orthorhombic space group *Pbcn*) near the Mg-rich
959 endmember; and (4) orthopyroxene (orthorhombic space group *Pbca*) for more ferroan
960 compositions.

961 Upon cooling, these four high-temperature pyroxene phases may undergo several types of
962 solid-state transformations of significance to meteorite mineralogy – inversions that depend
963 strongly on the thermal history of individual crystals. Some transitions are isochemical. For
964 example, protoenstatite transforms to orthoenstatite below ~1000 ºC and, given sufficient
965 annealing time, may further transform to clinoenstatite (monoclinic $P2_1/c$) below ~600 ºC. High-
966 temperature $C2/c$ pigeonite similarly transforms to the low-temperature $P2_1/c$ form on cooling.
967 Evidence for these isochemical transformations may be preserved in distinctive twinning (e.g.,
968 Takeda et al. 1989).

969 More commonly, shifting boundaries of miscibility gaps on cooling lead to exsolution of one
970 pyroxene composition from another. Most significantly, the augite-pigeonite miscibility gap
971 becomes wider with cooling below ~1200 ºC, with coexisting equilibrium compositions
972 approaching Wo_{05} and Wo_{45} below 1000 ºC for some Mg-Fe compositions. Consequently,
973 depending on cooling rates and annealing times, pigeonite with $Wo_{>05}$ may exsolve one or more
974 generations of augite, while augite with $Wo_{<45}$ may exsolve pigeonite (Harlow et al. 1979; Mori
975 and Takeda 1981a). Indeed, owing to multiple stages of exsolution, it is not uncommon for four
976 different compositions of pyroxene to coexist in a single igneous rock (Deer et al. 1997).

This is the peer-reviewed, final accepted version for American Mineralogist, published by the Mineralogical Society of America.
The published version is subject to change. Cite as Authors (Year) Title. American Mineralogist, in press.
DOI: https://doi.org/10.2138/am-2021-7632. http://www.minsocam.org/

977 This profligacy of potential compositional and morphological natural kinds of pyroxene
978 creates challenges. We choose to simplify pyroxene nomenclature, lumping as much as possible
979 pyroxenes that share their structure types within a continuous compositional field. Consequently,
980 three natural kinds encompass the vast majority of pyroxenes in non-chondritic meteorites.

981 1. *DA orthoenstatite*: Orthopyroxenes occur close to the En-Fs join with < 5 mol % Wo. The
982 official endmember names for this series are enstatite and orthoferrosilite. Almost all
983 meteoritic examples, with the exception of orthopyroxenes with augite exsolution in some
984 eucrites (En_{35-75}), are Mg-dominant. Therefore, we designate these occurrences as *DA*
985 *orthoenstatite*; we employ "orthoenstatite" instead of the IMA-approved name "enstatite"
986 (Morimoto et al. 1988) to reduce ambiguity.
987 2. *DA pigeonite*: Low-calcium clinopyroxenes (monoclinic space group $P2_1/c$) encompass a
988 range of Mg-Fe-Ca compositions, almost always with Mg > Fe in non-chondritic
989 meteorites. The clinoenstatite-clinoferrosilite series is defined as having less than 5 mol %
990 of the Wo component. However, these pyroxenes form a continuous solid solution with
991 the somewhat more calcic pyroxenes (Wo_{5-15}) designated "pigeonite" by IMA
992 conventions. Here we lump all low-Ca clinopyroxenes into *DA pigeonite*.
993 3. *DA augite*: A similar somewhat arbitrary division is applied by IMA to Ca-rich pyroxenes,
994 all of which are $C2/c$ monoclinic phases within a single-phase region. Therefore, we lump
995 examples with Wo_{45-50} close to the diopside-hedenbergite join together with somewhat
996 less calcic clinopyroxenes (Wo_{30-45}), defined by IMA conventions as augite, into *DA*
997 *augite*.

In addition to these common phases, we recognize three additional natural kinds of non-chondritic meteoritic pyroxene.

4. Near endmember hedenbergite from the Asuka 881371 angrite represents a clear outlier (Yanai 1994, Figure 8), which we name *DA hedenbergite*.
5. The Na-Cr clinopyroxene *DA kosmochlor* ($NaCr^{3+}Si_2O_6$; formerly ureyite) occurs in some iron meteorites.
6. Finally, calcic clinopyroxene nomenclature is further complicated by the occurrence of "fassaite," a Ca-Mg-dominant, Fe-poor clinopyroxene with Al and Ti, which result in compositions that lie significantly outside the pyroxene quadrilateral. Fassaite is closest compositionally to the IMA-approved species diopside ($CaMgSi_2O_6$), but it always incorporates significant fractions of other components, including kushiroite ($CaAl_2SiO_6$; also known as calcium-Tschermak's pyroxene), grossmanite ($CaTi^{3+}AlSiO_6$), and/or a hypothetical Ti^{4+} endmember ($CaMg_{0.5}Ti^{4+}_{0.5}AlSiO_6$). Sack and Ghiorso (2017) demonstrate that these compositions are separated by as many as three miscibility gaps from diopside; therefore, *DA fassaite*, though not officially recognized by the IMA, represents at least one additional pyroxene natural kind.

Orthoenstatite ($MgSiO_3$): *DA orthoenstatite* is a major primary igneous phase in several types of achondrites, with crystals sometimes exceeding 5 centimeters in maximum dimension (Mittlefehldt et al. 1998, and references therein). Orthoenstatite also forms through the inversion of pigeonite, which commonly leads to exsolution of augite lamellae (Deer et al. 1997). Diogenites incorporate from ~85 to 100 vol % orthoenstatite, typically with compositions close

This is the peer-reviewed, final accepted version for American Mineralogist, published by the Mineralogical Society of America.
The published version is subject to change. Cite as Authors (Year) Title. American Mineralogist, in press.
DOI: https://doi.org/10.2138/am-2021-7632. http://www.minsocam.org/

to En_{75}. (Mittlefehldt et al. 1998, Figure 42 and Table 30). Near endmember orthoenstatite ($En_{>98}$) is the dominant mineral in the unusual unbrecciated Shallowater enstatite achondrite, which has ~80 vol % orthoenstatite in crystals to 4.5-centimeters maximum dimension (Reid and Cohen 1967). This example contrasts with most aubrites, which have disordered enstatite, largely the result of impact alteration (Watters and Prinz 1979). Orthoenstatite also occurs in pallasites (Hiroi et al. 1993), in ureilites (Takeda 1987; Takeda et al. 1989), and in HED meteorites (Delany et al. 1984; Mittlefehldt 1994; Bowman et al. 1997).

Pigeonite [$(Mg,Fe,Ca)SiO_3$]: *DA pigeonite*, including both pigeonite and samples close to endmember clinoenstatite with < 5 mol % Wo, are significant minerals in many achondritic meteorites (Mittlefehldt et al. 1998). DA pigeonite is the dominant, and in some instances the only, pyroxene in ureilites, which are ultramafic restite achondrites (Takeda 1989; Takeda et al. 1992). In brachinites, which are olivine cumulate rocks, pigeonite is second in abundance to forsterite, constituting up to 15 modal percent (Kring et al. 1991; Nehru et al. 1992).

Augite [$(Ca,Mg,Fe)Si_2O_6$]: *DA augite*, including samples close to endmember diopside, occur as the principal calcium-bearing phase in several types of plagioclase-free ultramafic achondrites. Augite is found with pigeonite and/or orthopyroxene in some ureilites (Takeda 1989; Takeda et al. 1992). Unusually ferroan augite (~$Wo_{40}Fs_{40}$) occurs in igneous clasts of howardites, associated with fayalite, tridymite, and plagioclase (Ikeda and Takeda 1985). Essentially iron-free diopsidic augite occurs in enstatite achondrites (aubrites) as a common minor phase, accounting for up to ~8 vol % of some examples (Olsen et al. 1977b; Watters and Prinz 1979). In many meteorites, for example diogenites (Bowman et al. 1997), pigeonite has inverted to orthoenstatite that has exsolution lamellae of a range of calcic clinopyroxenes,

This is the peer-reviewed, final accepted version for American Mineralogist, published by the Mineralogical Society of America.
The published version is subject to change. Cite as Authors (Year) Title. American Mineralogist, in press.
DOI: https://doi.org/10.2138/am-2021-7632. http://www.minsocam.org/

1041 including diopsidic ($Di_{>90}$) and augitic ($Wo_{<45}Fs_{<25}$) examples (Mori and Takeda 1981b;
1042 Takeda and Mori 1985; Mittlefehldt and Lindstrom 1993).

1043 **Hedenbergite ($CaFeSi_2O_6$):** Near endmember *DA hedenbergite* of composition
1044 $[(Ca_{0.99}Mg_{0.01}Fe_{1.00})Si_2O_6]$, as well as other compositions on the Di-Hd join, occur in the
1045 Asuka 881371 angrite (Yanai 1994, Table 1), and in the D'Orbigny angrite (Hwang et al. 2019).

1046 **Fassaite [$Ca(Mg,Al,Ti^{3+},Ti^{4+})(Al,Si)SiO_6$]:** The Al- and/or Ti-rich calcic pyroxene, *DA*
1047 *fassaite*, is the major phase (93 vol %) in the unusual Angra dos Reis angrite (Prinz et al. 1977).
1048 With average composition $[(Ca_{0.97}Mg_{0.59}Fe^{2+}_{0.21}Al_{0.16}Ti_{0.06})(Al_{0.28}Si_{1.72})O_6]$, this
1049 clinopyroxene incorporates ~16 mol % Ca-Tschermak's and 21 mol % hedenbergite
1050 components, but only 6 mol % of the grossmanite component, in contrast to the more Ti-rich, Fe-
1051 poor fassaite in CAIs (Morrison and Hazen 2020). Fassaite occurs both as a groundmass of
1052 grains up to 0.5 millimeters maximum dimension and as larger grains to ~3 millimeters
1053 enclosing the groundmass. It occurs in association with olivine, hercynite, and troilite, as well as
1054 an unusual suite of accessory phases including kirschsteinite, celsian, Ti-rich magnetite, and
1055 baddeleyite. Fassaite is also present in other angrites (McKay et al. 1988, 1990; Prinz et al. 1988,
1056 1990), as well as in angrite-like clasts in polymict ureilites (Prinz et al. 1983b, 1986).

1057 **Kosmochlor ($NaCr^{3+}Si_2O_6$):** The Na-Cr clinopyroxene *DA kosmochlor* (formerly named
1058 ureyite; Morimoto et al. 1988) occurs in some iron meteorites, typically in association with
1059 graphite and chromite (Frondel and Klein 1965; Olsen and Fuchs 1968).
1060
1061 **Amphibole Group:** Amphiboles, a major group of rock-forming double-chain silicates, make
1062 their earliest appearances as minor accessory phases in silicate inclusions in iron meteorites and

in an aubrite. Two IMA-approved amphibole species, fluoro-richterite and kaersutite, have similar compositions and may represent endmembers of a continuous solid solution. However, they occur in different contexts and only fluoro-richterite has measurable F. Therefore, we consider *DA fluoro-richterite* and *DA kaersutite* to be distinct natural kinds.

Fluoro-richterite [$Na(NaCa)Mg_5Si_8O_{22}F_2$]: *DA fluoro-richterite* was reported from the Canyon Diablo and Wichita County (IAB) iron meteorites (Olsen 1967; Olsen et al. 1973). In addition, Bevan et al. (1977) reported anhydrous fluoro-richterite in needle-like crystals to ~1-millimeter maximum dimension from the Mayo Belwa aubrite, which contains 5 vol % crystal-lined vugs. Rubin (2010) suggested that fluoro-richterite may be an impact-related phase, formed when F-rich gas condensed in shock-induced vugs.

Kaersutite [$NaCa_2(Mg_3AlTi^{4+})(Si_6Al_2)O_{22}O_2$]: A single occurrence of *DA kaersutite* has been reported from silicate inclusions in the Sombrerete (IAB) iron meteorite (Prinz et al. 1982). DA kaersutite is associated with albitic glass (the dominant phase), orthoenstatite, anorthite, and chlorapatitie.

Feldspar Group [$(Ca,Na,K)Al(Al,Si)Si_2O_8$]: Calcic plagioclase is an abundant primary igneous phase in many types of non-chondritic meteorites (Mittlefehldt et al. 1998: Table 7, 11, 18, 20, 28, 33, 39, and 44). Albite, sanidine, and celsian, by contrast, are extremely minor phases, typically associated with residual silica-rich melts. In spite of the continuous solid solution of the plagioclase series, we draw a distinction between *DA anorthite*, which is typically An_{99-75} and, with the exception of brachinites, rarely displays compositions with $An_{<60}$, and *DA albite*, which is invariably close to the $NaAlSi_3O_8$ endmember ($An_{<10}$).

Anorthite ($CaAl_2Si_2O_8$): *DA anorthite* is an important component of many non-chondritic meteorites (Mittlefehldt et al. 1998, and references therein). It occurs in silicate inclusions in iron meteorites (An_{57-93}; Bunch and Olsen 1968; Bunch et al. 1970; Olsen et al. 1994); in aubrites (An_{75-95}; Watters and Prinz 1979); in HED group achondrites (An_{72-95}; Mittlefehldt et al. 1998, Table 33); in angrites ($An_{\sim 99}$; Prinz et al. 1977; Crozaz and McKay 1990; Mikouchi et al. 1996); in basaltic ($An_{>70}$) and cumulate eucrites (An_{91-98}; Mittlefehldt et al. 1998, Table 33), and in mesosiderites (An_{91-93}; Mittlefehldt et al. 1998).

Albite ($NaAl_3SiO_8$): Near endmember *DA albite* is a common, if minor, phase in non-chondritic meteorites. Albite occurs frequently in silica-rich clasts in numerous iron meteorites (Bunch and Olsen 1968; Wasserberg et al. 1968; Prinz et al. 1983a; Ruzicka 2014). For example, McCoy et al. (1994) report albite of composition ($Ab_{91}An_5Or_4$) from chlorapatite-dominant silicate inclusions in the Carlton (IIICD) iron meteorite.

Brachinites, which are dunites with up to 98 vol % forsterite, are an outlier with plagioclase compositions observed between An_{16} and An_{37} (Nehru et al. 1983, 1996; Mittlefehldt et al. 1998, Table 18), whereas aubrites typically contain minor albitic plagioclase (Rubin and Ma 2020).

Sanidine ($KAlSi_3O_8$): Potassic feldspars are rare phases in non-chondritic meteorites. Wasserburg et al. (1968) reported a sanidine crystal 11 centimeters in length from a silicate inclusion in the Colomera (IIE) iron meteorite, where it occurs in association with plagioclase-silica glass, clinoenstatite, and several minor phases. K feldspar is found in the Ni-rich San

Cristobal (unique IAB) iron meteorite (Wlotzka and Jarosewich 1977), and as exsolution lamellae in "antiperthite" with an albitic host from the Watson (IIE) iron meteorite (Olsen et al. 1994). Potassic feldspar also occurs in the Bilanga diogenite (Domanik et al. 2004) and in some eucrites (Barrat et al. 2007).

Celsian ($BaAl_2Si_2O_8$): *DA celsian* $[(Ba_{0.90}Ca_{0.08}Na_{0.02})(Al_{1.98}Si_{2.02})O_8]$ occurs in the Angra dos Reis angrite as a minor mineral in association with dominant fassaite, plus forsterite, hercynite, and troilite, as well as an unusual suite of accessory phases including kirschsteinite, Ti-rich magnetite, and baddeleyite (Prinz et al. 1977). Prinz et al. (1977) also describe minor co-existing anorthite from Angra dos Reis. This earliest known occurrence of a barium mineral may be the result of crystallization of a late-stage residual melt enriched in alkaline earth elements.

Feldspathic glass [Na-(K-Ca)-Al-Si]: *DA feldspathic glass*, in contrast to shock-induced maskelynite (see Part IVB below), occurs as a significant phase in a variety of silicate-rich inclusions that represent late-stage melt fractions (Ruzicka 2014). Sodium-dominant albitic glass is the major phase in silicate inclusions in the Sombrerete (IAB) iron meteorite, in which it is associated with enstatite, anorthite, chlorapatitie, and minor kaersutite, tridymite, and oxides (Prinz et al. 1982). Wasserburg et al. (1968) reported albitic glass from the Colomera (IIE) silicate-bearing iron meteorite, where it occurs in association with clinoenstatite, forsterite, and other phases. Na-K-Al-Si glass is reported from interstitial silicate assemblages in ureilites with clinoenstatite and augite (Goodrich 1986), while feldspathic glass with a significant anorthite content (An_{5-50}) occurs in lithic clasts from polymict ureilites (Prinz et al. 1986). Some brachinites contain Na-rich feldspathic glass (Nehru et al. 1983). Finally, feldspathic glass is a volumetrically minor component of some enstatite achondrites: Fuchs (1974) reported Na-K-Al-Si glass as ~5-micrometer-diameter trapped melt inclusions in orthoenstatite in the Bishopville,

Norton County, and Pena Blanca Springs aubrites, while Fogel (2005) described basaltic vitrophyre clasts in the Khor Temiki and LEW 87007 aubrite with 51 and 13 vol % albitic glass in the inclusions, respectively.

Other Silicates

Zircon ($ZrSiO_4$): *DA zircon* is a rare phase in non-chondritic meteorites, reported in basaltic eucrites (Gomes and Keil 1980) and the unique andesitic (30 vol % tridymite) achondrite NWA 11119 (Srinivasan et al. 2018). Ireland and Wlotzka (1992) analyzed two zircon grains from the Vaca Muerta mesosiderite, from which they obtained a $^{207}Pb/^{206}Pb$ age of 4.563 +/- 0.015 Ga.

Tranquillityite [$Fe^{2+}_8Ti_3Zr_2Si_3O_{24}$]: *DA tranquillityite* was identified by Srinivasan et al. (2018) as a minor phase in the unique NWA 11119 silica-rich achondrite – a silica-rich extrusive rock with numerous millimeter-diameter vesicles (comprising > 1 vol %) surrounded by quenched melt and 30 vol % tridymite associated with an unusual mineralogical suite, including zircon, fayalite, and tsangpoite.

Yagiite [$NaMg_2(AlMg_2Si_{12})O_{30}$]: *DA yagiite* is member of the milarite group, originally described by Bunch and Fuchs (1969b) from silicate inclusions in the Colomera (IIE) iron meteorite. With average composition $[Na_{1.20}K_{0.30})(Mg_{2.60}Fe_{0.34}Ti_{0.10}Al_{1.96})(Si_{10.22}Al_{1.78})O_{30}]$, yagiite occurs as inclusions in fassaite and in association with whitlockite, tridymite, and albite. It has subsequently been identified in a similar inclusion in the Sombrerete (IAB) iron meteorite (Ruzicka 2014).

Kuratite [$Ca_2(Fe^{2+}_5Ti)O_2[Si_4Al_2O_{18}]$: *DA kuratite* is a rare Fe^{2+} analog of rhönite that was characterized by Hwang et al. (2016) from the D'Orbigny angrite, where it occurs as euhedral to

anhedral crystals up to ~20 micrometers maximum dimension in close association with hedenbergite, ulvöspinel, fayalite, kirschsteinite, and iron sulfide. Hwang et al. (2016) suggested that this assemblage represents rapid cooling of an interstitial melt from > 1000 ºC.

Krinovite [$Na_4(Mg_8Cr^{3+}_4)O_4(Si_{12}O_{36})$]: Olsen and Fuchs (1968) described *DA krinovite*, a Cr-Mg isomorph of aenigmatite, from mineralogically unusual graphite-silicate inclusions in the Canyon Diablo, Wichita County, and Youndegin (IAB) iron meteorites. Subhedral grains up to 200 micrometers in diameter occur in association with graphite, albite, richterite, and roedderite.

Roedderite [$(Na,K)_2Mg_5Si_{12}O_{30}$]: *DA roedderite* was reported by Olsen and Fuchs (1968) from the Canyon Diablo and Wichita County (IAB) iron meteorites, where it occurs in graphite-silicate inclusions. Roedderite was also found in the Bustee aubrite by Hsu (1998) as an irregular ~500- x 200-micrometer grain associated with olivine and enstatite, as well as in the Khor Temiki and Pena Blanca Springs aubrites (Fogel 2001).

ORGANIC SOLIDS

Kerogen (C-H-O-N): Condensed organic material, here termed *DA kerogen*, is an important carbon-bearing phase in many ureilites (Vdovykin 1970). It occurs along silicate grain boundaries, as well as in grain fractures and cleavage planes.

This is the peer-reviewed, final accepted version for American Mineralogist, published by the Mineralogical Society of America.
The published version is subject to change. Cite as Authors (Year) Title. American Mineralogist, in press.
DOI: https://doi.org/10.2138/am-2021-7632. http://www.minsocam.org/

PART IVB: IMPACT MINERALIZATION OF ASTEROIDAL BODIES AND THEIR CONSTITUENTS

Among the earliest mineralizing processes in the solar nebula, commencing contemporaneously with asteroid formation at ~4.565 Ga and continuing throughout the history of the solar system, was shock alteration of preexisting phases (Buchwald 1975, 1977; Stöffler et al. 1988, 1991, 2018; Bischoff and Stöffler 1992; Scott et al. 1992; Rubin et al. 1997; Sharp and DeCarli 2006; Stöffler and Grieve 2007; Koeberl 2014; Rubin 2015a; Breen et al. 2016; Fritz et al. 2017; Tomioka and Miyahara 2017; Tschauner 2019). High-velocity collisions, as well as bow shocks in the early nebular environment, produced significant transient high-temperature and pressure events that transformed materials through shattering (Bunch and Rajan 1988), impact melting (Dodd and Jarosewich 1979, 1982; Rubin 1985; Fagan et al. 2000; Lunning et al. 2016), vaporization (El Goresy et al. 1997), and a range of solid-state alterations (Ashworth 1980, 1985; Madon and Poirier 1980, 1983; Price 1983; Rubin 2006). Large-scale impacts also initiated more gradual asteroidal heating and fluidization that are manifest in asteroid metamorphism (Rubin and Ma 2020) – effects revealed by a significant correlation in meteorites between the extent of thermal metamorphism (to be reviewed in Part V) and the degree of shock alteration.

Here we focus on rapid, shock-related changes that produced new kinds of minerals in meteorites. Shock events recorded in meteorites represent transient temperatures and pressures that can exceed 3,000 ºC and 100 GPa (Figure 3), with peak conditions lasting perhaps a few seconds (Ohtani et al. 2004; Xie et al. 2006; Tomioka and Miyahara 2017; Stöffler et al 2018, Tables 4 through 11). Under such extreme conditions, minerals transform in a variety of ways. Accordingly, Stöffler and colleagues have proposed a unified scale of shock metamorphism, with increasing stages of impact effects grading from S1 (for unshocked examples) to S7 (for whole-

rock melting and/or vaporization). They enumerated separate mineralogical and textural criteria to codify shock stages for each major parent lithology (which can be applied equally to meteorites and to planetary impact structures): felsic (F), mafic (M), anorthositic (A), ultramafic (U), chondritic rocks (C), sedimentary rocks (SR), unconsolidated sediments (SE), and regolith (RE). Note that shock effects in iron meteorites were not considered by Stöffler et al. (2018); however, see previous work (Buchwald 1975, 1977; Bennett and McSween 1996; Tomkins 2009; Breen et al. 2016).

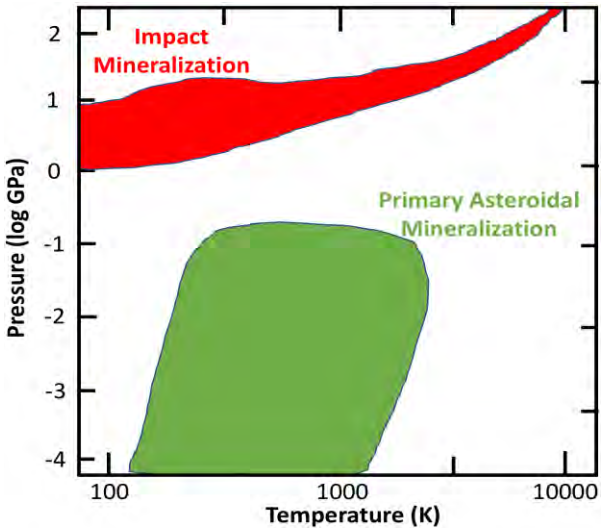

Figure 3. The ranges of pressure-temperature conditions for primary asteroidal mineralization (green) and impact mineralization (red) suggest that these processes represent distinct stages of mineral evolution.

A range of effects, from undulose extinction with crossed polarizers in transmitted light and irregular fracturing at low degrees of shock, to mosaic extinction and planar fracturing at intermediate shock, to melting and/or transformation to new denser phases at the highest shock states, are observed in meteorites. Phases generated from impact melting and subsequent igneous processes are often difficult to distinguish from minerals formed in molten differentiating asteroidal bodies; minerals that are thought to have crystallized at low pressure (< 0.1 GPa) were considered in Part IVA above, for example in discussions of nonmagmatic achondrites.

Likewise, minerals formed through condensation of impact-generated vapor are often similar to nebular condensates and are reviewed in previous sections of this evolutionary system. Here we focus exclusively on new high-pressure (> 0.1 GPa) meteorite phases that arose from short-lived impact events, either through solid-state transformation or crystallization from a shock-induced melt.

SYSTEMATIC IMPACT ALTERATION MINERALOGY

Minerals formed through shock processes and preserved in meteorites have been reviewed in the context of high-pressure mineralogy and/or meteorite mineralogy by several authors (Scott et al. 1992; Rubin et al. 1997; Mittlefehldt et al. 1998; Rubin and Ma 2017, 2020; Tomioka and Miyahara 2017; Ma 2018; Stöffler et al. 2018; Tshauner 2019). Here we list 40 kinds of dense, micrometer-scale phases (Table 2) that are thought to have formed rapidly as a byproduct of high-energy collisions between objects ranging in size from meters to hundreds of kilometers in diameter.

These impact minerals incorporate 14 different essential elements (Figure 4), all of which are among the major essential elements in primary asteroidal and planetesimal minerals from which they formed (compare with Figure 2).

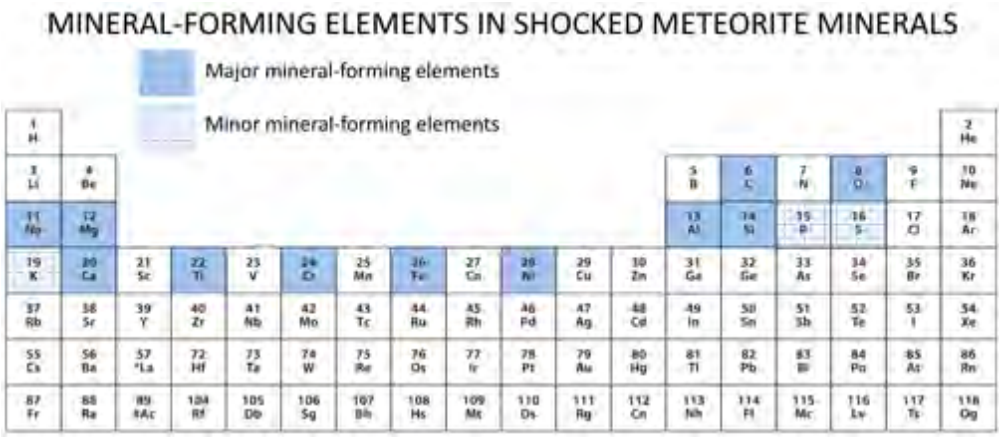

This is the peer-reviewed, final accepted version for American Mineralogist, published by the Mineralogical Society of America.
The published version is subject to change. Cite as Authors (Year) Title. American Mineralogist, in press.
DOI: https://doi.org/10.2138/am-2021-7632. http://www.minsocam.org/

Figure 4. Essential mineral-forming elements in 40 shocked meteorite minerals. All of these 14 elements are major mineral-forming elements in primary asteroidal minerals (compare with Figure 2).

We focus on irreversible high-pressure shock effects that likely occurred on asteroids and their precursors in the early solar nebula – events that led to new dense phases or diagnostic altered textures in preexisting minerals. However, unlike the time-restricted processes that formed minerals in CAIs, chondrules, or differentiated planetesimals in the earliest solar nebula, impact processes have continued throughout the 4.5-billion-year history of the solar system. Accordingly, many of the phases listed in Table 2 are only known from examples that are significantly younger than 4560 Ma. Indeed, nine impact phases known thus far exclusively from martian meteorites (i.e., feiite, liebermannite, liuite, seifertite, stoeflerite, tissintite, tschaunerite, zagamiite, and an unnamed silicate) formed much more recently. Nevertheless, these shock minerals formed from precursor phases that were present on differentiated planetesimals and thus all of these impact phases were also likely to have formed during the earliest stages of the solar system.

We distinguish between shock effects preserved in chondritic, non-chondritic, and martian meteorites versus more recent influences of meteor impacts on Earth, including effects of atmospheric passage. Terrestrial impact events have transformed a variety of crustal minerals that are not significant components of asteroids. Thus, high-pressure shock phases found exclusively in terrestrial impact structures, such as reidite ($ZrSiO_4$; Glass et al. 2002), akaogiite (TiO_2; El Goresy et al. 2010), maohokite ($MgFe_2O_4$; Chen et al. 2019), and reisite (TiO_2; Tschauner et al. 2020), will be considered in a later contribution. Note that we also defer to Part V discussion of enigmatic Al-bearing alloys and quasicrystals, for which extreme reduction

1250 associated with shock effects has been invoked as a possible origin (Hollister et al. 2014; Hu et
1251 al. 2019).

1252 Several high-pressure minerals that are thus far known only as impact phases in meteorites
1253 likely occur as major phases in Earth's mantle, as well. A few examples – ringwoodite, majorite,
1254 and amorphous $CaSiO_3$, for example – have been reported from both meteorites and as
1255 inclusions in mantle-derived diamond. However, other presumed mantle phases, including
1256 akimotoite, hemleyite, and bridgmanite (likely the most abundant mineral on Earth in terms of
1257 volume; Tschauner et al. 2014), are to date known only from meteorites.

1258 We employ a binomial nomenclature with IMA species names preceded by "impact," i.e.,
1259 *impact stishovite*. We deviate from IMA conventions in a few instances. We lump members of
1260 five continuous Mg-Fe solid solutions – periclase-wüstite, wadsleyite-asimowite, ringwoodite-
1261 ahrensite, akimotoite-hemleyite, and bridgmanite-hiroseite – into *impact magnesiowüstite*,
1262 *impact wadsleyite*, *impact ringwoodite*, *impact akimotoite*, and *impact bridgmanite*, respectively.
1263 In each of these cases, Mg-dominant examples are much more abundant, Fe-dominant examples
1264 are typically close to intermediate compositions, and all examples formed by the same
1265 mechanism. We include four minerals that have been partially characterized but are not yet
1266 approved by the IMA: *impact martensite* (α_2-Fe,Ni), *impact* $[(Mg,Fe)SiO_3]$, *impact*
1267 $[(Mg,Fe,Si)_2(Si,\square)O_4]$, and *impact* $[(Fe,Mg,Cr,Ti,Ca,\square)_2(Si,Al)O_4]$. We also recognize three
1268 amorphous phases: *impact silica glass*, *impact amorphous* $CaSiO_3$, and *impact maskelynite.*
1269
1270 **NATIVE ELEMENTS**

1271 **Fe-Ni Alloys:** Fe-Ni alloys commonly display significant shock effects (Buseck et al. 1966;
1272 Wood 1967; Begemann and Wlotzka 1969; Smith and Goldstein 1977; Bennett and McSween

1996). Etched samples of the Fe-Ni alloy kamacite often have shock-induced twinning known as Neumann bands (Buchwald 1975). These twins on the {211} planes of α-(Fe,Ni) form easily, perhaps in some cases on atmospheric entry. A range of more intense shock effects are observed in some meteoritic Fe-Ni alloys, including high-pressure transformation to the ε-iron phase, a high-density hexagonal close-packed structure requiring pressures > 13 GPa, but which is not quenchable. Fe-Ni alloys experience extensive impact melting, as well as transformation of impact Fe-Ni melt on cooling to the metastable α_2-Fe-Ni alloy called martensite.

Martensite (α_2-Fe,Ni): *Impact martensite* forms when shock heating of kamacite and taenite homogenizes the Fe-Ni alloy, which then cools rapidly to form the metastable (α_2-Fe,Ni) cubic form. Martensite, typically with 8 to 15 wt. % Ni, is known from a range of chondritic and non-chondritic meteorites (Rubin and Keil 1983; Mittlefehldt et al. 1998; Rubin and Ma 2020). Martensite transforms to plessite, an intimate mixture of stable kamacite and taenite, upon reheating in the $\alpha + \gamma$ iron stability field (Taylor and Heymann 1970; Scott and Rajan 1979).

Carbon Allotropes: Allotropes of carbon display a range of shock-induced effects. Rubin (1997a) and Rubin and Scott (1997) describe graphite as an exsolution phase in impact metal melt, while partially disordered graphite has also been attributed to impact alteration (Rubin 1997b; Rubin and Scott 1997). Here we list two high-pressure forms of carbon, diamond and chaoite, as impact phases.

Diamond (C): *Impact diamond*, as well as its disordered form "lonsdaleite," is an important diagnostic mineralogical marker of high-pressure impacts. Diamond formed through terrestrial impacts has been recognized since detailed studies of the Meteor Crater, Arizona (Frondel and Marvin 1967). Impact diamond typically has a significant density of stacking faults. Impact

diamond was subsequently described as a meteorite phase by several authors (Russell et al. 1992; Rubin et al. 1997; Mittlefehldt et al. 1998; Garvie et al. 2011). Note that "lonsdaleite," which was originally approved by the IMA as the hexagonal 2H variant of cubic diamond, has been shown by Németh et al. (2014) to be disordered diamond and is now discredited.

Chaoite (C): Chaoite, a high-pressure hexagonal (space group *P*6/*mmm*) form of carbon, was originally described by El Goresy and Donnay (1968) from the Reis Crater in Germany. *Impact chaoite* occurs in several carbon-rich ureilite achondrites (Vdovykin 1970).

SILICIDES

The origins of iron silicides, which are minor phases in many dimict and polymict ureilites, are enigmatic. Common occurrences of suessite (Fe_3Si; Keil et al. 1982; Ross et al. 2019) and rare xifengite (Fe_5Si_3; Ross et al. 2019), as well as unconfirmed reports of hapkeite (Fe_2Si; Smith et al. 2008) and naquite (FeSi; Moggi Cecchi et al. 2015), have been ascribed to reduction of Fe and Si from olivine (Keil et al. 1982) or Si-bearing metal (Ross et al. 2019), possibly in association with a reducing carbonaceous matrix, during shock-melting events and subsequent rapid quenching from high temperature.

Suessite (Fe_3Si): Keil et al. (1982) recorded *impact suessite* as a minor phase in the matrix of the North Haig polymict ureilite in association with troilite, kamacite, and a carbonaceous matrix. Ross et al. (2019) identified frequent occurrences of suessite, at times in association with rare xifengite, in several ureilites.

Xifengite (Fe_5Si_3): Ross et al. (2019) described rare grains of *impact xifengite* in association with suessite from the DaG 999 and EET 87720 ureilites.

PHOSPHIDES

Allabogdanite [$(Fe,Ni)_2P$]: *Impact allabogdanite* was discovered as elongated crystals in the Onello Ni-rich ataxite meteorite by Britvin et al. (2002), who originally ascribed it to primary asteroidal origins. Subsequent experimental research (Dera et al. 2008) and observations of natural material from several other occurrences (Britvin et al. 2019; Litasov et al. 2019) revealed allabogdanite to be a very-high-pressure impact phase in the Fe-Ni-P system.

SULFIDES

Meteoritic sulfides display shock effects; notably, shocked troilite may have a "bubbly" texture, twinning, shearing, and transformation to polycrystalline aggregates (Scott et al. 1992; Bennett and McSween 1996; Joreau et al. 1996). However, with the possible exception of shenzhuangite (see below), new dense forms of sulfide minerals have not been reported from shocked meteorite.

Shenzhuangite ($NiFeS_2$): Bindi and Xie (2018) described a shock-induced sulfide from the Suizhou (L6) chondrite, *impact shenzhuangite* with the chalcopyrite structure. They argue that Ni is incompatible in the chalcopyrite structure at low pressure; therefore, shenzhuangite is included in our list of impact-generated phases (Tschauner 2019).

PHOSPHATES

Tuite [γ-$Ca_3(PO_4)_2$]: Xie et al. (2002a, 2003) described *impact tuite*, a high-pressure transformation product of merrillite, which was discovered in shock veins from the Suizhou (L6) chondrite. Experiments by Murayama et al. (1986) demonstrated that pressures in excess of 10 GPa are required to stabilize tuite.

OXIDES

Magnesiowüstite [(Mg,Fe)O]: *Impact magnesiowüstite* occurs in several highly shocked meteorites in association with other high-pressure phases (Tschanuer 2019; Bindi et al. 2020). For example, magnesiowüstite of average composition [$(Mg_{0.54}Fe_{0.46})0$], found in the shocked (S6) Sixiangkou chondrite as 5-micrometer-diameter blebs in association with majorite (Chen et al. 1996), points to shock conditions exceeding 2050 ºC at 20 to 24 GPa.

Wangdaodeite ($FeTiO_3$): *Impact wangdaodeite*, a high-pressure polymorph of ilmenite with the $LiNbO_3$ perovskite-type structure, was discovered by Xie et al. (2016, 2020) from the Suizhou (L6) chondrite. Experimental studies point to formation at shock pressures above 20 GPa.

Liuite ($FeTiO_3$): *Impact liuite* was reported by Ma and Tschauner (2018a) from a shock-melt pocket in the Tissint martian meteorite. The rare phase was found at the rim of a transformed ilmenite-ülvospinel grain in association with other impact phases, feiite and tschaunerite. Liuite is closely related to wangdaodeite, another ilmenite polymorph. However, liuite with the $GdFeO_3$ perovskite structure has a significant bridgmanite component, with a composition close to [$(Fe,Mg)(Ti_{0.6}Si_{0.4})O_3$].

Chenmingite ($FeCr_2O_4$): Two shock-induced polymorphs of chromite are known from the Shizhiu (L6) chondrite (Chen et al. 2003a). Chen et al. (2003b) and Ma et al. (2019a) characterized *impact chenmingite*, $FeCr_2O_4$ in the $CaFe_2O_4$-type structure. Experiments demonstrate that chemmingite formed at pressures above 17 GPa at temperatures exceeding 1300 ºC.

This is the peer-reviewed, final accepted version for American Mineralogist, published by the Mineralogical Society of America.
The published version is subject to change. Cite as Authors (Year) Title. American Mineralogist, in press.
DOI: https://doi.org/10.2138/am-2021-7632. http://www.minsocam.org/

Xieite ($FeCr_2O_4$): Chen et al. (2008) described *impact xieite*, a high-pressure polymorph of $FeCr_2O_4$ with the $CaTi_2O_4$ structure type found as lamellae in host chromite in the Shizhiu (L6) chondrite. Experiments suggest that shock pressures must have exceeded 17 GPa while temperatures were below 1300 ºC.

Tschaunerite (Fe_2TiO_4): *Impact tschaunerite*, a polymorph of ülvospinel with the calcium ferrite structure, occurs in association with liuite and feiite from a shock-melt pocket in the Tissint martian meteorite (Ma and Prakapenka 2018).

Dmitryivanovite ($CaAl_2O_4$): Mikouchi et al. (2009) described a high-pressure polymorph of krotite, *impact dmitryivanovite*, from the Northwest Africa 470 CH3 chondrite.

Vestaite [$(Ti^{4+}Fe^{2+})Ti^{4+}_3O_9$]: *Impact vestaite* is a monoclinic high-pressure phase, identified in the eucrite NWA 8003, that crystallized from a shock melt at ≤10 GPa (Pang et al. 2018). It occurs in melt pockets and shock veins and presumably was produced after an impact on Vesta.

Feiite [$(Fe,Ti,Cr)_4O_5$]: *Impact feiite* from a shock-melt pocket in the Tissint martian meteorite was found at the rim of a transformed ilmenite-ülvospinel grain in association with other rare impact phases, liuite and tschaunerite (Ma and Tschauner 2018b).

SILICATES

Virtually all silicates at room pressure have Si in tetrahedral coordination. A key to understanding many high-pressure transformations in silicates, including those caused by very high shock pressures, is the attainment of denser states through structures with Si partially or completely in octahedral coordination (i.e., Hazen and Finger 1978; Tschauner 2019). In this

This is the peer-reviewed, final accepted version for American Mineralogist, published by the Mineralogical Society of America.
The published version is subject to change. Cite as Authors (Year) Title. American Mineralogist, in press.
DOI: https://doi.org/10.2138/am-2021-7632. http://www.minsocam.org/

regard, shock minerals provide important insights to possible major phases of Earth's deep interior – notably dense variants of silica, olivine, pyroxene, and feldspar.

Silica Polymorphs (SiO_2): A number of high-pressure polymorphs of SiO_2 have been synthesized and observed in nature as shock phases (Swamy et al. 1994; Kuwayama 2008; Tschauner 2019). We include impact-formed coesite, stishovite, seifertite, and densified silica glass.

Coesite (SiO_2): *Impact coesite*, the natural analog of the high-pressure silica polymorph synthesized by Coes (1953), was first reported by Chao et al. (1960) from shock-altered sandstone at Meteor Crater, Arizona, where it was found in association with *impact stishovite*. Coesite was subsequently identified in a number of meteorites, providing early evidence that shock transformations played a significant role in the early solar system (Ohtani et al. 2011; Hollister et al. 2014; Tomioka and Miyahara 2017, Tables 2 and 3).

Stishovite (SiO_2): Chao et al. (1962) described *impact stishovite* from Meteor Crater, Arizona, with subsequent studies by Fahey (1964), following its initial synthesis by Stishov and Popova (1961). Numerous occurrences of this rutile isomorph have been reported from shocked meteorites and lunar rocks (Holtstam et al. 2003; Garvie et al. 2011; Ohtani et al. 2011; Kaneko et al. 2015; see Tomioka and Miyahara 2017, Tables 2 and 3).

Seifertite (SiO_2): *Impact seifertite* is an extremely high-pressure shock phase with the orthorhombic (space group *Pbcn*) α-PbO_2 structure. It was initially synthesized by German et al. (1973), recognized in nature by TEM observations (Sharp et al. 1999), and further characterized

by Dera et al. (2002), El Goresy et al. (2008), and Miyahara et al. (2013a) from several shocked martian and lunar samples.

Silica glass (SiO_2): Dense *impact silica glass* is commonly associated with other high-pressure silica polymorphs (Grieve et al. 1996; Stöffler et al. 2018).

Olivine Polymorphs [$(Mg,Fe)_2SiO_4$]: At high shock pressures, olivine undergoes a sequence of phase transitions, first to the modified spineloid polymorph wadsleyite, then to the silicate spinel ringwoodite. Above ~25 GPa ringwoodite dissociates into perovskite-type [$(Mg,Fe)SiO_3$] plus masgnesiowüstite [(Mg,Fe)O] (e.g., Presnall 1995).

Wadsleyite [β-$(Mg,Fe)_2SiO_4$] and Asimowite [β-$(Fe,Mg)_2SiO_4$]: *Impact wadsleyite*, the modified β-spinel form of Mg_2SiO_4, was described by Putnis and Price (1979) and Price et al. (1983) from the Tenham and Peace River (L6) chondrites. Impact wadsleyite has been reported from more than a dozen varied meteorites (Tomioka and Miyahara 2017, Tables 2 and 3), including shocked lunar and martian material (Malavergne et al. 2001). It evidently forms through transformation from olivine along grain boundaries and fractures (Ozawa et al. 2009).

The Fe-rich analog of wadsleyite, asimowite, was characterized by Bindi et al. (2019) in shock-melted silicate droplets of the Suizhou and Quebrada Chimborazo 001 chondrites. The reported composition of impact asimowite, $[(Fe_{1.10}Mg_{0.80}Cr_{0.04}Mn_{0.02}Ca_{0.02}Al_{0.02})(Si_{0.97}Al_{0.03})O_4]$, is close to Fa_{55}. Given that a continuous solid solution exists between the Mg and Fe end members (e.g., Presnall 1995), that the only known example of asimowite is of intermediate composition and coexists with more numerous grains of wadsleyite ($Fo_{30\text{-}45}$), and that all meteoritic wadsleyite and asimowite grains

were formed by similar shock processes, we lump asimowite with impact wadsleyite as a single natural kind.

Ringwoodite [γ-$(Mg,Fe)_2SiO_4$] and Ahrensite [γ-$(Fe,Mg)_2SiO_4$]: Binns et al. (1969) discovered *impact ringwoodite*, the spinel-type (γ) form of Mg_2SiO_4 in a shock vein of the Tenham (L6) chondrite, and was subsequently reported from shock veins in numerous meteorites (Coleman 1977; Miyahara et al. 2008; Feng et al. 2011; Pittarello et al. 2015; Tomioka and Miyahara 2017, Tables 2 and 3). Impact ringwoodite also occurs as lamellae in meteoritic olivine, from which it transformed either within olivine crystals or adjacent to grain boundaries (Kerschhofer et al. 1996, 1998; Chen et al. 2004; Miyahara et al. 2010; Tomioka and Miyahara 2017). Compositions of impact ringwoodite vary from Fo_{82} to Fo_{46} (Kimura et al. 2003; Feng et al. 2011; Ma et al. 2016; Tomioka and Miayhara 2017).

Ma et al. (2016) described an Fe-dominant analog of ringwoodite, named ahrensite, from the Tissint martian meteorite – a mineral also previously reported from the Umbarger (L6) chondrite by Xie et al. (2002b). Ahrensite of composition [$(Fe_{1.06}Mg_{0.91}Mn_{0.02})SiO_4$], i.e., close to Fo_{45}, coexists with more numerous grains of ringwoodite with average compositions near Fo_{55} [$(Mg_{1.11}Fe_{0.85}Mn_{0.02})SiO_4$]. In accordance with the conventions of our evolutionary system, we lump all meteoritic examples of the solid solution between ahrensite and ringwoodite as a single natural kind, *impact ringwoodite*.

Poirierite [$(Mg,Fe)_2SiO_4$]: Tomioka et al. (2020) characterized *impact poirierite*, an orthorhombic (space group *Pmma*) dense polymorph of forsterite from the Suizhou (L6) chondrite. Details of composition, structure, and occurrence will be forthcoming.

This is the peer-reviewed, final accepted version for American Mineralogist, published by the Mineralogical Society of America.
The published version is subject to change. Cite as Authors (Year) Title. American Mineralogist, in press.
DOI: https://doi.org/10.2138/am-2021-7632. http://www.minsocam.org/

Pyroxene Polymorphs [$(Ca,Mg,Fe)_2Si_2O_6$]: Pyroxene group minerals experience a variety of transformations under shock conditions (e.g., Gasparik 1990). At temperatures above ~1600 ºC and ~16 GPA, endmember orthoenstatite ($MgSiO_3$) transforms initially to the garnet polymorph majorite with mixed tetrahedral and octahedral Si. Above ~17 GPa, majorite transforms to the ilmenite structure, akimotoite, and above ~22 GPa the perovskite form, bridgmanite with all Si in octahedral coordination appears. At high pressure below ~1600 ºC, enstatite dissociates to wadsleyite or ringwoodite plus the stishovite form of SiO_2, but bridgmanite is the stable phase above 22 GPa.

Additional complexities arise at lower pressures because orthoenstatite can partially to completely transform to clinoenstatite at pressures from 7 to 12 GPa, depending on temperature. This ortho- to clinoenstatite transformation is often blurred because lamellae of the two polymorphs can occur intimately intermixed in a disordered structure as the result of shock deformation.

Clinoenstatite ($MgSiO_3$): *Impact clinoenstatite* forms through the transformation of *DA orthoenstatite* to a disordered monoclinic structure (Reid and Cohen 1967; Tomioka and Fujino 1997; Rubin and Ma 2020).

Majorite ($MgSiO_3$): Mason et al. (1968) reported a high-pressure form of $MgSiO_3$ with the cubic (space group *Ia*{bar3}*d*) garnet structure from a shock vein in the Coorara (L6) chondrite. This phase, which can be represented by the structural formula [$Mg_3(MgSi)Si_3O_{12}$], was subsequently named majorite by Smith and Mason (1970). *Impact majorite* has been identified in more than 20 meteorites (Tomioka and Miyahara 2017, Tables 2 and 3), with compositions both

close to the Mg-Fe join (Coleman 1977; Walton 2013; Kato et al. 2017) and in solid solution with other garnet components, including pyrope ($Mg_3Al_2Si_3O_{12}$; Chen et al. 1996), almandine ($Fe_3Al_2Si_3O_{12}$; Ma and Tschauner 2016), and calcic garnet (Xie and Sharp 2007).

The majorite story is complicated by the discovery of a few occurrences of unambiguously tetragonal (space group $I4_1/a$) high-pressure garnets, in contrast to the familiar cubic symmetry (Xie and Sharp 2007; Ma and Tschauner 2016; Tomioka et al. 2016) – a difference that is difficult to document without electron diffraction of individual micrometer-scale grains. The lower symmetry results from Mg-Si ordering in octahedral sites, which may be a pervasive feature of meteoritic majorites (Angel et al. 1989; Heinemann et al. 1997; Tomioka et al. 2002). At this stage, we do not distinguish between completely disordered cubic majorite, which might occur in some rapidly quenched examples, and the pseudo-cubic tetragonal variant, which would obtain for samples with any degree of Mg-Si order.

Akimotoite [$(Mg,Fe)SiO_3$] and Hemleyite [$(Fe,Mg)SiO_3$]: The ilmenite structured polymorph of enstatite was reported by Sharp et al. (1997) from the Acfer 040 (L5-6) chondrite and by Tomioka and Fujino (1997) from the Tenham chondrite, and was subsequently named akimotoite (Tomioka and Fujino 1999). *Impact akimotoite* is now known from at least 17 meteorites (Tomioka and Miyahara 2017, Tables 2 and 3), including examples with significant Ca and minor Fe^{3+} (Ohtani et al. 2004; Xie and Sharp 2004; Xie et al. 2006; Miyajima et al. 2007; Ferroir et al. 2008; Chen and Xie 2015). Tomioka (2017) revealed the transformation mechanism from clinoenstatite to akimotoite as the result of oriented shear dislocations.

Bindi et al. (2017a, 2017b) described an Fe-dominant example of akimotoite in the shocked Suizhou (L6) chondrite – a phase they named hemleyite. Analyses span the range from 45 to 50

mol % $FeSiO_3$, with 33 to 39 mol % $MgSiO_3$, compared to reported akimotoite compositions from 20 to 30 mol % $FeSiO_3$, with 62 to 78 mol % $MgSiO_3$ (Bindi et al. 2017a; Figure 5). Because there appears to be a continuous akimotoite-hemleyite solid solution and all examples are formed by similar shock transformation of clinopyroxene, we lump hemleyite with *impact akimotoite*.

Bridgmanite [$(Mg,Fe)SiO_3$] and Hiroseite [$(Fe,Mg)SiO_3$]: Tschauner et al. (2014) characterized a natural occurrence of crystalline [$(Mg,Fe)SiO_3$] in the perovskite structure – a phase they named bridgmanite. The presence of this phase as a high-pressure shock mineral in meteorites was long suspected, based in part on amorphous regions of enstatite composition and the tendency of bridgmanite to invert to glass (Wang et al. 1992; Sharp et al. 1997), as well as transmission electron microscopy (TEM) evidence for the crystallinity of sub-micrometer grains of presumed $MgSiO_3$ perovskite coexisting with magnesiowüstite, which is the presumed post-ringwoodite assemblage (Tomioka and Fujino 1997).

Of note is the TEM description by Vollmer et al. (2007) of a 0.3-micrometer bridgmanite grain from the Acfer 094 carbonaceous chondrite. This grain has diagnostic isotopic anomalies, with extremely high $^{17}O/^{16}O$ and low $^{18}O/^{16}O$ characteristic of presolar grains from a low-mass AGB star. Consequently, Hazen and Morrison (2020) listed *AGB bridgmanite* as one of 41 stellar mineral natural kinds. However, we now consider this grain to be *impact bridgmanite* that formed from an isotopically anomalous *AGB enstatite* precursor grain.

Bindi and Xie (2019) and Bindi et al. (2020) characterized the Fe-dominant analog of bridgmanite of composition $[(Fe^{2+}_{0.44}Mg_{0.37}Fe^{3+}_{0.10}Al_{0.04}Ca_{0.03}Na_{0.02})(Si_{0.89}Al_{0.11})O_3]$,

which they named hiroseite. Crystal inclusions in magnesiowüstite (~5-micrometers diameter) were found in the Suizhou (L6) chondrite in association with other high-pressure shock phases. Bindi et al. (2020) demonstrated that a significant fraction of iron in meteoritic bridgmanite undergoes charge disproportionation ($3Fe^{2+} \rightarrow Fe^{0} + 2Fe^{3+}$), consistent with earlier analyses of experimental samples (McCammon 1997; Fialin et al. 2009; Sinmyo et al. 2017). This effect should be more pronounced in Fe-rich silicate perovskite; however, unless evidence is presented for a miscibility gap in the [$(Mg,Fe)SiO_3$] solid solution, we lump all examples of meteoritic bridgmanite and hiroseite into *impact bridgmanite*.

Amorphous $CaSiO_3$: Shock transformation of Ca-rich pyroxene above ~17 GPa leads to the formation of a high-pressure Mg-silicate (wadsleyite + stishovite; majorite; ringwoodite + stishovite; akimotoite; or bridgmanite, depending on the temperature and pressure), plus $CaSiO_3$ perovskite (Akaogi et al. 2004). Therefore, perovskite-type $CaSiO_3$ must have formed in many augite-rich meteorites. However, the crystalline phase is unstable at room conditions and inverts to amorphous $CaSiO_3$ (Liu and Ringwood 1975) – a non-crystalline phase found in a number of meteorites (Tomioka and Kimura 2003; Xie and Sharp 2007), which we designate *impact amorphous $CaSiO_3$*.

Tissintite [$(Ca,Na,\square)AlSi_2O_6$]: Ma et al. (2015) discovered a monoclinic (space group *C*2/*c*) defect pyroxene in the shocked Tissint martian meteorite. *Impact tissintite* has an unusual defect structure, with vacancies in the M2 site. The phase was subsequently synthesized at 6 to 8.5 GPa and 1000 to 1350 ºC by Rucks et al. (2018), who suggest it forms naturally from inversion of maskelynite.

1536 **Unnamed [(Mg,Fe)SiO_3]:** Xie et al. (2011) presented TEM evidence for a high-pressure
1537 shock mineral with the olivine structure but with pyroxene stoichiometry from the Tenham (L6)
1538 chondrite. Further investigation of this intriguing phase, which we designate *impact unnamed*
1539 *[(Mg,Fe)SiO_3]*, is warranted.
1540
1541 **Feldspar Polymorphs [(Ca,Na,K)Al(Al,Si)Si_2O_8]:** Feldspar-group minerals undergo a variety
1542 of high-pressure phase transformations under shock conditions, including meteorite minerals
1543 with the pyroxene, hollandite, and calcium ferrite structures, as well as amorphous shock phases
1544 (Liu 1978, 2006; Yagi et al. 1994; Liu and El Goresy 2007; Ozawa et al. 2014; Zhou et al. 2017).
1545 **Jadeite ($NaAlSi_2O_6$):** Albite transforms to jadeite plus a silica phase (quartz, coesite, or
1546 stishovite, depending on the maximum pressure) at pressures above ~2.5 GPa. Jadeite plus
1547 stishovite is the stable assemblage to at least 20 GPa, above which pressure jadeite transforms to
1548 the calcium ferrite structure. Consequently, *impact jadeite* is known from numerous meteorites
1549 (Kimura et al. 2000; Ohtani et al. 2004; Ozawa et al. 2009, 2014; Tomioka and Miyahara 2017,
1550 Table 2). In some instances, jadeite may represent a back reaction from crystallization of
1551 maskelynite (Miyahara et al. 2013b).
1552 **Maskelynite [(Ca,Na)Al(Al,Si)Si_2O_8]:** The amorphous phase of plagioclase, *impact*
1553 *maskelynite*, is found in numerous shocked anorthite-bearing meteorites (Ostertag 1983; Stöffler
1554 et al. 1986, 1991; Brearley and Jones 1998; Mittlefehldt et al. 1998; Rubin 2015b; Rubin and Ma
1555 2020).
1556 **Lingunite [(Na,Ca)$AlSi_3O_8$]:** Alkali feldspars with the hollandite structure do not appear to
1557 have a high-pressure stability field; however, they can be quenched metastably from high

pressure (Liu 2006; Zhou et al. 2017). The Na-rich endmember, first synthesized by Liu (2006), was characterized by Gillet et al. (2000) from the Sixiangkou meteorite and subsequently named lingunite. Natural examples of *impact lingunite* have been described from at least 20 shocked meteorites (Tomioka and Miyahara 2017, Tables 2 and 3).

Liebermannite [$(K,Na)AlSi_3O_8$]: A high-pressure hollandite structure polymorph of $KAlSi_3O_8$ was reported by Langenhorst and Poirier (2000) from the shocked Zagami meteorite – a phase synthesized by Liu and El Goresy (2007). Ma et al. (2018) characterized the mineral and named it liebermannite. *Impact liebermannite* with average composition $[(K_{0.6}Na_{0.2}Ca_{0.1})AlSi_3O_8]$ is found in close association with lingunite and maskelynite, both with compositions close to ~$[Na_{0.5}K_{0.02}Ca_{0.4})Al(Al_{0.35}Si_{2.65}O_8]$.

Stöfflerite ($CaAl_2Si_2O_8$): The hollandite-structured high-pressure polymorph of anorthite was recognized by Spray and Boonsue (2016) from Raman spectra of material from a terrestrial impact structure. *Impact stöfflerite* was subsequently characterized by Tschauner and Ma (2017) from the NWA 856 martian meteorite.

Other Silicates

Cordierite ($Mg_2Al_4Si_5O_{18}$): *Impact cordierite* is a rare phase in meteorites, first reported by Fuchs (1969b) from an unusual CAI in the Allende meteorite. It was subsequently identified in the Chaunskij anomalous mesosiderite, which was estimated to have equilibrated at 0.6 GPa (Petaev et al. 2000). Cordierite typically forms at pressures above 0.2 GPa (e.g., Deer et al. 1962), which is significantly greater than those of asteroid interiors; we thus assume a shock origin.

Zagamiite ($CaAl_2Si_{3.5}O_{11}$): Ma and colleagues (Ma and Tschauner 2017; Ma et al. 2017b, 2019b) characterized a high-pressure calcium aluminosilicate ($CaAl_2Si_{3.5}O_{11}$) found in shocked martian meteorites. *Impact zagamiite* was originally recognized by its distinctive Raman spectrum (Beck et al. 2004). This phase was synthesized by Irifune et al. (1994), who called it "CAS." It forms when calcic plagioclase is subjected to shock pressures greater than ~22 GPa (Akaogi et al. (2010).

Unnamed [$(Fe,Mg,Cr,Ti,Ca,\square)_2(Si,Al)O_4$]: Ma et al. (2019c) described a new high-pressure silicate phase, *impact* $(Fe,Mg,Cr,Ti,Ca,\square)_2(Si,Al)O_4$ with a tetragonal spinelloid structure, in a shock melt pocket from the Tissint Martian meteorite.

Unnamed [$(Mg,Fe,Si)_2(Si,\square)O_4$]: Ma et al. (2019d) reported a vacancy-rich, partially inverted spinelloid silicate, *impact* $(Mg,Fe,Si)_2(Si,\square)O_4$, as a major matrix phase in shock melt veins of the Tenham and Suizhou L6 chondrites.

IMPLICATIONS

Cosmic mineral evolution played out in a succession of stages, each of which explored new regimes of temperature, pressure, and composition, while adding to the diversity of condensed solid phases. The 130 meteorite minerals reviewed above (Tables 1 and 2) complement the 41 stellar natural kinds (Hazen and Morrison 2020), 67 interstellar and primary nebular condensates (Morrison and Hazen 2020), and 44 primary chondrule minerals (Hazen et al. 2021) described in earlier parts of this series.

In Part IV of the evolutionary system of mineralogy we encounter pressures significantly above 1 atmosphere for the first time, both in the contexts of asteroidal interiors (to $P < 0.5$ Gpa) and via shock events (to $P > 30$ GPa). The resulting inventory of meteorite minerals includes 90 kinds formed by primary asteroidal processes, as well as 40 high-pressure impact minerals. These 130 mineral natural kinds encompass 127 approved IMA mineral species, 10 of which are lumped with other species and thus do not appear as separate natural kinds in Tables 1 and 2. In addition, we include 7 crystalline phases, either not recognized as valid IMA species (e.g., fassaite; magnesiowüstite; martensite) or awaiting possible approval (e.g., unnamed $CuCrS_2$ and Mg-Fe silicates), as well as 6 amorphous phases.

Asteroidal processes resulted in many new mineral phases. Of the 90 primary asteroidal natural kinds (Table 1), 48 minerals appear for the first time, including the earliest known members of the apatite and amphibole groups, as well as zircon, potassic feldspar, and numerous phosphate minerals. Of the 40 impact minerals listed in Table 2, 38 occur for the first time; only diamond and clinopyroxene also formed previously at low pressure. This total of 86 new minerals in Part IV almost doubles the total of 181 phases tabulated to this stage of mineral evolution.

The observed diversity and distribution of asteroidal minerals appears to be consistent with previous studies in "mineral ecology," by which patterns of mineral occurrences on Earth can be used to document the relative frequencies of common versus rare species, as well as to predict Earth's "missing" minerals (Hazen et al. 2015a, 2015b, 2016; Hystad et al. 2015a, 2015b, 2017, 2019; Grew et al. 2017). Earlier studies demonstrate that the great majority of mineral occurrences (defined as a specific mineral species from one locality) represent a few abundant minerals, whereas the great majority of mineral species are rare (i.e., known from only a few

localities). Meteorite minerals are no exception to this trend. Of the 90 asteroidal primary minerals, fewer than 20 phases constitute 99.9 volume percent of almost all non-chondritic meteorites. By contrast, more than 50 of these minerals are rare and have only been reported as sub-millimeter- to sub-micrometer-scale grains, with at least two dozen of those phases only known as sub-micron crystals from a single meteorite. Accordingly, we estimate that the documented collective mass of these >50 rarest differentiated asteroidal minerals is no more than a few milligrams. We suggest that further statistical study of the diversity and distribution of meteorite minerals, employing the methods of mineral ecology, might provide estimates of the total diversity of meteorite minerals.

The characteristic "Large Numbers of Rare Events" (LNRE) distribution of minerals (Hystad et al. 2015a) observed for many mineralogical environments demonstrates that rare minerals play a disproportionate role in understanding natural processes (Hazen and Ausubel 2016), not unlike the role of trace elements and isotopes in petrology and geochemistry. In meteorites, rare minerals and their LNRE distributions document details of evolving pressure-temperature-composition niches and the important influence of transient and disequilibrium events, while revealing many remarkable new structural topologies and compositional permutations. Furthermore, in the case of shock-induced minerals, phases that are intrinsically rare at Earth's surface provide perhaps our best natural view of mantle minerals that represent more than half of Earth's volume (Tschauner 2019). In Part V of this series, which will focus on secondary meteorite minerals formed by a range of aqueous and thermal processes, we will find a significant pulse of new phases characterized by the same type of skewed distribution – a few common kinds accompanied by many more rare minerals.

ACKNOWLEDGMENTS

We are deeply grateful to Chi Ma, David Mittlefehldt, and Steven Simon, who provided detailed, thoughtful, and constructive reviews that significantly improved the manuscript. In addition, Timothy McCoy and Alan Rubin offered invaluable detailed reviews of an earlier version of this contribution, while McCoy contributed photographs of important meteorite specimens. Luca Bindi, Chi Ma, and Alan Rubin provided access to highly relevant work in press. We are grateful to Asmaa Boujibar, Carol Cleland, Robert T. Downs, Olivier Gagné, Peter Heaney, Sergey Krivovichev, Glenn MacPherson, Anirudh Prabhu, Michael Walter, and Shuang Zhang for thoughtful discussions and comments.

This publication is a contribution to the Deep Carbon Observatory, the 4D Initiative, and the Deep-time Digital Earth (DDE) program. Studies of mineral evolution and mineral ecology have been supported by the Deep Carbon Observatory, the Alfred P. Sloan Foundation, the W. M. Keck Foundation, the John Templeton Foundation, the NASA Astrobiology Institute ENIGMA team, a private foundation, and the Carnegie Institution for Science. Any opinions, findings, or recommendations expressed herein are those of the authors and do not necessarily reflect the views of the National Aeronautics and Space Administration.

References

Akaogi, M., Yano, M., Tejima, Y., Iijima, M., and Kojitani, H. (2004) High-pressure transitions of diopside and wollastonite: Phase equilibria and thermochemistry of $CaMgSi_2O_6$, $CaSiO_3$ and $CaSi_2O_5$–$CaTiSiO_5$ system. Physics of the Earth and Planetary Interiors, 143, 145–156.

Akaogi, M., Haraguchi, M., Nakanishi, K., Ajiro, H., and Kojitani, H. (2010) High-pressure phase relations in the system $CaAl_4Si_2O_{11}$–$NaAl_3Si_3O_{11}$ with implication for Narich CAS phase in shocked Martian meteorites. Earth and Planetary Science Letters, 289, 503–508.

Angel, R.J., Finger, L.W., Hazen, R.M., Kanzaki, M., Weidner, D.J., Liebermann, R.C., and Veblen, D.R. (1989) Structure and twinning of single-crystal $MgSiO_3$ garnet synthesized at 17 GPa and 1800°C. American Mineralogist, 74, 509–512.

Aoudjehane, H.C., and Jambon, A. (2007) Determination of silica polymorphs in eucrites by cathodoluminescence. Lunar and Planetary Science, 38, 1714.

Ashworth, J.R. (1980) Deformation mechanisms in mildly shocked chondritic diopside. Meteoritics, 15, 105-115.

Ashworth, J.R. (1985) Transmission electron microscopy of L-group chondrites: 1. Natural shock effects. Earth and Planetary Science Letters, 73, 17-32.

Axon, H.J., Kinder, J., Haworth, C.W., and Horsfield, J.W. (1981) Carlsbergite, CrN, in troilite, FeS, of the Sikhote Alin meteoritic iron. Mineralogical Magazine, 44, 107–109.

Bailey, K.D. (1994) Typologies and Taxonomies: An Introduction to Classification Techniques. Studies in Quantitative Applications in the Social Sciences, 102. SAGE Publications.

Bannister, F.A. (1941) Osbornite, meteoritic titanium nitride. Mineralogical Magazine, 26, 36-44.

1687 Barrat, J.-A., Yamaguchi, A., Greenwood, R.C., Bohn, M., Cotten, J., Benoit, M., and Franchi,
1688 I.A. (2007) The Stannern trend eucrites: Contamination of main group eucritic magmas by
1689 crustal partial melts. Geochimica et Cosmochimica Acta, 71, 4108-4124.
1690 Beck, P., Gillet, P., Gautron, L., Daniel, I., and El Goresy, A. (2004) A new natural high-
1691 pressure (Na,Ca)-hexaluminosilicate [$(Ca_xNa_{1-x})Al_{3+x}Si_{3-x}O_{11}$] in shocked Martian
1692 meteorites. Earth and Planetary Science Letters, 219, 1–12.
1693 Beck, A.W., Mittlefehldt, D.W., McSween, H.Y., Jr, Rumble, D., III, Lee, C.-T., and Bodnar,
1694 R.J. (2011) MIL 03443, a dunite from asteroid 4 Vesta: Evidence for its classification and
1695 cumulate origin. Meteoritics & Planetary Science, 46, 1133-1151.
1696 Begemann, F., and Wlotzka, F. (1969) Shock induced thermal metamorphism and mechanical
1697 deformations in the Ramsdorf chondrite. Geochimica et Cosmochimica Acta, 33, 1351-1370.
1698 Benedix, G.K., McCoy, T.J., Keil, K., Bogard, D.D., and Garrison, D.H. (1998) A petrologic and
1699 isotopic study of winonaites: Evidence for early partial melting, brecciation, and
1700 metamorphism. Geochimica et Cosmochimica Acta, 62, 2535-2553.
1701 Benedix, G.K., McCoy, T.J., Love, S.G., and Keil, K. (2000) A petrologic study of IAB iron
1702 meteorites: Constraints on the formation of the IAB-winonaite parent body. Meteoritics &
1703 Planetary Science, 35, 1127-1141.
1704 Benedix, G.K., Haack, H., and McCoy, T.J. (2014) Iron and stony-iron meteorites. Treatise on
1705 Geochemistry, 2nd edition, 1, 267-285.
1706 Bennett, M.E.I., and McSween, H.Y. Jr. (1996) Shock features in iron-nickel metal and troilite of
1707 L-group ordinary chondrites. Meteoritics & Planetary Science, 31, 255-264.
1708 Benz, W., and Asphaug, E. (1999) Catastrophic disruptions revisited. Icarus, 142, 5-20.

1709 Berkley, J.L., and Jones, J.H. (1982) Primary igneous carbon in ureilites: Petrological
1710 implications. Journal of Geophysical Research, 87, A353-A364.
1711 Bevan, A.W.R., Bevan, J.C., and Francis, J.G. (1977) Amphibole in the Mayo Belwa meteorite:
1712 First occurrence in an enstatite achondrite. Mineralogical Magazine, 41, 531-534.
1713 Bild, R.W., and Wasson, J.T. (1977) Netschaëvo: A new class of chondritic meteorite. Science,
1714 197, 58-62.
1715 Bindi, L., and Xie, X.D. (2018) Shenzhaungite, $NiFeS_2$, the Ni-analogue of chalcopyrite from
1716 the Suizhou L6 chondrite. European Journal of Mineralogy, 30, 165-169.
1717 Bindi, L., and Xie, X. (2019) Hiroseite, IMA 2019-019. Mineralogical Magazine, 83, 615-620.
1718 Bindi, L., Steinhardt, P.J., Yao, N., and Lu, P.J. (2011) Icosahedrite, $Al_{63}Cu_{24}Fe_{13}$, the first
1719 natural quasicrystal. American Mineralogist, 96, 928-931.
1720 Bindi, L., Eiler, J.M., Guan, Y., Hollister, L.S., MacPherson, G., Steinhardt, P.J., and Yao. N.
1721 (2012) Evidence for the extraterrestrial origin of a natural quasicrystal. Proceedings of the
1722 National Academy of Science USA, 109, 1396-1401.
1723 Bindi, L., Lin, C., Ma, C., and Steinhardt, P.J. (2016) Collisions in outer space produced an
1724 icosahedral phase in the Khatyrka meteorite never observed previously in the laboratory.
1725 Scientific Reports, 6, 38117.
1726 Bindi, L., Chen, M., and Xie, X. (2017a) Discovery of the Fe-analogue of akimotoite in the
1727 shocked Suizhou L6 chondrite. Scientific Reports, 7, 42674, 1-8.
1728 Bindi, L., Chen, M., and Xie, X. (2017b) Hemleyite, IMA 2016-085. Mineralogical Magazine,
1729 81, 209-213.
1730 Bindi, L., Brenker, F.E., Nestola, F., Koch, T.E., Prior, D.J., Lilly, K., Krot, A.N., Bizzarro, M.,
1731 and Xie, X. (2019) Discovery of asimowite, the Fe-analog of wadsleyite, in shock-melted

1732 silicate droplets of the Suizhou L6 and the Quebrada Chimborazo 001 CB3.0 chondrites.
1733 American Mineralogist, 104, 775-778.
1734 Bindi, L., Shim, S-H., Sharp, T.G., and Xie, X. (2020) Evidence for the charge
1735 disproportionation of iron in extraterrestrial bridgmanite. Science Advances, 6, eaay7893 (6
1736 p.).
1737 Binns, R.A., Davis, R.J., and Reed, S.J.B. (1969) Ringwoodite, natural $(Mg,Fe)_2SiO_4$ spinel in
1738 the Tenham meteorite. Nature, 221, 943-944.
1739 Bischoff, A., and Stöffler, D. (1992) Shock metamorphism as a fundamental process in the
1740 evolution of planetary bodies: information from meteorites. European Journal of Mineralogy,
1741 4, 707-755.
1742 Blichert-Toft, J., Moynier, F., Lee, C.A., Telouk, P., and Albare`de, F. (2010) The early
1743 formation of the IV iron meteorite parent body. Earth and Planetary Science Letters, 296,
1744 469–480.
1745 Bogard, D., Burnett, D., Eberhardt, P., and Wasserburg, G.J. (1967) ^{40}Ar-^{40}K ages of silicate
1746 inclusions in iron meteorites. Earth and Planetary Science Letters, 3, 275-283.
1747 Bogard, D.D., Burnett, D.S., and Wasserburg, G.J. (1969) Cosmogenic rare gases and the ^{40}K-
1748 ^{40}Ar age of the Kodaikanal iron meteorite. Earth and Planetary Science Letters, 5, 273-281.
1749 Boesenberg, J.S., Prinz, M., Weisberg, M.K., Davis, A.M., Clayton, R.N., Mayeda, T.K., and
1750 Wasson, J.T. (1995) Pyroxene-pallasites: A new pallasite grouplet. Meteoritics, 30, 488-489.
1751 Boesenberg, J.S., Delaney, J.S., and Hewins, R.H. (2012) A petrological and chemical
1752 reexamination of Main Group pallasite formation. Geochimica et Cosmochimica Acta, 89,
1753 134-158.

1754 Bowman, L.E., Spilde, M.N., and Papike, J.J. (1997) Automated energy dispersive spectrometer
1755 modal analysis applied to the diogenites. Meteoritics & Planetary Science, 32, 869-875.
1756 Boyd, R. (1991) Realism, anti-foundationalism and the enthusiasm for natural kinds.
1757 Philosophical Studies, 61, 127-148.
1758 Brearley, A.J., and Jones, R.H. (1998) Chondritic meteorites. Reviews in Mineralogy, 36, 3.01-
1759 3.398.
1760 Breen, J. P., Rubin, A. E., and Wasson, J. T. (2016) Variations in impact effects among IIIE iron
1761 meteorites. Meteoritics & Planetary Science, 51, 1611-1631.
1762 Britvin, S.N., Rudashevsky, N.S., Krivovichev, S.V., Burns, P.C., and Polekhovsky, Y.S. (2002)
1763 Allabogdanite, $(Fe,Ni)_2P$, a new mineral from the Onello meteorite: The occurrence and
1764 crystal structure. American Mineralogist, 87, 1245-1249.
1765 Britvin, S.N., Shilovskikh, V.V., Pagano, R., Vlasenko, N.S., Zaitsev, A.N., Krzhizhanovskaya,
1766 M.G., Lozhkin, M.S., Zolotarev, A.A., and Gurzhiy, V.V. (2019) Allabogdanite, the high-
1767 pressure polymorph of $(Fe,Ni)_2P$, a stishovite-grade indicator of impact processes in the Fe–
1768 Ni–P system. Scientific Reports, 9, 1047 (8 p.).
1769 Britvin, S.N., Murashko, M.N., Vapnik, Y., Polekhovsky, Y.S., Krivovichev, S.V.,
1770 Krzhizhanovskaya, M.O., Vereshchagin, O.S., Shilovskikh, V.V., and Vlasenko, N.S. (2020a)
1771 Transjordanite, Ni_2P, a new terrestrial and meteoritic phosphide, and natural solid solutions
1772 barringerite-transjordanite (hexagonal Fe_2P–Ni_2P). American Mineralogist, 105, 428–436.
1773 Britvin, S.N., Krivovichev, S.V., Obolonskaya, E.V., Vlasenko, N.S., Bocharov, V.N., and
1774 Bryukhanova, V.V. (2020b) Xenophyllite, $Na_4Fe_7(PO_4)_6$, an exotic meteoritic phosphate:

New mineral description, Na-ions mobility and electrochemical implications. Minerals, 10, 300 (13 pp.).

Buchwald, V.F. (1975) Handbook of Iron Meteorites. University of California Press.

Buchwald, V.F. (1977) The mineralogy of iron meteorites. Philosophical Transactions of the Royal Society of London, A286, 453-491.

Buchwald, V.F., and Scott, E.R.D. (1971) First nitride (CrN) in iron meteorites. Nature Physical Science, 233, 113-114.

Bunch, T.E., and Fuchs, L.H. (1969a) A new mineral: brezinaite, Cr_3S_4, and the Tucson meteorite. American Mineralogist, 54,1509-1518.

Bunch, T.E., and Fuchs, L.H. (1969b) Yagiite, a new sodium-magnesium analogue of osumilite, American Mineralogist, 54, 14-18.

Bunch, T.E., and Keil, K. (1971) Chromite and ilmenite in non-chondritic meteorites. American Mineralogist, 56, 146-157.

Bunch, T.E., and Olsen, E. (1968) Potassium feldspar in Weekeroo Station, Kodaikanal, and Colomera iron meteorites. Science, 160, 1223-1225.

Bunch, T.E., and Rajan, R.S. (1988) Meteorite regolith breccias. In J.F. Kerridge and M.S. Matthews, Eds., Meteorites and the Early Solar System, pp. 144-164. University of Arizona Press.

Bunch, T.E., Keil, K., and Olsen, E. (1970) Mineralogy and petrology of silicate inclusions in iron meteorites. Contributions to Mineralogy and Petrology, 25, 297-240.

Burke, E.A.J. (2006) The end of CNMMN and CCM—Long live the CNMNC! Elements, 2, 388.

1797 Burkhardt, C., Kleine, T., Oberli, F., Pack, A., Bourdon, B., and Wieler, R. (2011) Molybdenum
1798 isotopic anomalies in meteorites: Constraints on solar nebula evolution and the origin of the
1799 Earth. Earth and Planetary Science Letters, 312, 390-400.
1800 Buseck, P.R. (1969) Phosphide from meteorites: Barringerite, a new iron-nickel mineral.
1801 Science, 165, 169-171.
1802 Buseck, P.R. (1977) Pallasite meteorites-mineralogy, petrology, and geochemistry. Geochimica
1803 et Cosmochimica Acta, 41, 711-740.
1804 Buseck, P.R., and Goldstein, J.I. (1969) Olivine compositions and cooling rates of pallasitic
1805 meteorites. Geological Society of America Bulletin, 80, 2141-2158.
1806 Buseck, P.R., and Holdsworth, E. (1977) Phosphate minerals in pallasite meteorites.
1807 Mineralogical Magazine, 41, 91-102.
1808 Buseck, P.R., Mason, B., and Wiik, H.-B. (1966) The Farmington meteorite-mineralogy and
1809 petrology. Geochimica et Cosmochimica Acta, 30, 1-8.
1810 Casanova, I., McCoy, T.J., and Keil, K. (1993) Metal-rich meteorites from the aubrite parent
1811 body. Lunar and Planetary Science, 24, 259-260.
1812 Casanova, I., Graf, T., and Marti, K. (1995) Discovery of an unmelted H-chondrite inclusion in
1813 an iron meteorite. Science, 268, 540-542.
1814 Chabot, N.L., and Drake, M.J. (1999) Crystallization of magmatic iron meteorites: The role of
1815 mixing in the molten core. Meteoritics & Planetary Science, 34, 235–246.
1816 Chabot, N.L., and Drake, M.J. (2000) Crystallization of magmatic iron meteorites: The effects of
1817 phosphorus and liquid immiscibility. Meteoritics & Planetary Science, 35, 807–816.
1818 Chen, M., and Xie, X.D. (2015) Shock-produced akimotoite in the Suizhou L6 chondrite.
1819 Science China Earth Sciences, 58, 876–880.

1820 Chen, M., Sharp, T.G., El Goresy, A., Wopenka, B., and Xie, X. (1996) The majorite-pyrope-
1821 magnesiowustite assemblage: Constraints on the history of shock veins in chondrites. Science
1822 271, 1570-1573.
1823 Chen, M., Shu, J., Mao, H.-K.., Xie, X., and Hemley, R.J. (2003a) Natural occurrence and
1824 synthesis of two new post-spinel polymorphs of chromite. Proceedings of the National
1825 Academy of Sciences (USA), 100, 14651–14654.
1826 Chen, M., Shu, J., Xie, X., and Mao, H.-K. (2003b) Natural $CaTi_2O_4$-structured $FeCr_2O_4$
1827 polymorph in the Suizhou meteorite and its significance in mantle mineralogy. Geochimica et
1828 Cosmochimica Acta, 67, 3937–3942.
1829 Chen, M., El Goresy, A., and Gillet, P. (2004) Ringwoodite lamellae in olivine: clues to olivine–
1830 ringwoodite phase transition mechanisms in shocked meteorites and subducting slabs.
1831 Proceedings of the National Academy of Scineces USA, 101, 15033–15037.
1832 Chen, M., Shu, J., and Mao, H.K. (2008) Xieite, a new mineral of high-pressure $FeCr_2O_4$
1833 polymorph. Chinese Science Bulletin, 53, 3341-3345.
1834 Chen, M., Shu, J., Xie, X., and Tan, D. (2019) Maohokite, a post-spinel polymorph of $MgFe_2O_4$
1835 in shocked gneiss from the Xiuyan crater in China. Meteoritics & Planetary Science, 54, 495-
1836 502.
1837 Choi, B.-G., Ouyang, X., and Wasson, J.T. (1995) Classification and origin of IAB and IIICD
1838 iron meteorites. Geochimica et Cosmochimica Acta, 59, 593-612.
1839 Chao, E.C.T., Shoemaker, E.M., and Madsen, B.M. (1960) First natural occurrence of coesite.
1840 Science, 132, 220-222.

1841 Chao, E.C.T., Fahey, J.J., Littler, J., and Milton, D.J. (1962) Stishovite, SiO_2, a very high
1842 pressure new mineral from Meteor Crater, Arizona. Journal of Geophysical Research, 67,
1843 419-421.
1844 Clarke, R.S. Jr., and Scott, E.R.D. (1980) Tetrataenite - ordered FeNi, a new mineral in
1845 meteorites. American Mineralogist, 65, 624-630.
1846 Clayton, R.N., and Mayeda, T.K. (1996) Oxygen-isotope studies of achondrites. Geochimica et
1847 Cosmochimica Acta, 60, 1999–2018.
1848 Clayton, D.D. and Nittler, L.R. (2004) Astrophysics with presolar stardust. Annual Reviews of
1849 Astronomy and Astrophysics, 42, 39-78.
1850 Coes, L. (1953) A new dense crystalline silica. Science, 118, 131–132.
1851 Cohen, B.A., Goodrich, C.A., and Keil, K. (2004) Feldspathic clast populations in polymict
1852 ureilites: Stalking the missing basalts from the ureilite parent body. Geochimica et
1853 Cosmochimica Acta, 68, 4249–4266.
1854 Coleman, L.C. (1977) Ringwoodite and majorite in the Catherwood meteorite. Canadian
1855 Mineralogist, 15, 97-101.
1856 Crozaz, G., and McKay, G. (1990) Rare earth elements in Angra dos Reis and Lewis Cliff
1857 86010, two meteorites with similar but distinct magma evolutions. Earth and Planetary
1858 Science Letters, 97, 369-381.
1859 Davis, A.M. (2011) Stardust in meteorites. Proceedings of the National Academy of Sciences
1860 USA, 108, 19142-19146.
1861 Davis, A.M. (2014) Meteorites and Cosmochemical Processes: Treatise on Geochemistry,
1862 Volume 1, Second edition. Elsevier-Pergamon.

1863 Davis, A.M., and Olsen, E.J. (1991) Phosphates in pallasite meteorites as probes of mantle
1864 processes in small planetary bodies. Nature, 353, 637-640.
1865 Davison, T.M., Collins, G.S., and Ciesla, F.J. (2010) Numerical modeling of heating in porous
1866 planetesimal collisions. Icarus, 208, 468–481.
1867 Day, J.M.D., Ash, R.D., Liu, Y., Bellucci, J.J., Rumble, D., McDonough, W.F., Walker, R.J.,
1868 and Taylor, L.A. (2009) Early formation of evolved asteroidal crust. Nature, 457, 179–182.
1869 Day, J.M.D., Walker, .R.J, Ash, R.D., Liu, Y., Rumble, D., Irving, A.J., Goodrich, C.A., Tait, K.,
1870 McDonough, W.F., and Taylor, L.A. (2012) Origin of felsic achondrites Graves Nunataks
1871 06128 and 06129, and ultramafic brachinites and brachinite-like achondrites by partial
1872 melting of volatile-rich primitive parent bodies. Geochimica et Cosmochimica Acta, 81, 94–
1873 128.
1874 Deer, W.A., Howie, R.A., and Zussman, J. (1962) Rock-Forming Minerals. Volume 1B.
1875 Disilicates and Ring Silicates. Longman Scientific & Technical.
1876 Deer, W.A., Howie, R.A., and Zussman, J. (1997) Rock-Forming Minerals. Volume 2A. Single-
1877 Chain Silicates. The Geological Society of London.
1878 Delaney, J.S., Prinz, M., and Takeda, H. (1984) The polymict eucrites. Journal of Geophysical
1879 Research, 89, C251-C288.
1880 Dera, P., Prewitt, C.T., Boctor, N.Z., and Hemley, R.J. (2002) Characterization of a high-
1881 pressure phase of silica from the Martian meteorite Shergotty. American Mineralogist, 87,
1882 1018-1023.
1883 Dera, P., Lavina, B., Borkowski, L.A., Prakapenka, V.B., Sutton, S.R., Rivers, M.L., Downs,
1884 R.T., Boctor, N.Z., and Prewitt, C.T. (2008) High-pressure polymorphism of Fe_2P and its
1885 implications for meteorites and Earth's core. Geophysical Research Letters, 35, #L10301.

1886 Dodd, R.T., and Jarosewich, E. (1979) Incipient melting in and shock classification of L-group
1887 chondrites. Earth and Planetary Science Letters, 44, 335-340.
1888 Dodd, R.T., and Jarosewich, E. (1982) The composition of incipient shock melts in L6
1889 chondrites. Earth and Planetary Science Letters, 59, 355-363.
1890 Domanik, K., Kolar, S., Musselwhite, D., and Drake, M.J. (2004) Accessory silicate mineral
1891 assemblages in the Bilanga diogenite: A petrographic study. Meteoritics & Planetary Science,
1892 39, 567-579.
1893 Downes, H., Mittlefehldt, D.W., Kita, N.T., and Valley, J.W. (2008) Evidence from polymict
1894 ureilite meteorites for a disrupted and re-accreted single ureilite parent asteroid gardened by
1895 several distinct impactors. Geochimica et Cosmochimica Acta, 72, 4825–4844.
1896 Drake, M.J. (2001) The eucrite/Vesta story. Meteoritics & Planetary Science, 36, 501–513.
1897 Dupré, J. (1981) Natural kinds and biological taxa. Philosophical Review, 90, 66-90.
1898 Ebihara, M., Ikeda, Y., and Prinz, M. (1997) Petrology and chemistry of the Miles IIE iron. II:
1899 Chemical characteristics of the Miles silicate inclusions. Proceedings of the NIPR Symposium
1900 on Antarctic Meteorites, 21, 373-388.
1901 El Goresy, A. (1971) Meteoritic rutile: a niobium bearing mineral. Earth and Planetary Science
1902 Letters, 11, 359-361.
1903 El Goresy, A., and Donnay, G. (1968) A new allotropic form of carbon from the Ries Crater.
1904 Science, 161, 363-364.
1905 El Goresy, A., Wopenka, B., Chen, M., Weinbruch, S., and Sharp, T. (1997) Evidence for two
1906 different shock induced high-pressure events and alkali-vapor metasomatism in Peace River
1907 and Tenham (L6) chondrites. Lunar and Planetary Science, 28, #1044.

El Goresy, A., Dera, P., Sharp, T.G., Prewitt, C.T., Chen, M., Dubrovinsky, L., Wopenka, B., Boctor, N.Z., and Hemley, R.J. (2008) Seifertite, a dense orthorhombic polymorph of silica from the Martian meteorites Shergotty and Zagami. European Journal of Mineralogy, 20, 523-528.

El Goresy, A., Dubrovinsky, L., Gillet, P., Graup, G., and Chen, M. (2010) Akaogiite: An ultra-dense polymorph of TiO_2 with the baddeleyite-type structure, in shocked garnet gneiss from the Ries Crater, Germany. American Mineralogist, 95, 892-895.

Fagan, T.J., Scott, E.R.D., Keil, K., Cooney, T.F., and Sharma, S.K. (2000) Formation of feldspathic and metallic melts by shock in enstatite chondrite Reckling Peak A80259. Meteoritics & Planetary Science, 35, 319-329.

Fahey, J.J. (1964) Recovery of coesite and stishovite from Coconino Sandstone of Meteor Crater, AZ. American Mineralogist, 49, 1643-1647.

Feng, L., Lin, Y., Hu, S., Xu, l., and Miao, B. (2011) Estimating compositions of natural ringwoodite in the heavily shocked Grove Mountains 052049 meteorite from Raman spectra. American Mineralogist, 96, 1480–1489.

Ferroir, T., Beck, P., Van de Moortèle, B., Bohn, M., Reynard, B., Simonovici, A., El Goresy, A., and Gillet, P. (2008) Akimotoite in the Tenham meteorite: Crystal chemistry and high-pressure transformation mechanisms. Earth and Planetary Science Letters, 275, 26–31.

Fialin, M., Catillon, G., and Andrault, D. (2009) Disproportionation of Fe^{2+} in Al-free silicate perovskite in the laser heated diamond anvil cell as recorded by electron probe microanalysis of oxygen. Physics and Chemistry of Minerals, 36, 183–191.

1929 Floran, R.J. (1978) Silicate petrography, classification, and origin of the mesosiderites: Review
1930 and new observations. Proceedings of the Lunar and Planetary Science Conference, 9, 1053-
1931 1081.
1932 Floss, C., and Crozaz, G. (1993) Heterogeneous REE patterns in oldhamite from the aubrites:
1933 Their nature and origin. Geochimica et Cosmochimica Acta, 57, 4039-4057.
1934 Fogel, R.A. (2001) The role of roedderite in the formation of aubrites. Lunar and Planetary
1935 Science, 32, #2177.
1936 Fogel, R.A. (2005) Aubrite basalt vitrophyres: The missing basaltic component and high-sulfur
1937 silicate melts. Geochimica et Cosmochimica Acta, 69, 1633-1648.
1938 Fritz, J., Greshake, A., and Fernandes, V.A. (2017) Revising the shock classification of
1939 meteorites. Meteoritics & Planetary Science, 52, 1216-1232.
1940 Frondel, C., and Klein, C. (1965) Ureyite, $NaCrSi_2O_6$: A new meteoritic pyroxene. Science, 149,
1941 742-744.
1942 Frondel, C., and Marvin, U.B. (1967) Lonsdaleite, a hexagonal polymorph of diamond. Nature,
1943 214, 587-589.
1944 Fuchs, L.H. (1966) Djerfisherite, alkali copper-iron sulfide, a new mineral from the Kota-Kota
1945 and St. Mark's enstatite chondrites. Science, 153, 166-167.
1946 Fuchs, L.H. (1967) Stanfieldite: A new phosphate mineral from stony-iron meteorites. Science,
1947 158, 910-911.
1948 Fuchs, L.H. (1969a) The phosphate mineralogy of meteorites. In P.M. Millman, Ed., Meteorite
1949 Research, pp. 683-695. Reidel.
1950 Fuchs, L.H. (1969b) Occurrence of cordierite and aluminous orthoenstatite in the Allende
1951 meteorite. American Mineralogist, 4, 1645-1653.

1952 Fuchs, L.H. (1974) Glass inclusions of granitic compositions in orthopyroxene from three
1953 enstatite achondrites. Meteoritics, 9, 342.
1954 Fuchs, L.H., Olsen, E., and Henderson, E.P. (1967) On the occurrence of brianite and panethite,
1955 two new phosphate minerals from the Dayton meteorite. Geochimica et Cosmochimica Acta,
1956 31, l711-1719.
1957 Garvie, L.A.J., Németh, P., and Buseck, P.R. (2011) Diamond, bucky-diamond, graphite-
1958 diamond, Al-silicate, and stishovite in the Gujba CB chondrite. Meteoritics & Planetary
1959 Science, 46, Supplement 1, 5227.
1960 Garvie, L.A.J., Ma, C., Ray, S., Domanik, K., Wittmann, A., and Wadhwa, M. (2020)
1961 Carletonmooreite, Ni_3Si, a new silicide from the Norton County, aubrite meteorite. American
1962 Mineralogist, in press.
1963 Gasparik, T. (1990) Phase relations in the transition zone. Journal of Geophysical Research, 95,
1964 15,751–15,769.
1965 German, V.N., Podurets, M.A., and Trunin, R.F. (1973) Shock compression of quartz to 90 GPa.
1966 Soviet Physics, Journal of Experimental and Theoretical Physics, 37, 107–115.
1967 Gillet, P., Chen, M., Dubrovinsky, L., and El Goresy, A. (2000) Natural $NaAlSi_3O_8$-hollandite in
1968 the shocked Sixiangkou meteorite. Science, 287, 1633-1636.
1969 Glass, B.P., Liu, S., and Leavens, P.B. (2002) Reidite: an impact-produced high-pressure
1970 polymorph of zircon found in marine sediments. American Mineralogist, 87, 562-565.
1971 Goldstein, J.I., and Michael, J.R. (2006) The formation of plessite in meteoritic metal.
1972 Meteoritics & Planetary Science, 41, 553-570.
1973 Goldstein, J.I., Scott, E.R.D., and Chabot, N.L. (2009) Iron meteorites: Crystallization, thermal
1974 history, parent bodies, and origin. Chemie der Erde, 69, 293–325.

1975 Gomes, C.B., and Keil, K. (1980) Brazilian Stone Meteorites. University of New Mexico Press.

1976 Goodrich, C.A. (1986) Trapped primary silicate liquid in ureilites. Lunar and Planetary Science,
1977 17, 273-274.

1978 Goodrich, C.A. (1992) Ureilites: A critical review. Meteoritics, 27, 252–327.

1979 Goodrich, C.A., and Berkley, J.L. (1986) Primary magmatic carbon in ureilites: Evidence from
1980 cohenite-bearing spherules. Geochimica et Cosmochimica Acta, 50, 681-691.

1981 Goodrich, C.A., Scott, E.R.D., and Fioretti, A.M. (2004) Ureilitic breccias: Clues to the
1982 petrologic structure and impact disruption of the ureilite parent asteroid. Chemie der Erde –
1983 Geochemistry, 64, 283–327.

1984 Goodrich, C.A., Van Orman, J.A., and Wilson, L. (2007) Fractional melting and smelting on the
1985 ureilite parent body. Geochimica et Cosmochimica Acta, 71, 2876-2895.

1986 Goodrich, C.A., Hutcheon, I.D., Kita, N.T., Huss, G.R., Cohen, B.A., and Keil, K. (2010) ^{53}Mn–
1987 ^{53}Cr and ^{26}Al–^{26}Mg ages of a feldspathic lithology in polymict ureilites. Earth and Planetary
1988 Science Letters, 295, 531–540.

1989 Goodrich, C.A., Wilson, L., Van Orman, J.A., and Michel, P. (2013) Comment on 'Parent body
1990 depth-pressure-temperature relationships and the style of the ureilite anatexis' by PH Warren
1991 (MAPS 47: 209–227). Meteoritics & Planetary Science, 48, 1096-1106.

1992 Goodrich, C.A., Harlow, G.E., Van Orman, J.A., Sutton, S.R., Jercinovic, M.J., and Mikouchi, T.
1993 (2014) Petrology of chromite in ureilites: Deconvolution of primary oxidation states and
1994 secondary reduction processes. Geochimica et Cosmochimica Acta, 135, 126-169.

1995 Göpel, C., Manhès, G., and Allègre, C.J. (1985) Concordant 3,676 Ma U-Pb formation age for
1996 the Kodaikanal iron meteorite. Nature, 317, 341-344.

1997 Grady, M.M., and Wright, I. (2006) Types of extraterrestrial material available for study. In:
1998 D.S. Lauretta and H.Y. McSween Jr, Eds., Meteorites and the Early Solar System II, pp. 3-18.
1999 University of Arizona Press.
2000 Graham, A.L., Easton, A.J., and Hutchison, R. (1977) The Mayo Belwa meteorite: a new
2001 enstatite achondrite fall. Mineralogical Magazine, 41, 487-492.
2002 Grew, E.S., Yates, M.G., Beane, R.J., Floss, C., and Gerbi, C. (2010) Chopinite-sarcopside solid
2003 solution, $[(Mg,Fe)_3\square](PO_4)_2$, in GRA95209, a transitional acapulcoite: Implications for
2004 phosphate genesis in meteorites. American Mineralogist, 95, 260-272.
2005 Grew, E.S., Hystad, G., Hazen, R.M., Krivovichev, S.V., and Gorelova, L.A. (2017) How many
2006 boron minerals occur in Earth's upper crust? American Mineralogist, 102, 1573-1587.
2007 Grieve, R.A.F., Langenhorst, F., and Stöffler, D. (1996) Shock metamorphism of quartz in nature
2008 and experiment. 2. Significance in geoscience. Meteoritics & Planetary Science, 31, 6-35.
2009 Haack, H., Rasmussen, K.L., and Warren, P.H. (1990) Effects of regolith/megaregolith
2010 insulation on the cooling histories of differentiated asteroids. Journal of Geophysical
2011 Research, 95, 5111-5124.
2012 Haba, M.K., Yamaguchi, A., Horie, K., and Hidaka, H. (2014) Major and trace elements of
2013 zircons from basaltic eucrites: Implications for the formation of zircons on the eucrite parent
2014 body. Earth and Planetary Science Letters, 387, 10-21.
2015 Harlow, G.E., Nehru, C.E., Prinz, M., Taylor, G.J., and Keil, K. (1979) Pyroxenes in Serra de
2016 Mage: Cooling history in comparison with Moama and Moore County. Earth and Planetary
2017 Science Letters, 43, 173-181.
2018 Hawley, K. and Bird, A. (2011) What are natural kinds? Philosophical Perspectives, 25, 205-221.

Hazen, R.M. (2019) An evolutionary system of mineralogy: Proposal for a classification based on natural kind clustering. American Mineralogist, 104, 810-816.

Hazen, R.M. and Ausubel, J.H. (2016) On the nature and significance of rarity in mineralogy. American Mineralogist, 101, 1245-1251.

Hazen, R.M., and Finger, L.W. (1978) Crystal chemistry of silicon-oxygen bonds at high pressure: Implications for the Earth's mantle mineralogy. Science, 201, 1122-1123.

Hazen, R.M., and Morrison, S.M. (2020) An evolutionary system of mineralogy, Part I: stellar mineralogy (>13 to 4.6 Ga). American Mineralogist, 105, 627-651.

Hazen, R.M., Papineau, D., Bleeker, W., Downs, R.T., Ferry, J.M., McCoy, T.L., Sverjensky, D.A., and Yang, H. (2008) Mineral evolution. American Mineralogist, 93, 1693-1720.

Hazen, R.M., Grew, E.S., Downs, R.T., Golden, J., and Hystad, G. (2015) Mineral ecology: Chance and necessity in the mineral diversity of terrestrial planets. Canadian Mineralogist, 53, 295-323.

Hazen, R.M., Hystad, G., Downs, R.T., Golden, J., Pires, A., and Grew, E.S. (2015) Earth's "missing" minerals. American Mineralogist, 100, 2344-2347.

Hazen, R.M., Hummer, D.R., Hystad, G., Downs, R.T., and Golden, J.J. (2016) Carbon mineral ecology: Predicting the undiscovered minerals of carbon. American Mineralogist, 101, 889-906.

Hazen, R.M., Morrison, S.M., and Prabhu, A. (2021) An evolutionary system of mineralogy, part III: Primary chondrule mineralogy (4.566 to 4.561 Ga). American Mineralogist, in press.

Heinemann, S., Sharp, T.G., Seifert, F., and Rubie, D.C. (1997) The cubic-tetragonal phase transition in the system majorite ($Mg_4Si_4O_{12}$)–pyrope ($Mg_3Al_2Si_3O_{12}$), and garnet symmetry in the Earth's transition zone. Physics and Chemistry of Minerals, 24, 206–221.

2042 Henderson, E.P. (1941) Chilean hexahedrites and the composition of all hexahedrites. American
2043 Mineralogist, 26, 546-550.
2044 Herrin, J.S., Zolensky, M.E., Ito, M., Le, L., Mittlefehldt, D.W., Jenniskens, P., Ross, A.J., and
2045 Shaddad, M.H. (2010) Thermal and fragmentation history of ureilitic asteroids: insights from
2046 the Almahata Sitta fall. Meteoritics & Planetary Science, 45, 1789–1803.
2047 Hewins, R.H. (1983) Impact versus internal origins for mesosiderites. Journal of Geophysical
2048 Research, 88, B257–B266.
2049 Hewins, R.H., Jones, R.H., and Scott, E.R.D. [Eds.] (1996) Chondrules and the Protoplanetary
2050 Disk. Cambridge University Press.
2051 Hiroi, T., Bell, J.F., Takeda, H., and Pieters, C.M. (1993) Spectral comparison between olivine-
2052 rich asteroids and pallasites. Proceedings of the NIPR Symposium on Antarctic Meteorites, 6,
2053 234-245.
2054 Hollister, L.S., Bindi, L., Yao, N., Poirier, G.R., Andronicos, C.L., MacPherson, G.J., Lin, C.,
2055 Distler, V.V., Eddy, M.P., Kostin, A., Kryachko, V., Steinhardt, W.M., Yudovskaya, M.,
2056 Eiler, J.M., Guan, Y., Clarke, J.J., and Steinhardt P.J. (2014) Impact-induced shock and the
2057 formation of natural quasicrystals in the early solar system. Nature Communications, 5, 4040.
2058 Holtstam, D., Broman, C., Söderhielm, J., and Zetterqvist, A. (2003) First discovery of stishovite
2059 in an iron meteorite. Meteoritics & Planetary Science, 38, 1579–1583.
2060 Hsu, W. (1998) Geochemical and petrographic studies of oldhamite, diopside, and roedderite in
2061 enstatite meteorites. Meteoritics & Planetary Science, 33, 291-301.
2062 Hu, J., Asimow, P.D., and Ma, C. (2019) First shock synthesis of khatyrkite, stolperite and a
2063 newly-found natural quasicrystal: Implciations for the impact origin of quasicrystals from the
2064 Khatyrka meteorite. Lunar and Planetary Science, 50, 3126.

Hubbard, A. (2016) Ferromagnetism and particle collisions: Applications to protoplanetary disks and the meteoritical record. The Astrophysical Journal, 826, 152 (10 pp).

Hutchison, R. (2004) Meteorites: A Petrologic, Chemical and Isotopic Synthesis. Cambridge University Press.

Hwang, S.L., Shen, P., Chu, H.T., Yui, T.F., Varela, M.E., and Iizuka, Y. (2016) Kuratite, $Ca_4(Fe_{10}^{2+}Ti_2)O_4[Si_8Al_4O_{36}]$, the Fe^{2+}-analogue of rhönite, a new mineral from the D'Orbigny angrite meteorite. Mineralogical Magazine, 80, 1067-1076.

Hwang, S.L., Shen, P., Chu, H.T., Yui, T.F., Varela, M.E., and Iizuka, Y. (2019) New minerals tsangpoite $Ca_5(PO_4)_2(SiO_4)$ and matyhite $Ca_9(Ca_{0.5}\square_{0.5})Fe(PO_4)_7$ from the D'Orbigny angrite. Mineralogical Magazine, 83, 293-313.

Hystad, G., Downs, R.T., and Hazen, R.M. (2015) Mineral frequency distribution data conform to a LNRE model: Prediction of Earth's "missing" minerals. Mathematical Geosciences, 47, 647-661.

Hystad, G., Downs, R.T., Grew, E.S., and Hazen, R.M. (2015) Statistical analysis of mineral diversity and distribution: Earth's mineralogy is unique. Earth and Planetary Science Letters, 426, 154-157.

Hystad, G., Downs, R.T., Hazen, R.M., and Golden, J.J. (2017) Relative abundances for the mineral species on Earth: A statistical measure to characterize Earth-like planets based on Earth's mineralogy. Mathematical Geosciences, 49, 179-194.

Hystad, G., Eleish, A., Downs, R.T., Morrison, S.M., and Hazen, R.M. (2019) Bayesian estimation of Earth's undiscovered mineralogical diversity using noninformative priors. Mathematical Geosciences, 51, 401-417.

2087 Ikeda, Y., and Takeda, H. (1985) A model for the origin of basaltic achondrites based on the
2088 Yamato 7308 howardite. Journal of Geophysical Research, 90, C649-C663.
2089 Ireland T.R., and Wlotzka F. (1992) The oldest zircons in the solar system. Earth and Planetary
2090 Science Letters, 109, 1-10.
2091 Irifune T., Ringwood, A.E., and Hibberson, W.O. (1994) Subduction of continental crust and
2092 terrigenous and pelagic sediments: An experimental study. Earth and Planetary Science
2093 Letters, 126, 351-368.
2094 Isa, J., Ma, C., and Rubin, A.E. (2016) Joegoldsteinite: A new sulfide mineral ($MnCr_2S_4$) from
2095 the Social Circle IVA iron meteorite. American Mineralogist, 101, 1217-1221.
2096 Ivanov, A.V., Zolensky, M.E., Saito, A., Ohsumi, K., MacPherson, G.J., Yang S.V., Kononkova,
2097 N.N., and Mikouchi, T. (2000) Florenskyite, FeTiP, a new phosphide from the Kaidun
2098 meteorite. American Mineralogist, 85, 1082–1086.
2099 Jambon, A., Barrat, J.A., Boudouma, O., Fonteilles, M., Badia, D., Göpel, C., and Bohn, M.
2100 (2005) Mineralogy and petrology of the angrite Northwest Africa 1296. Meteoritics &
2101 Planetary Science, 40, 361–375.
2102 Jambon, A., Boudouma, O., Fonteilles, M., Le Guillou, C., Badia, D., and Barrat, J.A. (2008)
2103 Petrology and mineralogy of the angrite Northwest Africa 1670. Meteoritics & Planetary
2104 Science, 43, 1783–1795.
2105 Johansen, A., Oishi, J.S., Mac Low, M.-M., Klahr, H., Henning, T., and Youdin, A. (2007) Rapid
2106 planetesimal formation in turbulent circumstellar disks. Nature 448, 1022-1025.
2107 Joreau, P., Leroux, H., and Doukhan, J.C. (1996) A transmission electron microscopy (TEM)
2108 investigation of opaque phases in shocked chondrites. Meteoritics, 31, 305-312.

2109 Kaneko, S., Miyahara, M., Ohtani, E., Arai, T., Hirao, N., and Sato, K. (2015) Discovery of
2110 stishovite in Apollo 15299 sample. American Mineralogist, 100, 1308–1311.
2111 Karwowski, Ł., Kusz, J., MuszyŃski, A., Kryza, R., Sitarz, M., and Galuskin, E.V. (2015)
2112 Moraskoite, $Na_2Mg(PO_4)F$, a new mineral from the Morasko IAB-MG iron meteorite
2113 (Poland). Mineralogical Magazine, 79, 387-398.
2114 Kato, Y., Sekine, T., Kayama, M., Miyahara, M., and Yamaguchi, A. (2017). High-pressure
2115 polymorphs in Yamato-790729 L6 chondrite and their significance for collisional conditions.
2116 Meteoritics & Planetary Science, 52, 2570-2585.
2117 Keil, K. (2000) Thermal alteration of asteroids: Evidence from meteorites. Planetary and Space
2118 Science, 48, 887–903.
2119 Keil, K. (2010) Enstatite achondrite meteorites (aubrites) and the histories of their asteroidal
2120 parent bodies. Chemie der Erde – Geochemistry, 70, 295–317.
2121 Keil, K. (2012) Angrites, a small but diverse suite of ancient, silica-undersaturated asteroidal
2122 volcanic-plutonic mafic meteorites, and the history of their parent asteroid. Chemie der Erde –
2123 Geochemistry, 72, 191–218.
2124 Keil, K., and Brett, R. (1974) Heideite, $(Fe,Cr)_{1+x}(Ti,Fe)_2S_4$: a new mineral in the Bustee
2125 enstatite achondrite. American Mineralogist, 59, 465-470.
2126 Keil, K., and Fredriksson, K. (1963) Electron microprobe analysis of some rare minerals in the
2127 Norton County achondrite. Geochimica et Cosmochinca Acta, 27, 939-947.
2128 Keil, K., and Snetsinger, K.G. (1967) Niningerite, a new meteoritic sulfide. Science, 155, 451-
2129 453.

2130 Keil, K., Berkley, J.L., and Fuchs, L.H. (1982) Suessite, Fe_3Si: A new mineral in the North Haig
2131 ureilite. American Mineralogist, 67, 126-131.
2132 Keil, K., Haack, H., and Scott, E.R.D. (1994) Catastrophic fragmentation of asteroids – evidence
2133 from meteorites. Planetary and Space Science, 42, 1109–1122.
2134 Kelly, W.R., and Larimer, J.W. (1977) Chemical fractionation in meteorites-VII. Iron meteorites
2135 and the cosmochemical history of the metal phase. Geochimica et Cosmochimica Acta, 41,
2136 93-111.
2137 Kerridge, J.F., and Matthews, M.S. (1988) Meteorites and the Early Solar System. University of
2138 Arizona Press.
2139 Kerschhofer, L., Sharp, T.G., and Rubie, D.C. (1996) Intracrystalline transformation of olivine to
2140 wadsleyite and ringwoodite under subduction zone conditions. Science, 274, 79–81.
2141 Kerschhofer, L., Dupas, C., Liu, M., Sharp, T.G., Durham, W.B., and Rubie, D.C. (1998)
2142 Polymorphic transformations between olivine, wadsleyite and ringwoodite: Mechanisms of
2143 intracrystalline nucleation and the role of elastic strain. Mineralogical Magazine, 62, 617–638.
2144 Kimura, M., Suzuki, A., Kondo, T., Ohtani, E., and El Goresy, A. (2000) Natural occurrence of
2145 high-pressure phases jadeite, hollandite, wadsleyite, and majorite-pyrope garnet in an H
2146 chondrite, Yamato 75100. Meteoritics & Planetary Sciences, 35, A87–A88.
2147 Kimura, M., Chen, M., Yoshida, T., El Goresy, A., and Ohtani, E. (2003) Back-transformation of
2148 high-pressure phases in a shock melt vein of an H-chondrite during atmospheric passage:
2149 Implications for the survival of high-pressure phases after decompression. Earth and Planetary
2150 Science Letters, 217, 141–150.
2151 Koeberl, C. (2014) The geochemistry and cosmochemistry of impacts. Treatise on
2152 Geochemistry, 2nd edition, 1, 73-118.

2153 Kracher, A., and Wasson, J.T. (1982) The role of S in the evolution of the parental cores of the
2154 iron meteorites. Geochimica et Cosmochimica Acta, 46, 2419–2426.
2155 Kracher, A., Kurat, G., and Buchwald, V.F. (1977) Cape York: The extraordinary mineralogy of
2156 an ordinary iron meteorite and its implication for the genesis of III AB irons. Geochemical
2157 Journal, 11, 207-217.
2158 Kring, D.A., Boynton, W.V., Hill, D.H., and Haag, R.A. (1991) Petrologic description of Eagles
2159 Nest: A new olivine achondrite. Meteoritics, 26, 360.
2160 Krot, A.N., Keil, K., Scott, E.R.D., Goodrich, C.A., and Weisberg, M.K. (2014) Classification of
2161 meteorites and their genetic relationships. Treatise on Geochemistry, 2nd edition, 1, 2-63.
2162 Kruijer, T.S., Burkhardt, C., Budde, G., and Kleine, T. (2017) Age of Jupiter from the distinct
2163 genetics and formation times of meteorites. Proceedings of the National Academy of Sciences
2164 USA, 114, (5 p.). Doi: 10.1073/pnas.1704461114.
2165 Kuwayama, Y. (2008) Ultrahigh pressure and high temperature experiments using a laser heated
2166 diamond anvil cell in multimegabar pressures region. The Review of High-Pressure Science
2167 and Technology, 18, 3–10.
2168 Langenhorst, F., and Poirier, J.-P. (2000) 'Eclogitic' minerals in a shocked basaltic meteorite.
2169 Earth and Planetary Science Letters, 176, 259-265.
2170 Litasov, K.D., Teplyakova, S.N., Shatskiy, A., and Kuper, K.E. (2019) Fe-Ni-PS melt pockets in
2171 Elga IIE iron meteorite: Evidence for the origin at high pressures up to 20 Gpa. Minerals, 9,
2172 616 (11 p.).
2173 Liu, L.G. (1978) High-pressure phase transformations of albite, jadeite and nepheline. Earth and
2174 Planetary Science Letters, 37, 438–444.

Liu, X. (2006) Phase relations in the system $KAlSi_3O_8$—$NaAlSi_3O_8$ at high pressure-high temperature conditions and their implication for the petrogenesis of lingunite. Earth and Planetary Science Letters, 246, 317-325.

Liu, L.G., and El Gorsey, A. (2007) High-pressure phase transitions of the feldspars, and further characterization of lingunite. International Geology Review, 49, 854-860.

Liu, L.G., and Ringwood, A.E. (1975) Synthesis of a perovskite-type polymorph of $CaSiO_3$. Earth and Planetary Science Letters, 28, 209–211.

Lodders, K. (1996) An experimental and theoretical study of rare-earth-element partitioning between sulfides (FeS,CaS) and silicate and applications to enstatite achondrites. Meteoritics & Planetary Science, 31, 749-766.

Lodders, K., and Amari, S. (2005) Presolar grains from meteorites: Remnants from the early times of the solar system. Chemie der Erde, 65, 93-166.

Longhi, J. (1999) Phase equilibrium constraints on angrite petrogenesis. Geochimica et Cosmochimica Acta, 63, 573–585.

Lovering, J.F. (1975) The Moama eucrite-A pyroxene-plagioclase adcumulate. Meteoritics, 10, 101-114.

Lugaro, M. (2005) Stardust from Meteorites: An Introduction to Presolar Grains. World Scientific.

Lunning, N.G., Corrigan, C.M., McSween, H.Y., Tenner, T.J., Kita, N.T., and Bodnar, R.J. (2016) CV and CM chondrite impact melts. Geochimica et Cosmochimica Acta, 189, 338-358.

Ma, C. (2018) A closer look at shock meteorites: Discovery of new high-pressure minerals. American Mineralogist, 103, 1521-1522.

2198 Ma, C., and Prakapenka, V. (2018) Tschaunerite, IMA 2017-032a. Mineralogical Magazine, 82,
2199 1369-1379.

2200 Ma, C., and Rubin, A.E. (2019) Edscottite, Fe_5C_2, a new iron carbide mineral from the Ni-rich
2201 Wedderburn IAB meteorite. American Mineralogist, 104, 1351-1355.

2202 Ma, C. and Tschauner, O. (2016) Discovery of tetragonal almandine,
2203 $(Fe,Mg,Ca,Na)_3(Al,Si,Mg)_2Si_3O_{12}$, a new high-pressure mineral in Shergotty. Meteoritics &
2204 Planetary Science, 51, Supplement 1, #6124.

2205 Ma, C., and Tschauner, O. (2017) Zagamiite, IMA 2015-022a. European Journal of Mineralogy,
2206 29, 339–344.

2207 Ma, C., and Tschauner, O. (2018a) Liuite, IMA 2017-042a. Mineralogical Magazine, 82, 1369-
2208 1379.

2209 Ma, C., and Tschauner, O. (2018b) Feiite, IMA 2017-041a. Mineralogical Magazine, 82, 1369-
2210 1379.

2211 Ma, C., Beckett, J.R., and Rossman, G.R. (2012a) Buseckite, (Fe,Zn,Mn)S, a new mineral from
2212 the Zakłodzie meteorite. American Mineralogist, 97, 1226-1233.

2213 Ma, C., Beckett, J.R., and Rossman, G.R. (2012b) Browneite, MnS, a new sphalerite-group
2214 mineral from the Zakłodzie meteorite. American Mineralogist, 97, 2056-2059.

2215 Ma, C., Tschauner, O., Beckett, J.R., Liu, Y., Rossman, G.R., Zhuravlev, K., Prakapenka, V.,
2216 Dera, P,, and Taylor, L.A. (2015) Tissintite, $(Ca,Na,\square)AlSi_2O_6$, a highly-defective, shock-
2217 induced, high-pressure clinopyroxene in the Tissint martian meteorite. Earth and Planetary
2218 Science Letters, 422, 194-205.

2219 Ma, C., Tschauner, O., Beckett, J.R., Liu, Y., Rossman, G.R., Sinogeikin, S.V., Smith, J.S., and
2220 Taylor, L.A. (2016) Ahrensite, γ-Fe_2SiO_4, a new shock-metamorphic mineral from the Tissint
2221 meteorite: Implications for the Tissint shock event on Mars. Geochimica et Cosmochimica
2222 Acta, 184, 240-256.
2223 Ma, C., Lin, C., Bindi, L., and Steinhardt, P. J. (2017a) Hollisterite (Al_3Fe), kryachkoite
2224 $(Al,Cu)_6(Fe,Cu)$, and stolperite (AlCu): Three new minerals from the Khatyrka CV3
2225 carbonaceous chondrite. American Mineralogist, 102, 690-693.
2226 Ma, C., Tschauner, O., and Beckett, J.R. (2017b) A new high-pressure calcium aluminosilicate
2227 ($CaAl_2Si_{3.5}O_{11}$) in martian meteorites: another after-life for plagioclase and connections to
2228 the CAS phase. Lunar and Planetary Science, 48, 1128.
2229 Ma, C., Tschauner, O., Beckett, J.R., Rossman, G.R., Prescher, C., Prakapenka, V.B., Bechtel
2230 H.A., and MacDowell, A. (2018) Liebermannite, $KAlSi_3O_8$, a new shock-metamorphic, high-
2231 pressure mineral from the Zagami Martian meteorite. Meteoritics & Planetary Science, 53,
2232 50-61.
2233 Ma, C., Tschauner, O., Beckett, J.R., Liu, Y., Greenberg, E., and Prakapenka, V.B. (2019a)
2234 Chenmingite, $FeCr_2O_4$ in the $CaFe_2O_4$-type structure, a shock-induced, high-pressure mineral
2235 in the Tissint martian meteorite. American Mineralogist, 104, 1521-1525.
2236 Ma, C., Tschauner, O., and Beckett, J.R. (2019b) A closer look at Martian meteorites: Discovery
2237 of the new mineral zagamiite, $CaAl_2Si_{3.5}O_{11}$, a shock-metamorphic, high-pressure, calcium
2238 aluminosilicate. International Conference on Mars, 9, 6138.

2239 Ma, C., Tschauner, O., and Beckett, J.R. (2019c) Discovery of a new high-pressure silicate
2240 phase, $(Fe,Mg,Cr,Ti,Ca,\square)_2(Si,Al)O_4$ with a tetragonal spinelloid structure, in a shock melt
2241 pocket from the Tissint Martian meteorite. Lunar and Planetary Science Conference, 50,
2242 1460.
2243 Ma, C., Tschauner, O., Bindi, L., Beckett, J.R., and Xie, X. (2019d) A vacancy-rich, partially
2244 inverted spinelloid silicate, $(Mg,Fe,Si)_2(Si,\square)O_4$, as a major matrix phase in shock melt veins
2245 of the Tenham and Suizhou L6 chondrites. Meteoritics & Planetary Science, 54, 1907-1918.
2246 Madon, M., and Poirier, J.P. (1980) Dislocations in spinel and garnet high-pressure polymorphs
2247 of olivine and pyroxene: Implications for mantle rheology. Science, 207, 66–68.
2248 Madon, M., and Poirier, J.P. (1983) Transmission electron microscope observation of a, b and c
2249 $(Mg,Fe)_2SiO_4$ in shocked meteorites: Planar defects and polymorphic transitions. Physics of
2250 the Earth and Planetary Interiors, 33, 31–44.
2251 Magnus, P.D. (2012) Scientific Enquiry and Natural Kinds: From Mallards to Planets. Palgrave
2252 MacMillan.
2253 Malavergne, V., Guyot, F., Benzerara, K., and Martinez, I. (2001). Description of new shock-
2254 induced phases in the Shergotty, Zagami, Nakhla and Chassigny meteorites. Meteoritics &
2255 Planetary Science, 36, 1297-1305.
2256 Marvin, U.B. (1962) Cristobalite in the Carbo Iron Meteorite. Nature, 196, 634-636.
2257 Marvin, U.B., Petaev, M.I., Croft, W.J., and Killgore, M. (1997) Silica minerals in the Gibeon
2258 IVA iron meteorite. Lunar and Planetary Science, 28, 879-880.
2259 Mason, B., Nelen, J., and White, J.S. Jr. (1968) Olivine-garnet transformation in a meteorite.
2260 Science, 160, 66–67.

McCammon, C.A. (1997) Perovskite as a possible sink for ferric iron in the lower mantle. Nature, 387, 694–696.

McCord, T.B., Adams, J.B., and Johnson, T.V. (1970) Asteroid Vesta: Spectral reflectivity and compositional implications. Science, 168, 1445–1447.

McCoy, T.J. (1998) A pyroxene-oldhamite clast in Bustee: Igneous aubritic oldhamite and a mechanism for the Ti enrichment in aubritic troilite. Antarctic Meteorite Research, 11, 34-50.

McCoy, T.J., Scott, E.R.D., and Haack, H. (1993) Genesis of the IIICD iron meteorites: Evidence from silicate-bearing inclusions. Meteoritics, 28, 552-560.

McCoy, T.J., Steele, I.M., Keil, K., Leonard, B.F., and Endress, M. (1994) Chladniite, $Na_2CaMg_7(PO_4)_6$: A new mineral from the Carlton (IIICD) iron meteorite. American Mineralogist, 79, 375-380.

McCoy, T.J., Ehlmann, A.J., Benedix, G.K., Keil, K., and Wasson, J.T. (1996) The Lueders, Texas, IAB iron meteorite with silicate inclusions. Meteoritics and Planetary Science, 31, 419-422.

McCoy, T.J., Mittlefehldt, D., and Wilson, L. (2006) Asteroid differentiation. In D.S. Lauretta and H.Y. McSween Jr., Eds., Meteorites and the Early Solar System II, pp. 733-745. University of Arizona Press.

McKay, G., Lindstrom, D., Yang, S.-R., and Wagstaff, J. (1988) Petrology of a unique achondrite Lewis Cliff 86010. Lunar and Planetary Science, 19, 762-763.

McKay, G., Crozaz, G., Wagstaff, J., Yang, S.-R., and Lundberg, L. (1990) A petrographic, electron microprobe, and ion microprobe study of mini-angrite Lewis Cliff 87051. Lunar and Planetary Science, 21, 771-772.

2283 McSween, H.Y. Jr. (1999) Meteorites and Their Parent Planets, Second Edition. Cambridge
2284 University Press.
2285 McSween, H.Y., Mittlefehldt, D.W., Beck, A.W., Mayne, R.G., and McCoy, T.J. (2011) HED
2286 meteorites and their relationship to the geology of Vesta and the Dawn Mission. Space
2287 Science Reviews, 163, 141–174.
2288 Mikouchi, T., Takeda, H., Miyamoto, M., Ohsumi, K., and McKay, G.A. (1995) Exsolution
2289 lamellae of kirschsteinite in magnesium-iron olivine from an angrite meteorite. American
2290 Mineralogist, 80, 585-592.
2291 Mikouchi, T., Miyamoto, M., and McKay, G.A. (1996) Mineralogical study of angrite Asuka-
2292 881371: Its possible relation to angrite LEW87051. Proceedings of the NIPR Symposium on
2293 Antarctic Meteorites, 9, 174–188.
2294 Mikouchi, T., Zolensky, M.E., Ivanova, M., Tachikawa, O., Komatsu, M., Le, L., and Gounelles,
2295 M. (2009) Dmitryivanovite: A new high-pressure calcium aluminum oxide from the
2296 Northwest Africa 470 CH3 chondrite characterized using electron back-scatter diffraction
2297 analysis. American Mineralogist, 94, 746-750.
2298 Mikouchi, T., Sugiyama, K., Satake, W., and Amelin, Y. (2011) Mineralogy and crystallography
2299 of calcium silico-phosphate in Northwest Africa 4590 angrite. Lunar and Planetary Science,
2300 42, 2026.
2301 Mills, S.J., Hatert, F., Nickel, E.H., and Ferrais, G. (2009) The standardization of mineral group
2302 hierarchies: Application to recent nomenclature proposals. European Journal of Mineralogy,
2303 21, 1073-1080.
2304 Mittlefehldt, D.W. (1994) The genesis of diogenites and HED parent body petrogenesis.
2305 Geochimica et Cosmochimica Acta, 58, 1537-1552.

2306 Mittlefehldt, D.W. (2014) Achondrites. Treatise on Geochemistry, 2nd edition, 1, 235-266.

2307 Mittlefehldt, D.W., and Lindstrom, M.M. (1990) Geochemistry and genesis of the angrites.
2308 Geochimica et Cosmochimica Acta, 54, 3209–3218.

2309 Mittlefehldt, D.W., and Lindstrom, M.M. (1993) Geochemistry and petrology of a suite of ten
2310 Yamato HED meteorites. Proceedings of the NIPR Symposium on Antarctic Meteorites, 6,
2311 268-292.

2312 Mittlefehldt, D.W., McCoy, T.J., Goodrich, C.A., and Kracher, A. (1998) Non-chondritic
2313 meteorites from asteroidal bodies. Reviews in Mineralogy, 36, 4.1-4.195.

2314 Mittlefehldt, D.W., Killgore, M., and Lee, M.T. (2002) Petrology and geochemistry of
2315 D'Orbigny, geochemistry of Sahara 99555, and the genesis of angrites. Meteoritics &
2316 Planetary Science, 37, 345–369.

2317 Miyahara, M., El Goresy, A., Ohtani, E., Nagase, T., Nishijima, M., Vashaei, Z., Ferroir, T.,
2318 Gillet, P., Dubrovinsky, L., and Simionovici, A. (2008) Evidence for fractional crystallization
2319 of wadsleyite and ringwoodite from olivine melts in chondrules entrained in shock-melt veins.
2320 Proceedings of the National Academy of Sciences USA, 105, 8542–8547.

2321 Miyahara, M., Ohtani, E., Kimura, M., El Goresy, A., Ozawa, S., Nagase, T., Nishijima, M., and
2322 Hiraga, K. (2010) Coherent and subsequent incoherent ringwoodite growth in olivine of
2323 shocked L6 chondrites. Earth and Planetary Science Letters, 295, 321–327.

2324 Miyahara, M., Kaneko, S., Ohtani, E., Sakai, T., Nagase, T., Kayama, M., Nishido, H., and
2325 Hirao, N. (2013a) Discovery of seifertite in a shocked lunar meteorite. Nature
2326 Communications, 4, 1737.

2327 Miyahara, M., Ozawa, S., Ohtani, E., Kimura, M., Kubo, T., Sakai, T., Nagase, T., Nishijima,
2328 M., and Hirao, N. (2013b) Jadeite formation in shocked ordinary chondrites. Earth and
2329 Planetary Science Letters, 373, 102–108.
2330 Miyajima, N., El Goresy, A., Dupas-Bruzek, C., Seifert, F., Rubie, D.C., Chen, M., and Xie, X.
2331 (2007): Ferric iron in Al-bearing akimotoite coexisting with iron-nickel metal in a shock-melt
2332 vein in an L-6 chondrite. American Mineralogist, 92, 1545-1549.
2333 Moggi Cecchi, V., Caporali, S., and Pratesi, G. (2015) DaG 1066: a newfound anomalous ureilite
2334 with chondritic inclusions. Meteoritics & Planetary Science, 50, Supplement 1, 5252.
2335 Mori, H., and Takeda, H. (1981a) Thermal and deformational histories of diogenites as inferred
2336 from their microtextures of orthopyroxene. Earth and Planetary Science Letters, 53, 266-274.
2337 Mori, H., and Takeda, H. (1981b) Evolution of the Moore County pyroxenes as viewed by an
2338 analytical transmission electron microprobe (ATEM). Meteoritics, 16, 362-363.
2339 Morimoto, N., Fabries, J., Ferguson, A.K., Ginzburg, I.V., Ross, M., Seifert, F.A., Zussman, J.,
2340 Aoki, K., and Gottardi, G. (1988) Nomenclature of pyroxenes. American Mineralogist, 73,
2341 1123–1133.
2342 Moore, C.B., Lewis, C.F., and Nava, D. (1969) Superior analysis of iron meteorites. In: P.M.
2343 Millman, Ed., Meteorite Research, pp. 738–748. Reidel.
2344 Morrison, S.M., and Hazen, R.M. (2020) An evolutionary system of mineralogy, Part II:
2345 interstellar and solar nebula primary condensation mineralogy (> 4.565 Ga). American
2346 Mineralogist, in press.
2347 Mostefaoui, S., Lugmair, G.W., and Hoppe, P. (2005) ^{60}Fe: A heat source for planetary
2348 differentiation from a nearby Supernova explosion. The Astrophysical Journal, 625, 271–277.

Murayama, J.K., Nakai, S., Kato, M., and Kumazawa, M. (1986) A dense polymorph of $Ca_3(PO_4)_2$: A high pressure phase of apatite decomposition and its geochemical significance. Physics of the Earth and Planetary Interiors 44:293–303.

Nehru, C.E., Delaney, J.S., Harlow, G.E., and Prinz, M. (1980) Mesosiderite basalts and the eucrites. Meteoritics, 15, 337-338.

Nehru, C.E., Prinz, M., and Delaney, J.S. (1982) The Tucson iron and its relationship to enstatite meteorites. Journal of Geophysical Research, B87, Supplement I, A365-A373.

Nehru, C.E., Prinz, M., Delaney, J.S., Dreibus, G., Palme, H., Spettel, B., and Wanke, H. (1983) Brachina: A new type of meteorite, not a Chassignite. Journal of Geophysical Research, 88, B237-B244.

Nehru, C.E., Prinz, M., Weisberg, M.K., Ebihara, M.E., Clayton, R.N., and Mayeda, T.K. (1992) Brachinites: A new primitive achondrite group. Meteoritics, 27, 267.

Nehru, C.E., Prinz, M., Weisberg, M.K., Ebihara, M.E., Clayton, R.N., and Mayeda, T.K. (1996) A new brachinite and petrogenesis of the group. Lunar and Planetary Science, 27, 943-944.

Németh, P, Garvie, L.A., Aoki. T., Dubrovinskaia, N., Dubrovinsky, L., and Buseck, P.R. (2014) Lonsdaleite is faulted and twinned cubic diamond and does not exist as a discrete material. Nature Communications, 5, 5447.

Nielsen, H.P., and Buchwald, V.F. (1981) Roaldite, a new nitride in iron meteorites. Geochimica et Cosmochimica Acta, Supplement, 16, 1343-1348.

Niemeyer, S. (1979a) I-Xe dating of silicate and troilite from IAB iron meteorites. Geochimica et Cosmochimica Acta, 43, 843-860.

Niemeyer, S. (1979b) ^{40}Ar-^{39}Ar dating of inclusions from IAB iron meteorites. Geochimica et Cosmochimica Acta, 43, 1829-1840.

2372 Nittler, L.R., and Ciesla, F. (2016) Astrophysics with extraterrestrial materials. Annual Reviews
2373 of Astronomy and Astrophysics, 54, 53-93.
2374 Ohtani, E., Kimura, Y., Kimura, M., Takata, T., Kondo, T., and Kubo, T. (2004) Formation of
2375 high-pressure minerals in shocked L6 chondrite Yamato 791384: Constraints on shock
2376 conditions and parent body size. Earth and Planetary Science Letters, 227, 505–515.
2377 Ohtani, E., Ozawa, S., Miyahara, M., Ito, Y., Mikouchi, T., Kimura, M., Arai, T., Sato, K., and
2378 Hiraga, K. (2011). Coesite and stishovite in a shocked lunar meteorite, Asuka-881757, and
2379 impact events in lunar surface. Proceedings of the National Academy of Sciences, 108, 463-
2380 466.
2381 Okada, A., and Keil, K. (1982) Caswellsilverite, $NaCrS_2$: A new mineral in the Norton County
2382 enstatite achondrite. American Mineralogist, 67, 132-136.
2383 Okada, A., Keil, K., Taylor, G.J., and Newsom, H. (1988) Igneous history of the aubrite parent
2384 asteroid: Evidence from the Norton County enstatite achondrite. Meteoritics, 23, 59-74.
2385 Olsen, E.J. (1967) Amphibole: First occurrence in a meteorite. Science, 156, 61-62.
2386 Olsen, E.J., and Fredriksson, K. (1966) Phosphates in iron and pallasite meteorites. Geochimica
2387 et Cosmochimica Acta, 30, 459–470.
2388 Olsen, E.J., and Fuchs, L. (1968) Krinovite, $NaMg_2CrSi_3O_{10}$: A new meteorite mineral. Science,
2389 161, 786-787.
2390 Olsen, E.J., and Jarosewich, E. (1971) Chondrules: First occurrence in an iron meteorite.
2391 Science, 174, 583-585.
2392 Olsen, E., and Steele, I. (1993) New alkali phosphates and their associations in the IIIAB iron
2393 meteorites. Meteoritics, 28, 415.

2394 Olsen, E.J., and Steele, I.A. (1997) Galileiite: A new meteoritic phosphate mineral. Meteoritics
2395 & Planetary Science, 32, AI55-A156.
2396 Olsen, E.J., Huebner, J.S., Douglas, J.A.V., and Plant, A.G. (1973) Meteoritic amphibole.
2397 American Mineralogist, 58, 869-872.
2398 Olsen, E.J., Erlichman. J., Bunch, T.E., and Moore, P.B. (1977a) Buchwaldite, a new meteoritic
2399 phosphate mineral. American Mineralogist, 63, 362-364.
2400 Olsen, E.J., Bunch, T.E., Jarosewich, E., Noonan, A.F., and Huss, G.I. (1977b) Happy Canyon:
2401 A new type of enstatite achondrite. Meteoritics, 12, 109-123.
2402 Olsen, E.J., Davis, A., Clarke, R.S. Jr., Schultz, L., Weber, H.W., Clayton, R., Mayeda, T.,
2403 Jarosewich, E., Sylvester, P., Grossman, L., Wang, M.-S., Lipschutz, M.E., Steele, I.M., and
2404 Schwade, J. (1994) Watson: A new link in the IIE iron chain. Meteoritics, 29, 200-213.
2405 Olsen, E.J., Kracher, A., Davis, A.M., Steele, I.M., Hutcheon, I.D., and Bunch, T.E. (1999) The
2406 phosphates of IIIAB iron meteorites. Meteoritics & Planetary Science, 34, 285–300.
2407 Ostertag, R. (1983) Shock experiments on feldspar crystals. Journal of Geophysical Research,
2408 88, 364–376.
2409 Ozawa, S., Ohtani, E., Miyahara, M., Suzuki, A., Kimura, M., and Ito, Y. (2009) Transformation
2410 textures, mechanisms of formation of high-pressure minerals in shock melt veins of L6
2411 chondrites, and pressure-temperature conditions of the shock events. Meteoritics & Planetary
2412 Sciences, 44, 1771–1786.
2413 Ozawa, S., Miyahara, M., Ohtani, E., Koroleva, O.N., Ito, Y., Litasov, K.D., and Pokhilenko,
2414 N.P. (2014) Jadeite in Chelyabinsk meteorite and the nature of an impact event on its parent
2415 body. Scientific Reports, 4, 5033. https://doi.org/10.1038/srep05033.

2416 Pang, R.-L. Harries, D., Pollok, K., Zhang, A.-C., and Langenhorst, F. (2018) Vestaite,
2417 $(Ti^{4+}Fe^{2+})Ti^{4+}_3O_9$, a new mineral in the shocked eucrite Northwest Africa 8003. American
2418 Mineralogist, 103, 1502-1511.
2419 Petaev, M.I., Clarke, R.S. Jr., Jarosewich, E., Zaslavskaya, N.I., Kononkova, N.N., Wang, M.-S.,
2420 Lipschutz, M.E., Olsen, E.J., Davis, A.M., Steele, I.M., Clayton, R.N., Mayeda, T.K., and
2421 Kallemeyn, G. (2000) The Chaunskij anomalous mesosiderite: Petrology, chemistry, oxygen
2422 isotopes, classification and origin. Geochemistry International, 38, S322–S350.
2423 Pittarello, L., Ji, G., Yamaguchi, A., Schryvers, D., Debaille, V., and Claeys, P. (2015) From
2424 olivine to ringwoodite: A TEM study of a complex process. Meteoritics & Planetary Science,
2425 50, 944–957.
2426 Powell, B.N. (1969) Petrology and chemistry of meso siderites-I. Textures and composition of
2427 nickel-iron. Geochimica et Cosmochimica Acta, 33, 789-810.
2428 Pratesi, G., Bindi, L., and Moggi-Cecchi, V. (2006) Icosahedral coordination of phosphorus in
2429 the crystal structure of melliniite, a new phosphide mineral from the Northwest Africa 1054
2430 acapulcoite. American Mineralogist, 91, 451-454.
2431 Presnall, D.C. (1995) Phase diagrams of Earth-forming minerals. In: T.J. Ahrens, Ed., Mineral
2432 Physics & Crystallography: A Handbook of Physical Constants, pp. 248-268. American
2433 Geophysical Union.
2434 Price, G.D. (1983) The nature and significance of stacking faults in wadsleyite, natural b-(Mg,
2435 $Fe)_2SiO_4$ from the Peace River meteorite. Physics of the Earth and Planetary Interiors, 33,
2436 137–147.
2437 Price, G.D., Putnis, A., Agrell, S.O., and Smith, D.G.W. (1983) Wadsleyite, natural beta-
2438 $(Mg,Fe)_2SiO_4$ from the Peace River meteorite. Canadian Mineralogist, 21, 29-35.

2439 Prinz, M., and Weisberg, M.K. (1995) Asuka 881371 and the angrites: Origin in a
2440 heterogeneous, CAI-enriched, differentiated, volatile depleted body. Antarctic Meteorites, 20,
2441 207–210.
2442 Prinz, M., Keil, K., Hlava, P.F., Berkley, J.L., Gomes, C.B., and Curvello, W.S. (1977) Studies
2443 of Brazilian meteorites, III. Origin and history of the Angra dos Reis achondrite. Earth and
2444 Planetary Science Letters, 35, 317-330.
2445 Prinz, M., Nehru, C.E., and Delaney, J.S. (l982) Sombrerete: An iron with highly fractionated
2446 amphibole-bearing Na-P-rich silicate inclusions. Lunar and Planetary Science, 13, 634-635.
2447 Prinz, M., Nehru, C.E., Delaney, J.S., Weisberg, M., and Olsen, E. (1983a) Globular silicate
2448 inclusions in lIE irons and Sombrerete: Highly fractionated minimum melts. Lunar and
2449 Planetary Science, 14, 618-619.
2450 Prinz, M., Delaney, J.S., Nehru, C.E., and Weisberg, M.K. (l983b) Enclaves in the Nilpena
2451 polymict ureilite. Meteoritics, 18, 376-377.
2452 Prinz, M., Weisberg, M.K., and Nehru, C.E. (1986) North Haig and Nilpena: Paired polymict
2453 ureilites with Angra dos Reis-related and other clasts. Lunar and Planetary Science, 17, 681-
2454 682.
2455 Prinz, M., Weisberg, M.K., and Nehru, C.E. (l988) LEW86010, a second angrite: Relationship to
2456 CAl's and opaque matrix. Lunar and Planetary Science, 19, 949-950.
2457 Prinz, M., Weisberg, M.K., and Nehru, C.E. (1990) LEW 87051, a new angrite: Origin in a Ca-
2458 Al-enriched eucritic planetesimal? Lunar and Planetary Science, 21, 979-980.
2459 Prinz, M., Weisberg, M.K., and Nehru, C.E. (1994) LEW88774: A new type of Cr-rich ureilite.
2460 Lunar and Planetary Science, 25, 1107-1108.

Putnis, A., and Price, G.D. (1979) High-pressure $(Mg,Fe)_2SiO_4$ phases in the Tenham chondritic meteorite. Nature, 280, 217–218.

Ramdohr, P. (1963) The opaque minerals in stony meteorites. Journal of Geophysical Research, 68, 2011-2036.

Ramdohr, P. (1973) The Opaque Minerals in Stony Meteorites. Akademie Verlag.

Randich, E., and Goldstein, J.I. (1978) Cooling rates of seven hexahedrites. Geochimica et Cosmochimica Acta, 42, 221–234.

Rasmussen, K.L. (1989) Cooling rates and parent bodies of iron meteorites from group IIICD, lAB, and IVB. Physica Scripta, 39, 410-416.

Reid, A.M., and Cohen, A.J. (1967) Some characteristics of enstatite from enstatite achondrites. Geochimica et Cosmochimica Acta, 31, 661-672.

Reid, A.M., Williams, R.J., and Takeda, H. (1974) Coexisting bronzite and clinobronzite and the thermal evolution of the Steinbach meteorite. Earth and Planetary Science Letters, 22, 67-74.

Reuter, K.B., Williams, D.B., and Goldstein, J.I. (1988) Low temperature phase transformations in the metallic phases of iron and stony-iron meteorites. Geochimica et Cosmochimica Acta, 52, 617-626.

Ross, A. J., Downes, H., Herrin, H.S., Mittlefehldt, D.W., Humayun, M., and Smith, C. (2019) The origin of iron silicides in ureilite meteorites. Geochemistry, 79, 125539 (15 pp.).

Rubin, A.E. (1985) Impact melt products of chondritic material. Reviews of Geophysics, 23, 277-300.

Rubin, A.E. (1997a) Igneous graphite in chondritic meteorites. Mineralogical Magazine, 61, 699-703.

2483 Rubin, A.E, (1997b) Mineralogy of meteorite groups. Meteoritics & Planetary Science, 32, 231-
2484 247.
2485 Rubin, A.E. (2006) Shock, post-shock annealing and post-annealing shock in ureilites.
2486 Meteoritics & Planetary Science, 41, 125-133.
2487 Rubin, A.E. (2010) Impact melting in the Cumberland Falls and Mayo Belwa aubrites.
2488 Meteoritics & Planetary Science, 45, 265-275.
2489 Rubin, A.E. (2015a) Impact features of enstatite-rich meteorites. Chemie der Erde, 75, 1-28.
2490 Rubin, A.E. (2015b) Maskelynite in asteroidal, lunar and planetary basaltic meteorites: An
2491 indicator of shock pressure during impact ejection from their parent bodies. Icarus, 257, 221-
2492 229.
2493 Rubin, A.E., and Keil, K. (1983) Mineralogy and petrology of the Abee enstatite chondrite
2494 breccia and its dark inclusions. Earth and Planetary Science Letters, 64, 118-131.
2495 Rubin, A.E., and Ma, C. (2017) Meteoritic minerals and their origins. Chemie der Erde, 77, 325-
2496 385.
2497 Rubin, A.E., and Ma, C. (2020) Meteorite Mineralogy. Cambridge University Press, in press.
2498 Rubin, A.E., and Mittlefehldt, D.W. (1992) Classification of mafic clasts from mesosiderites:
2499 Implications for endogenous igneous processes. Geochimica et Cosmochimica Acta, 56, 827-
2500 840.
2501 Rubin, A.E. and Scott, E.R.D. (1997) Abee and related EH chondrite impact-melt breccias.
2502 Geochimica et Cosmochimica Acta, 61, 425-435.
2503 Rubin, A.E., Scott, E.R.D., and Keil, K. (1997) Shock metamorphism of enstatite chondrites.
2504 Geochimica et Cosmochimica Acta, 61, 847-858.

2505 Rucks, M.J., Whitaker, M.L., Glotch, T.D., Parise, J.B., Jaret, S.J., Catalano, T., and Dyar, M.D.
2506 (2018) Making tissintite: Mimicking meteorites in the multi-anvil. American Mineralogist,
2507 103, 1516–1519.
2508 Russell, S.S., Pillinger, C.T., Arden, J.W., Lee, M.R., and Ott, U. (1992) A new type of
2509 meteoritic diamond in the enstatite chondrite Abee. Science, 256, 206-209.
2510 Russell, S.A., Connelly, H.C., and Krot, A.N. [Eds]. (2018) Chondrules: Records of
2511 Protoplanetary Disk Processes. Cambridge University Press.
2512 Ruzicka, A. (2014) Silicate-bearing iron meteorites and their implications for the evolution of
2513 asteroidal parent bodies. Chemie der Erde, 74, 3-48.
2514 Sack, R.O., and Ghiorso, M.S. (2017) Ti^{3+}- and Ti^{4+}-rich fassaites at the birth of the solar
2515 system: Thermodynamics and applications. American Journal of Science, 317, 807-845.
2516 Schertl, H.-P., Mills, S.J., and Maresch, W.V. (2018) A Compendium of IMA-Approved Mineral
2517 Nomenclature. International Mineralogical Association.
2518 Scott, E.R.D. (1972) Chemical fractionation in iron meteorites and its interpretation. Geochimica
2519 et Cosmochimica Acta, 36, 1205–1236.
2520 Scott, E.R.D. (1977a) Pallasites-metal composition, classification and relationships with iron
2521 meteorites. Geochimica et Cosmochimica Acta, 41, 349-360.
2522 Scott, E.R.D. (1977b) Formation of olivine-metal textures in pallasite meteorites. Geochimica et
2523 Cosmochimica Acta, 41, 693–710.
2524 Scott, E.R.D. (1979) Origin of anomalous iron meteorites. Mineralogical Magazine, 43, 415-421.
2525 Scott, E.R.D. (1982) Origin of rapidly solidified metal-troilite grains in chondrites and iron
2526 meteorites. Geochimica et Cosmochimica Acta, 46, 813-823.

2527 Scott, E.R.D., and Agrell, S.O. (1971) The occurrence of carbides in iron meteorites. Meteoritics,
2528 6, 312-131.
2529 Scott, E.R.D., and Bild, R.W. (1974) Structure and formation of the San Cristobal meteorite,
2530 other IB irons and group I1ICD. Geochimica et Cosmochimica Acta, 38, 1379-1391.
2531 Scott, E.R.D., and Krot, A.N. (2014) Chondrites and their components. In: A.M. Davis,
2532 H.D.Holland, and K.K.Turekian, Eds., Treatise on Geochemistry, Vol. 1: Meteorites, Comets,
2533 and Planets, Second Edition, pp. 65-137. Elsevier-Pergamon.
2534 Scott, E.R.D., and Rajan, R.S. (1979) Thermal history of the Shaw chondrite. Proceedings of the
2535 Lunar and Planetary Science Conference, 10, 1031-1043.
2536 Scott, E.R.D., and Wasson, J.T. (1975) Classification and properties of iron meteorites. Reviews
2537 of Geophysics and Space Physics, 13, 527–546.
2538 Scott, E.R.D., Keil, K., and Steffler, D. (1992) Shock metamorphism of carbonaceous
2539 chondrites. Geochimica et Cosmochimica Acta, 56, 4281-4293.
2540 Scott, E.R.D., Haack, H., and McCoy, T.J. (1996) Core crystallization and silicate-metal mixing
2541 in the parent body of the IVA iron and stony-iron meteorites. Geochimica et Cosmochimica
2542 Acta, 60, 1615-1631.
2543 Scott, E.R.D., Haack, H., and Love, S.G. (2001) Formation of mesosiderites by fragmentation
2544 and reaccretion of a large differentiated asteroid. Meteoritics & Planetary Science, 36, 869–
2545 881.
2546 Sharp, T.G., and DeCarli, P.S. (2006) Shock effects in meteorites. In: D.S. Lauretta and H.Y.
2547 McSween Jr, Eds., Meteorites and the Early Solar System II, pp. 653-677. University of
2548 Arizona Press.

2549 Sharp, T.G., Lingemann, C.M., Dupas, C., and Stöffler, D. (1997) Natural occurrence of
2550 $MgSiO_3$-ilmenite and evidence for $MgSiO_3$-perovskite in a shocked chondrite. Science, 277,
2551 352-355.
2552 Sharp, T.G., El Goresy, A., Wopenka, B., and Chen, M. (1999) A post-stishovite SiO_2
2553 polymorph in the meteorite Shergotty: Implications for impact events. Science, 284, 1511–
2554 1513.
2555 Sharygin, V.V. (2020) Phase $CuCrS_2$ in iron meteorite Uakit (IIAB), Buryatia, Russia:
2556 Preliminary data. In S. Votyakov, D. Kiseleva, V. Grokhovsky, and Y. Shchapova, Eds.,
2557 Minerals: Structure, Properties, Methods of Investigation: 9th Geoscience Conference for
2558 Young Scientists, Ekaterinburg, Russia, February 5–8, pp. 229-234. Springer.
2559 Sharygin, V.V., Ripp, G.S., Yakovlev, G.A., Seryotkin, Y.V., Karmanov, N.S., Izbrodin, I.A.,
2560 Grokhovsky, V.I., and Khromova, E.A. (2020) Uakitite VN, a new mononitride mineral from
2561 Uakit iron meteorite (IIAB). Minerals, 10, 150. https://doi.org/10.3390/min10020150
2562 Shearer, C.K., Burger, P.V., Neal, C., Sharp, Z., Spivak-Birndorf, L., Borg, L., Fernandes, V.A.,
2563 Papike, J.J., Karner, J., Wadha, M., Gaffney, A., Shafer, J., Geisman, J., Atudorei, N.-V.,
2564 Herd, C., Weiss, B.P., King, P.L., Crowther, S.A., and Golmour, J.D. (2010) Non-basaltic
2565 asteroidal magmatism during the earliest stages of Solar System evolution. A view from
2566 Antarctic achondrites Graves Nunataks 06128 and 06129. Geochimica et Cosmochimica
2567 Acta, 74, 1172–1199.
2568 Shimizu, M., Yoshida, H., and Mandarino, J.A. (2002) The new mineral species keilite,
2569 (Fe,Mg)S, the iron-dominant analogue of niningerite. The Canadian Mineralogist, 40, 1687-
2570 1692.

2571 Singletary, S., and Grove, T.L. (2006) Experimental constraints on ureilite petrogenesis.
2572 Geochimica et Cosmochimica Acta, 70, 1291-1308.

2573 Sinmyo, R., McCammon, C.A., and Dubrovinsky, L. (2017) The spin state of Fe^{3+} in lower
2574 mantle bridgmanite. American Mineralogist, 102, 1263–1269.

2575 Shukolyukov, A., and Lugmair, G. (1992) ^{60}Fe-Light my fire. Meteoritics, 27, 289.

2576 Smith, B.A., and Goldstein, J.I. (1977) The metallic microstructures and thermal histories of
2577 severely reheated chondrites. Geochimica et Cosmochimica Acta, 41, 1061-1072.

2578 Smith, C.L., Downes, H., and Jones, A.P. (2008) Metal and sulphide phases in interstitial veins
2579 in “dimict” ureilites – insights into the history and petrogenesis of the ureilite parent body.
2580 Lunar and Planetary Science, 39, 1669.

2581 Smith, J.V., and Mason, B. (1970) Pyroxene-garnet transformation in Coorara meteorite.
2582 Science, 168, 832-833.

2583 Spray, J.G., and Boonsue, S. (2016) Monoclinic and tetragonal plagioclase (AN54) in shock
2584 veins from the central uplift of the Manicougan impact structure. Meteoritics & Planetary
2585 Science, 51, A590.

2586 Srinivasan, G., Goswami, J.N., and Bhandari, N. (1999) ^{26}Al in eucrite Piplia Kalan: Plausible
2587 heat source and formation chronology. Science, 284, 1348–1350.

2588 Srinivasan, P., Dunlap, D.R., Agee, C.B., Wadhwa, M., Coleff, D., Ziegler, K., Ziegler, R., and
2589 McCubbin, F.M. (2018). Silica-rich volcanism in the early solar system dated at 4.565 Ga.
2590 Nature Communications, 9, 3036 (8 pp.).

2591 Steele, I.M., Olsen, E., Pluth, J., and Davis, A.M. (1991) Occurrence and crystal structure of Ca-
2592 free beusite in the El Sampal IIIA iron meteorite. American Mineralogist, 76, 1985-1989.

2593 Stewart, B., Papanastassiou, D.A., and Wasserburg, G.J. (1996) Sm-Nd systematics of a silicate
2594 inclusion in the Caddo IAB iron meteorite. Earth and Planetary Science Letters, 143, 1-12.
2595 Stishov, S.M., and Popova, S.V. (1961) A new dense modification of silica. Geokhimiya, 10,
2596 837–839.
2597 Stöffler, D., and Grieve R.A.F. (2007). Impactites. In: D. Fettes and J. Desmons, Eds.,
2598 Metamorphic Rocks: A Classification and Glossary of Terms, Recommendations of the
2599 International Union of Geological Sciences Cambridge, pp. 82–92. Cambridge University
2600 Press.
2601 Stöffler, D., Ostertag, R., Jammes, C., Pfannschmidt, G., Sen Gupta, P.R., Simon, S.B., Papike,
2602 J.J., and Beauchamp, R.H. (1986) Shock metamorphism and petrography of the Shergotty
2603 achondrite. Geochimica et Cosmochimica Acta, 50, 889–903.
2604 Stöffler, D., Bischoff, A., Buchwald, V., and Rubin, A.E. (1988) Shock effects in meteorites. In
2605 J.F. Kerridge and M.S. Matthews, Eds., Meteorites and the Early Solar System, pp.165-202.
2606 University of Arizona Press.
2607 Stöffler, D., Keil, K., and Scott, E. R. D. (1991) Shock metamorphism of ordinary chondrites.
2608 Geochimica et Cosmochimica Acta, 55, 3845-3867.
2609 Stöffler, D., Hamann C., and Metzler K. (2018) Shock metamorphism of planetary silicate rocks
2610 and sediments: Proposal for an updated classification system. Meteoritics & Planetary
2611 Science, 53, 5-49.
2612 Swamy, V., Saxena, S.K., Sundman, B., and Zhang, J. (1994) A thermodynamic assessment of
2613 silica phase diagram. Journal of Geophysical Research, 99, 11,787–11,794.

2614 Swindle, T.D., Kring, D.A., Burkland, M.K., Hill, D.H., and Boynton, W.V. (1998) Noble gases,
2615 bulk chemistry, and petrography of olivine-rich achondrites Eagles Nest and Lewis Cliff
2616 88763: Comparison to brachinites. Meteoritics & Planetary Science, 33, 31-48.
2617 Takeda, H. (1987) Mineralogy of Antarctic ureilites and a working hypothesis for their origin
2618 and evolution. Earth and Planetary Science Letters, 81, 358-370.
2619 Takeda, H. (1989) Mineralogy of coexisting pyroxenes in magnesian ureilites and their
2620 formation conditions. Earth and Planetary Science Letters, 93, 181-194.
2621 Takeda, H., and Mori, H. (1985) The diogenite-eucrite links and the crystallization history of a
2622 crust of their parent body. Journal of Geophysical Research, 90, C636-C648.
2623 Takeda, H., Mori, H., and Ogata, H. (1989) Mineralogy of augite-bearing ureilites and the origin
2624 of their chemical trends. Meteoritics, 24, 73-81.
2625 Takeda, H., Babi, T., and Mori, H. (1992) Mineralogy of a new orthopyroxene-bearing ureilite
2626 LEW88201 and the relationship between magnesian ureilites and lodranites. Lunar and
2627 Planetary Science, 23, 1403-1404.
2628 Takeda, H., Mori, H., Hiroi, T., and Saito, J. (1994) Mineralogy of new Antarctic achondrites
2629 with affinity to Lodran and a model of their evolution in an asteroid. Meteoritics, 29, 830-842.
2630 Takeda, H., Yugami, K., Bogard, D., and Miyamoto, M. (1997a) Plagioclase-augite-rich gabbro
2631 in the Caddo County IAB Iron and the missing basalts associated with iron meteorites. Lunar
2632 and Planetary Science, 28, 1409-1410.
2633 Takeda, H., Ishii, T., Arai, T., and Miyamoto, M. (1997b) Mineralogy of the Asuka 87 and 88
2634 eucrites and the crustal evolution of the HED parent body. Antarctic Meteorite Research, 10,
2635 401-413.

2636 Taylor, G.J., and Heymann, D. (1970) Electron microprobe study of metal particles in the
2637 Kingfisher meteorite. Geochimica et Cosmochimica Acta, 34, 677-687.
2638 Taylor, G.J., Okada, A., Scott, E.R.D., Rubin, A.E., Huss, G.R., and Keil, K. (1981) The
2639 occurrence and implications of carbide-magnetite assemblages in unequilibrated ordinary
2640 chondrites. Lunar and Planetary Science Conference, 12, 1076-1078.
2641 Tomioka, N. (2007) A model for the shear mechanism in the enstatite-akimotoite phase
2642 transition. Journal of Mineralogical and Petrological Sciences, 102, 226–232.
2643 Tomioka, N., and Fujino, K. (1997) Natural (Mg,Fe)SiO_3-ilmenite and -perovskite in the
2644 Tenham meteorite. Science, 277, 1084–1086.
2645 Tomioka, N., and Fujino, K. (1999) Akimotoite, (Mg,Fe)SiO_3, a new silicate mineral of the
2646 ilmenite group in the Tenham chondrite. American Mineralogist, 84, 267-271.
2647 Tomioka, N., and Kimura, M. (2003) The breakdown of diopside to Ca-rich majorite and glass in
2648 a shocked H chondrite. Earth and Planetary Science Letters, 208, 271–278.
2649 Tomioka, N., and Miyahara, M. (2017) High-pressure minerals in shocked meteorites:
2650 Meteoritics & Planetary Science, 52, 2017-2039.
2651 Tomioka, N., Fujino, K., Ito, E., Katsura, T., Sharp, T., and Kato, T. (2002) Microstructures and
2652 structural phase transition in (Mg,Fe)SiO_3 majorite. European Journal of Mineralogy, 14, 7–
2653 14.
2654 Tomioka, N., Miyahara, M., and Ito, M. (2016) Discovery of natural $MgSiO_3$ tetragonal garnet
2655 in a shocked chondritic meteorite. Science Advances, 2, e1501725.
2656 Tomioka, N., Okuchi, T., Iitaka, T., Miyahara, M., Bindi, L., and Xie, X. (2020) Poirierite, IMA
2657 No. 2018-026b. European Journal of Mineralogy, 32, in press.

2658 Tomkins, A. G. (2009) What metal-troilite textures can tell us about post-impact metamorphism
2659 in chondrite meteorites. Meteoritics & Planetary Science, 44, 1133–1149.
2660 Tonks, W.B., and Melosh, H.J. (1992) Core formation by giant impacts. Icarus, 100, 326-346.
2661 Treiman, A.H., and Berkley, J.L. (1994) Igneous petrology of the new ureilites Nova 001 and
2662 Nullarbor 010. Meteoritics, 29, 843-848.
2663 Trinquier, A., Birck, J., and Allegre, C.J. (2007) Widespread ^{54}Cr heterogeneity in the inner
2664 solar system. The Astrophysical Journal, 655, 1179-1185.
2665 Trinquier, A., Elliott, T., Ulfbeck, D., Coath, C., Krot, A.N., and Bizzarro, M. (2009) Origin of
2666 nucleosynthetic isotope heterogeneity in the solar protoplanetary disk. Science, 324, 374-376.
2667 Tschauner, O. (2019) High-pressure minerals. American Mineralogist, 104, 1701-1731.
2668 Tschauner, O., and Ma, C. (2017) Stöfflerite, IMA 2017-062. Mineralogical Magazine, 81,
2669 1279–1286.
2670 Tschauner, O., Ma, C., Beckett, J.R., Prescher, C., Prakapenka, V.B., and Rossman, G.R. (2014)
2671 Discovery of bridgmanite, the most abundant mineral in Earth, in a shocked meteorite.
2672 Science, 346, 1100-1102.
2673 Tschauner, O., Ma, C., Lanzirotti, A., and Newville, M.G. (2020) Riesite, a new high pressure
2674 polymorph of TiO_2 from the Ries impact structure. Minerals, 10, 78 (8 pp.).
2675 Ulff-Møller, F., Rasmussen, K.L., Prinz, M., Palme, H., Spettel, B., and Kallemeyn, G.W. (1995)
2676 Magmatic activity on the IVA parent body: Evidence from silicate-bearing iron meteorites.
2677 Geochimica et Cosmochimica Acta, 59, 4713-4728.
2678 Ulff-Møller, F., Tran, J., Choi, B.-G., Haag, R., Rubin, A.E., and Wasson, J.T. (1997) Esquel:
2679 Implications for pallasite formation processes based on the petrography of a large slab. Lunar
2680 and Planetary Science, 28, 1465–1466.

2681 Ulff-Møller, F., Choi, B.-G., Rubin, A.E., Tran, J., and Wasson, J.T. (1998) Paucity of sulfide in
2682 a large slab of Esquel: New perspectives on pallasite formation. Meteoritics & Planetary
2683 Science, 33, 221-227.
2684 van Kooten, E.M.M.E., Schiller, M., and Bizzarro, M. (2017) Magnesium and chromium isotope
2685 evidence for initial melting by radioactive decay of ^{26}Al and late stage impact-melting of the
2686 ureilite parent body. Geochimica et Cosmochimica Acta, 208, 1–23.
2687 Vdovykin, G.P. (1970) Ureilites. Space Science Reviews, 10, 483-510.
2688 Vollmer, C., Hoppe, P., Brenker, F.E., and Holzapfel, C. (2007) Stellar $MgSiO_3$ perovskite: A
2689 shock-transformed stardust silicate found in a meteorite. The Astrophysical Journal Letters,
2690 666, L49–L52.
2691 Wallner, A., Bichler, M., Buczak, K., Dressler, R., Fifield, L.K., Schumann, D., Sterba, J.H.,
2692 Tims, S.G., Wallner, G., and Kutschera, W. (2015) Settling the half-life of ^{60}Fe: Fundamental
2693 for a versatile astrophysical chronometer. Physical Review Letters, 114, 041101 (6 pp).
2694 Walton, E. L. (2013) Shock metamorphism of Elephant Moraine A79001: Implications for
2695 olivine-ringwoodite transformation and the complex thermal history of heavily shocked
2696 Martian meteorites. Geochimica et Cosmochimica Acta, 107, 299-315.
2697 Wang, Y., Guyot, F., and Liebermann, R.C. (1992) Electron Microscopy of $(Mg,Fe)SiO_3$
2698 perovskite: Evidence for structural phase transitions and implications for the lower mantle.
2699 Journal Geophysical Research, 97,12,327–12,347.
2700 Warren, P. (2011) Stable-isotopic anomalies and the accretionary assemblage of the Earth and
2701 Mars: A subordinate role for carbonaceous chondrites. Earth and Planetary Science Letters,
2702 311, 93-100.

2703 Warren, P.H. (2012) Parent body depth–pressure–temperature relationships and the style of the
2704 ureilite anatexis. Meteoritics & Planetary Science, 47, 209-227.
2705 Warren, P.H., and Kallemeyn, G.W. (1994) Petrology of LEW88774: An extremely Chromium-
2706 rich ureilite. Lunar and Planetary Science, 25, 1465-1466.
2707 Wasserburg, G.J., Sanz, H.G., and Bence, A.E. (1968) Potassium-feldspar phenocrysts in the
2708 surface of Colomera, an iron meteorite. Science, 161, 684-687.
2709 Wasson, J.T. (1967) Chemical classification of iron meteorites: I. A study of iron meteorites with
2710 low concentrations of gallium and germanium. Geochimica et Cosmochimica Acta, 31, 161–
2711 180.
2712 Wasson, J.T. (1970) Chemical classification of iron meteorites: IV. Irons with Ge concentrations
2713 greater than 190 ppm and other meteorites associated with group I. Icarus, 12, 407–423.
2714 Wasson, J.T. (1971) Chemical classification of iron meteorites: V. Groups IIIC and IIID and
2715 other irons with germanium concentrations between 1 and 25 ppm. Icarus, 14, 59–70.
2716 Wasson, J.T. (1974) Meteorites: Classification and Properties. Springer-Verlag.
2717 Wasson, J.T. (1990) Ungrouped iron meteorites in Antarctica: Origin of anomalously high
2718 abundance. Science, 249, 900–902.
2719 Wasson, J.T. (2016) Formation of the Treysa quintet and the main-group pallasites by impact-
2720 generated processes in the IIIAB asteroid. Meteoritics & Planetary Science, 51, 773-784.
2721 Wasson, J.T., and Choe, W.H. (2009) The IIG iron meteorites: Probable formation in the IIAB
2722 core. Geochimica et Cosmochimica Acta, 73, 4879–4890.
2723 Wasson, J.T., and Kallemeyn, G.W. (2002) The IAB iron-meteorite complex: A group, five
2724 subgroups, numerous grouplets, closely related, mainly formed by crystal segregation in
2725 rapidly cooling melts. Geochimica et Cosmochimica Acta, 66, 2445–2473.

2726 Wasson, J.T., and Rubin, A.E. (1985) Formation of mesosiderites by low-velocity impacts as a
2727 natural consequence of planet formation. Nature, 318, 168–170.
2728 Wasson, J.T., and Wang, J.M. (1986) A nonmagmatic origin of group IIE iron meteorites.
2729 Geochimica et Cosmochimica Acta, 50, 725–732.
2730 Wasson, J.T., and Wei, C.M. (1970) Composition of metal, schreibersite and perryite of enstatite
2731 achondrites and the origin of enstatite chondrites and achondrites. Geochimica et
2732 Cosmochimica Acta, 31, 169-184.
2733 Wasson, J.T., Willis, .J, Wai, C.M., and Kracher, A. (1980) Origin of iron meteorite groups IAB
2734 and IIICD. Zeitschrift für Naturforschung, 35A, 781-795.
2735 Wasson, J.T., Ouyang, X.W., Wang, J.M., and Jerde, E. (1989) Chemical classification of iron
2736 meteorites: XI. Multi-element studies of 38 new irons and the high abundance of ungrouped
2737 irons from Antarctica. Geochimica et Cosmochimica Acta, 53, 735–744.
2738 Wasson, J.T., Choi, B.G., Jerde, E.A., and Ulff-Møller, F. (1998) Chemical classification of iron
2739 meteorites: XII. New members of the magmatic groups. Geochimica et Cosmochimica Acta,
2740 62, 715–724.
2741 Watters, T.R., and Prinz, M. (1979) Aubrites: Their origin and relationship to enstatite
2742 chondrites. Proceedings of the Lunar and Planetary Science Conference, 10, 1073-1093.
2743 Weisberg, M.K., McCoy, T.J., and Krot, A.N. (2006) Systematics and evaluation of meteorite
2744 classification. In: D.S. Lauretta, and H.Y. McSween, Jr., Eds., Meteorites and the Early Solar
2745 System II, pp. 19–52. University of Arizona Press.
2746 Wenk, H.-R., and Bulakh, A. (2003) Minerals: Their Constitution and Origin. Cambridge
2747 University Press.

2748 Wheelock, M.M., Keil, K., Floss, C., Taylor, G.J., and Crozaz, G. (1994) REE geochemistry of
2749 oldhamite-dominated clasts from the Norton County aubrite: Igneous origin of oldhamite.
2750 Geochimica et Cosmochimica Acta, 58, 449-458.
2751 Willis, J. (1980) The bulk composition of iron meteorite parent bodies. PhD Dissertation,
2752 University of California at Los Angeles, 208 p.
2753 Wlotzka, F., and Jarosewich, E. (1977) Mineralogical and chemical compositions of silicate
2754 inclusions in the El Taco, Camp del Cielo, iron meteorite. Smithsonian Contributions to Earth
2755 Science, 19, 104-125.
2756 Wood, J.A. (1967) Chondrites: Their metallic minerals, thermal histories, and parent planets.
2757 Icarus, 6, 1-49.
2758 Woolum, D., and Cassen, P. (1999) Astronomical constraints on nebular temperatures:
2759 Implications for planetesimal formation. Meteoritics & Planetary Science, 34, 897-907.
2760 Xie, Z., and Sharp, T.G. (2004) High-pressure phases in shock-induced melt veins of the
2761 Umbarger L6 chondrite: Constraints of shock pressure. Meteoritics & Planetary Science,
2762 3912, 2043–2054.
2763 Xie, Z., and Sharp, T.G. (2007) Host rock solid-state transformation in a shock-induced melt
2764 vein of Tenham L6 chondrite. Earth and Planetary Science Letters, 254, 433–445.
2765 Xie, X., Minitti, M.E., Chen, M., Mao, H.-K., Wang, D., Shu, J., and Fei, Y. (2002a) Natural
2766 high-pressure polymorph of merrillite in the shock veins of the Suizhou meteorite.
2767 Geochimica et Cosmochimica Acta, 66, 2439–2444.
2768 Xie, Z., Tomioka, N., and Sharp, T.G. (2002b) Natural occurrence of Fe_2SiO_4-spinel in the
2769 shocked Umbarger L6 chondrite. American Mineralogist, 87, 1257–1260.

2770 Xie, X., Minitti, M.E., Chen, M., Mao, H.-K., Wang, D., Shu, J., and Fei, Y. (2003) Tuite, γ-
2771 $Ca_3(PO_4)_2$ – A new mineral from the Suizhou L6 chondrite. European Journal of Mineralogy,
2772 15, 1001-1005.
2773 Xie, Z., Sharp, T.G., and DeCarli, P.S. (2006) High-pressure phases in a shock-induced melt vein
2774 of the Tenham L6 chondrite: Constraints on shock pressure and duration. Geochimica et
2775 Cosmochimica Acta, 70, 504–515.
2776 Xie, Z.D., Sharp, T.G., Leinenweber, K., DeCarli, P.S., and Dera, P. (2011) a new mineral with
2777 an olivine structure and pyroxene composition in the shock-induced melt veins of Tenham L6
2778 chondrite. American Mineralogist, 96, 430-436.
2779 Xie, X., Gu, X., Yang, H., Chen, M., and Li, K. (2016) Wangdaodeite, IMA 2016-007.
2780 Mineralogical Magazine, 80, 691–697.
2781 Xie, X., Gu, X., Yang, H., Chen, M., and Li, K. (2020) Wangdaodoeite, the $LiNbO_3$-structured
2782 high-pressure polymorph of ilmenite, a new mineral from the Suizhou L6 chondrite.
2783 Meteoritics & Planetary Science, 55, 184-192.
2784 Yagi, T., Suzuki, T., and Akaogi, M. (1994) High pressure transitions in the system $KAlSi_3O_8$–
2785 $NaAlSi_3O_8$. Physics and Chemistry of Minerals, 21, 12–17.
2786 Yanai, K. (1994) Angrite Asuka-881371: Preliminary examination of a unique meteorite in the
2787 Japanese collection of Antarctic meteorites. Proceedings of the NIPR Symposium on
2788 Antarctic Meteorites, 7, 30-41.
2789 Yang, J., and Goldstein, J.I. (2005) The formation of the Widmanstätten structure in iron
2790 meteorites. Meteorites & Planetary Science, 40, 239–253.

Yang, J., and Goldstein, J.I. (2006) Metallographic cooling rates of the IIIAB iron meteorites. Geochimica et Cosmochimica Acta, 70, 3197–3215.

Yang, C.-W., Williams, DB., and Goldstein, J.I. (1996) A revision of the Fe-Ni phase diagram at low temperatures (<400°C). Journal of Phase Equilibria, 17, 522-531.

Yang, C.-W., Williams, D.B., and Goldstein, J.I. (1997a) A new empirical cooling rate indicator for meteorites based on the size of the cloudy zone of the metallic phases. Meteoritics & Planetary Science, 32, 423-429.

Yang, C.-W., Williams, D.B., and Goldstein, J.I. (1997b) Low-temperature phase decomposition in metal from iron, stony-iron and stony meteorites. Geochimica et Cosmochim Acta, 61, 2943-2956.

Yang, J., Goldstein, J.I., and Scott, E.R.D. (2008) Metallographic cooling rates and origin of IVA iron meteorites. Geochimica et Cosmochimica Acta, 72, 3043–3061.

Youdin, A.N., and Goodman, J. (2005) Streaming instabilities in protoplanetary disks. The Astrophysical Journal, 620, 459-469.

Yugami, K., Takeda, H., Kojima, H., and Miyamoto, M. (1997) Modal abundances of primitive achondrites and the end member mineral assemblage of the differentiation trend. Symposium on Antarctic Meteorites, 22, 220-222.

Zhou, Y., Irifune, T., Ohfuji, H., Shinmei, T., and Du, W. (2017) Stability region of $K_{0.2}Na_{0.8}AlSi_3O_8$ hollandite at 22 GPa and 2273 K. Physics and Chemistry of Minerals, 44, 33-42.

Zinner, E.K. (2014) Presolar grains. In: A.M. Davis, H.D. Holland, and K.K. Turekian, Eds., Treatise on Geochemistry, Vol. 1: Meteorites, Comets, and Planets, Second Edition., pp.17-39. Elsevier-Pergamon.

2814 Zolensky, M., Gounelle, M., Mikouchi, T., Ohsumi, K., Le, L., Hagiya, K., and Tachikawa, O.
2815 (2008) Andreyivanovite: A second new phosphide from the Kaidun meteorite. American
2816 Mineralogist, 93, 1295-1299.

This is the peer-reviewed, final accepted version for American Mineralogist, published by the Mineralogical Society of America.
The published version is subject to change. Cite as Authors (Year) Title. American Mineralogist, in press.
DOI: https://doi.org/10.2138/am-2021-7632. http://www.minsocam.org/

Table 1. Primary phases in iron, stony iron, and achondrite meteorites from differentiated asteroidal (DA)parent bodies

Group Species (Formula)	Natural Kind	Characteristics	References
NATIVE ELEMENTS AND ALLOYS			
Iron or "kamacite" (α-Fe,Ni)	*DA iron*	The most abundant metal phase in most iron and stony-iron meteorites, typically with ~6 wt. % Ni.	1-6
Taenite (γ-Fe,Ni)	*DA taenite*	A common Fe-Ni alloy with 25 to 35 wt % Ni; exsolves from DA iron to form Widmanstätten patterns.	1,2,4,5,7
Tetrataenite (Fe,Ni)	*DA tetrataenite*	An ordered tetragonal (*P*4/*mmm*) phase of Fe-Ni	7,8
Awaruite (Ni_2Fe to Ni_3Fe)	*DA awaruite*	Forms thin layer that separate tetrataenite from kamacite in Widmanstätten patterns of some iron meteorites	7,9
Copper (Cu)	*DA copper*	A rare accessory phase in enstatite achondrites (aubrites)	3,10
Graphite (C)	*DA graphite*	A common accessory phase in iron meteorites	4,11,12
CARBIDES			
Cohenite [$(Fe,Ni)_3C$]	*DA cohenite*	A common accessory phase in iron meteorites	1,13
Haxonite [$(Fe,Ni)_{23}C_6$]	*DA haxonite*	An accessory mineral in some iron meteorites	4,14
Edscottite (Fe_5C_2)	*DA edscottite*	A rare phase in iron meteorites	15,16
SILICIDES			
Perryite [$(Ni,Fe)_8(Si,P)_3$]	*DA perryite*	A minor accessory phase in enstatite achondrites	3,17
Carletonmooreite (Ni_3Si)	*DA carletonmooreite*	A rare phase from the Norton County aubrite	18
PHOSPHIDES			
Schreibersite [$(Fe,Ni)_3P$]	*DA schreibersite*	The most important P-bearing phase in iron meteorites	1,3,4,19
Barringerite [$(Fe,Ni)_2P$]	*DA barringerite*	A rare phase in pallasites and iron meteorites	20,21
NITRIDES			
Osbornite (TiN)	*DA osbornite*	An occasional accessory mineral in enstatite achondrites	3,22
Carlsbergite (CrN)	*DA carlsbergite*	A rare accessory mineral in enstatite achondrites	23,24
Uakitite (VN)	*DA uakatite*	A rare accessory mineral in the Uakit (IIAB) iron meteorite	25
Roaldite [$(Fe,Ni)_4N$)]	*DA roaldite*	A scarce phase in iron meteorites	26
Sinoite (Si_2N_2O)	*DA sinoite*	A minor phase in the Zakłodzie enstatite achondrite	27
SULFIDES			

Troilite (FeS)	*DA troilite*	The most common sulfide phase in iron meteorites; also in stony-iron meteorites and achondrites	1,3,4,19,28-32
NaCl-type Monosulfide Group [(Mg,Fe,Ca,Mn)S]			
Niningerite [(Mg,Fe)S]	*DA niningerite*	Found in enstatite achondrites in association with other sulfides	27,33
Oldhamite (CaS)	*DA oldhamite*	Found in many enstatite achondrites with other sulfides	3,34
Alabandite (MnS)	*DA alabandite*	Found in many enstatite achondrites with other sulfides	3,35
Sphalerite Monosulfide Group [(Zn,Fe,Mn)S]			
Sphalerite (ZnS)	*DA sphalerite*	A rare phase in iron meteorites, possibly exsolved from alabandite	10
Browneite (MnS)	*DA browneite*	A minor phase in the Zakłodzie enstatite achondrite	37
Buseckite [(Fe,Zn,Mn)S]	*DA buseckite*	A minor phase in the Zakłodzie enstatite achondrite	27
Thiospinel Group [(Fe,Mn,Cr,Zn)Cr_2S_4]			
Daubréelite ($FeCr_2S_4$)	*DA daubréelite*	A common minor phase in iron and achondrite meteorites	1,3,29
Joegoldsteinite ($MnCr_2S_4$)	*DA joegoldsteinite*	Found in the Social Circle (IVA) iron meteorite	38
Kalininite ($ZnCr_2S_4$)	*DA kalininite*	Discovered as a trace phase in the Uakit (IIAB) iron meteorite	39
Wilkmanite Group [(Fe,Cr)$(Fe,Cr,Ti)_2S_4$]			
Brezinaite (Cr_3S_4)	*DA brezinaite*	A rare phase in iron and ureilite meteorites	40,41
Heideite [$(Fe,Cr)_{1.15}(Ti,Fe)_2S_4$]	*DA heideite*	Found in the Bustee enstatite achondrites with other sulfides	3,42
Other Sulfides			
Pentlandite [$(Ni,Fe)_9S_8$]	*DA pentlandite*	A rare phase in brachinites, coexisting with taenite and troilite	30,43
Caswellsilverite ($NaCrS_2$)	*DA caswellsilverite*	Occurs as inclusions in oldhamite in the Norton County aubrite	3,44
Unnamed ($CuCrS_2$)	*DA $CuCrS_2$*	A single occurrence from the Uakit (IIAB) iron meteorite	40
Djerfisherite [$K_6(Fe,Cu,Ni)_{25}S_{26}Cl$]	*DA djerfisherite*	Found in enstatite achondrites with other sulfides	3,45
PHOSPHATES			
Chlorapatite [$Ca_5(PO_4)_3Cl$]	*DA chlorapatite*	A common phosphate in iron and achondrite meteorites	4,30,46, 47
Whitlockite [$Ca_9Mg(PO_3OH)(PO_4)_6$]	*DA whitlockite*	A common phosphate in non-chondritic meteorites	1,46,48-53
Matyhite [$Ca_9(Ca_{0.5}\square_{0.5})Fe(PO_4)_7$]	*DA matyhite*	A rare phase from the D'Orbigny angrite	54
Graftonite [$(Fe,Mn)_3(PO_4)_3$]	*DA graftonite*	Occurs in troilite nodules in iron meteorites; often Mn-rich	55
Farringtonite [$(Fe,Mn)_3(PO_4)_3$]	*DA farringtonite*	Found in pallasites with fairfieldite and whitlockite	2,56
Sarcopside [$(Fe,Mn)_3(PO_4)_3$]	*DA sarcopside*	Occurs in troilite nodules of iron meteorites	57

	Stanfieldite [$Ca_4Mg_5(PO_4)_6$]	*DA stanfieldite*	A minor phase in pallasites	2,56,58
	Buchwaldite ($NaCaPO_4$)	*DA buchwaldite*	From troilite nodules in the Cape York (IIIAB) iron meteorite	10,59
	Maríćite ($NaFePO_4$)	*DA maríćite*	From troilite nodules in the Cape York (IIIAB) iron meteorite	10
	Moraskoite [$Na_2Mg(PO_4)F$]	*DA moraskoite*	A rare phase in the Morasko (IAB) iron meteorite	60
	Xenophyllite [$Na_4Fe_7(PO_4)_6$]	*DA xenophyllite*	A rare phase in the Austinovka (IIIAB) iron meteorite	61
	Brianite [$Na_2CaMg(PO_4)_2$]	*DA brianite*	A rare phase in iron meteorites associated with whitlockite	46,62,63
	Panethite [$Na_2(Fe,Mn)_2(PO_4)_2$]	*DA panethite*	A rare phase in the Dayton (IAB) iron meteorite	46,62,64
	Johnsomervilleite [$Na_2Ca(Fe,Mg,Mn)_7(PO_4)_6$]	*DA johnsomervilleite*	A rare phase in iron meteorites	57,65
	Chladniite [$Na_2CaMg_7(PO_4)_6$]	*DA Chladniite*	Only known from the Carlton (IIICD) iron meteorite	64
	Galileiite [$Na(Fe,Mn)_4(PO_4)_3$]	*DA galileiite*	A rare phase in iron meteorites	57
	Tsangpoite [$Ca_5(PO_4)_2(SiO_4)$]	*DA tsangpoite*	A rare silico-phosphate from the D'Orbigny angrite	54
OXIDES				
Oxide Spinel Group [$(Mg,Fe^{2+})(Al,Fe^{3+},Cr^{3+},Ti)_2O_4$]				
	Chromite ($Fe^{2+}Cr_2O_4$)	*DA chromite*	Often the most abundant oxide; found in all meteorite groups	1,2,4,31,43,66
	Magnetite (Fe_3O_4)	*DA magnetite*	An accessory phase in angrites	67,68
	Hercynite ($Fe^{2+}Al_2O_4$)	*DA hercynite*	A minor phase in angrites	67,68
	Ulvöspinel ($Fe^{2+}{}_2Ti^{4+}O_4$)	*DA ulvöspinel*	A minor phase in angrites	69
Other Oxides				
	Ilmenite ($FeTiO_3$)	*DA ilmenite*	Reported from diogenites, eucrites, and iron meteorites	48,70-72
	Corundum (Al_2O_3)	*DA corundum*	One report from the LEW 88774 Cr-rich ureilite	73
	Eskolaite (Cr_2O_3)	*DA eskolaite*	One report from the LEW 88774 Cr-rich ureilite	74
	Rutile (TiO_2)	*DA rutile*	A minor phase in the Sombrerete (IAB) iron meteorite	48
	Baddeleyite (ZrO_2)	*DA baddeleyite*	Found in the Angra dos Reis angrite as a minor phase	67
	Perovskite ($CaTiO_3$)	*DA perovskite*	One report from an oxide inclusion in aubrite ALH 84008	75
	Geilkeilite ($MgTiO_3$)	*DA geikeilite*	One report from an oxide inclusion in aubrite ALH 84008	75
	Armalcolite [$(Mg,Fe^{2+})Ti_2O_5$]	*DA armalcolite*	A rare phase in silicate inclusions of iron meteorites	72,76
SILICATES				
Silica Group (SiO_2)				
	Tridymite (SiO_2)	*DA tridymite*	Tridymite is the commonest silica polymorph; it is found in	1,4,48,71,77

		iron meteorites and in mafic meteorite lithologies	
Cristobalite (SiO_2)	*DA cristobalite*	A minor phase in eucrites, aubrites, and iron meteorites	27,78,79
Quartz (SiO_2)	*DA quartz*	A minor phase in eucrites, aubrites, and iron meteorites	4,27,80
Silica glass (SiO_2)	*DA silica glass*	In silicate inclusions of iron meteorites	72
Olivine Group [$(Mg,Fe,Ca)_2SiO_4$]			
Forsterite [$(Mg,Fe)_2SiO_4$]	*DA forsterite*	A major meteorite mineral in many stony-irons and achondrites, comprising >98 vol % of some brachinites,	2-4,30,81
Fayalite (Fe_2SiO_4)	*DA fayalite*	Near end-member fayalite occurs in howardites and angrites	52,82,83
Kirschteinite ($CaFe^{2+}SiO_4$)	*DA kirschsteinite*	Occurs as a minor accessory phase in angrites	53,67,68
Pyroxene Group [$(Ca,Mg,Fe,Ti,Al)_2(Al,Si)_2O_6$]			
Orthoenstatite ($MgSiO_3$)	*DA orthoenstatite*	A major phase in several types of non-chondritic meteorites	3,4,31,71,84
Pigeonite [$(Mg,Fe,Ca)SiO_3$]	*DA pigeonite*	A major phase in many achondrites	4,30,85
Augite [$(Ca,Mg,Fe)Si_2O_6$]	*DA augite*	The major Ca-bearing phase in many achondrites	3,4,31,52,70,85
Hedenbergite ($CaFeSi_2O_6$)	*DA hedenbergite*	Near end-member examples occur in angrites	54,82
Fassaite [$Ca(Mg,Al,Ti^{3+},Ti^{4+})(Al,Si)SiO_6$]	*DA fassaite*	A common phase in angrite meteorites	53,68,86,87
Kosmochlor ($NaCr^{3+}Si_2O_6$)	*DA kosmochlor*	A minor phase in some iron meteorites	88,89
Amphibole Group			
Fluoro-richterite [$Na(NaCa)Mg_5Si_8O_{22}F_2$]	*DA fluoro-richterite*	A rare phase in iron and aubrite meteorites	90,91
Kaersutite [$NaCa_2(Mg_3AlTi^{4+})(Si_6Al_2)O_{22}O_2$]	*DA kaersutite*	Repoprted from the Sombrerete (IAB) iron meteorite	48
Feldspar Group [$(Ca,Na,K)Al(Al,Si)Si_2O_8$]			
Anorthite ($CaAl_2Si_2O_8$)	*DA anorthite*	A major phase in many non-chondritic meteorites	3,4,50,69
Albite ($NaAl_3SiO_8$)	*DA albite*	A common minor phase in brachinites, aubrites, and iron meteorites	4,6,51,72
Sanidine ($KAlSi_3O_8$)	*DA sanidine*	K-rich feldspars are rare in non-chondritic meteorites. They occur in silicate inclusions in iron meteorites as crystals and in antiperthite	92-94
Celsian ($BaAl_2Si_2O_8$)	*DA celsian*	Occurs as a minor phase in the Angra dos Reis angrite	67
Feldspathic glass (Na,K,Ca,Al,Si)	*DA feldspathic glass*	A significant phase in late-stage melt fractions from Ureilites, brachinites, aubrites, and iron meteorites	8,48,72,92,95-97
Other Silicates			

Zircon ($ZrSiO_4$)	*DA zircon*	A rare phase in basaltic meteorite lithologies	83,98,99
Tranquillityite [$Fe^{2+}_8Ti_3Zr_2Si_3O_{24}$]	*DA tranquillityite*	One occurrence from NWA 11119 Si-rich achondrite	83
Yagiite [$NaMg_2(AlMg_2Si_{12})O_{30}$]	*DA yagiite*	A rare phase in iron meteorites	72,100
Kuratite [$Ca_2(Fe^{2+}_5Ti)O_2[Si_4Al_2O_{18}]$	*DA kuratite*	Known only from the D'Orbigny angrite	101
Krinovite [$Na_4(Mg_8Cr^{3+}_4)O_4(Si_{12}O_{36})$]	*DA krinovite*	A rare mineral in iron meteorites	89
Roedderite [$(Na,K)_2Mg_5Si_{12}O_{30}$]	*DA roedderite*	A rare mineral in iron and enstatite achondrite meteorites	89,102,103
ORGANIC SOLIDS			
Kerogen (C-H-O-N)	*DA kerogen*	An important carbon-bearing phase in many ureilites	104

References: 1. Buchwald 1977; 2. Buseck (1977); 3. Watters and Prinz (1979); 4. Mittlefehldt et al. (1998); 5. Benedix et al. (2014); 6. Rubin and Ma (2020); 7. Yang et al. 1997a; 8. Okada et al. (1988); 9. Yang et al. (1997b); 10. Ramdohr (1973); 11. Berkley & Jones (1982); 12. Treiman & Berkley (1994); 13. Goodrich & Berkley (1986); 14. Taylor et al. (1981); 15. Scott & Agrell (1971); 16. Ma & Rubin (2019); 17. Wasson & Wei (1970); 18. Garvie et al. (2020); 19. Benedix et al. (2000); 20. Buseck (1969); 21. Britvin et al. (2020a); 22. Bannister (1941); 23. Buchwald & Scott (1971); 24. Axon et al. (1981); 25. Sharygin et al. (2020); 26. Nielsen & Buchwald (1981); 27. Ma et al. (2012a); 28. Prinz et al. (1988); 29. Scott et al. (1996); 30. Nehru et al. (1992); 31. Bowman et al. (1997); 32. McCoy (1998); 33. McCoy et al. (1996); 34. Graham et al. (1977); 35. Keil & Fredriksson (1963); 36. Kracher et al. (1977); 37. Ma et al. (2012b); 38. Isa et al. (2016); 39. Sharygin (2020); 40. Bunch & Fuchs (1969a); 41. Nehru et al. (1982); 42. Keil & Brett (1974); 43. Nehru et al. (1983); 44. Okada & Keil (1982); 45. Ramdohr (1963); 46. McCoy et al. (1993); 47. Swindle et al. (1998); 48. Prinz et al. (1982); 49. Rubin & Mittlefehldt (1992); 50. Bunch et al. (1970); 51. Nehru et al. (1996); 52. Ikeda & Takeda (1985); 53. McKay et al. (1990); 54. Hwang et al. (2019); 55. Steele et al. (1991); 56. Buseck & Holdsworth (1977); 57. Olsen & Steele (1997); 58. Davis & Olsen (1991); 59. Olsen et al. (1977a); 60. Karwowski et al. (2015); 61. Britvin et al. (2020b); 62. Fuchs et al. (1967); 63. Scott & Bild (1974); 64. McCoy et al. (1994); 65. Olsen & Steele (1993); 66. Lovering (1975); 67. Prinz et al. (1977); 68. McKay et al. (1988); 69. Mikouchi et al. (1996); 70. Mittlefehldt & Lindstrom (1993); 71. Delany et al. (1984); 72. Ruzicka (2014); 73. Prinz et al. (1994); 74. Warren & Kallemeyn (1994); 75. Rosenshein et al. (2006); 76. Ebihara et al. (1997); 77. Nehru et al. (1980); 78. Marvin (1962); 79. Aoudjehane & Jambon (2007); 80. Marvin et al. (1997); 81. Ulff-Møller et al. (1998); 82. Yanai (1994); 83. Srinivasan et al. (2018); 84. Hiroi et al. (1993); 85. Takeda et al. (1992); 86. Prinz et al. (1986); 87. Prinz et al. (1990); 88. Frondel & Klein (1965); 89. Olsen & Fuchs (1968); 90. Olsen et al. (1973); 91. Bevan et al. (1977); 92. Wasserburg et al. (1968); 93. Wlotzka & Jarosewich (1977); 94. Olsen et al. (1994); 95. Goodrich (1986); 96. Fuchs (1974); 97. Fogel (2005); 98. Gomes & Keil (1980); 99. Ireland & Wlotzka (1992); 100. Bunch & Fuchs (1969b); 101. Hwang et al. (2016); 102. Hsu (1998); 103. Fogel (2001); 104. Vdovykin (1970)

146

This is the peer-reviewed, final accepted version for American Mineralogist, published by the Mineralogical Society of America.
The published version is subject to change. Cite as Authors (Year) Title. American Mineralogist, in press.
DOI: https://doi.org/10.2138/am-2021-7632. http://www.minsocam.org/

Table 2. Summary of 38 high-pressure impact phases in meteorites

Group Species (Formula)	Natural Kind	Characteristics	References
NATIVE ELEMENTS AND ALLOYS			
Martensite (α_2-Fe,Ni)	*Impact martensite*	Common in shocked meteorites; typically 8-15 wt. % Ni	1-3
Diamond (C)	*Impact diamond*	Often occurs as "lonsdaleite" with stacking faults	2,4-6
Chaoite (C)	*Impact chaoite*	Occurs in carbon-rich ureilite achondrites	7,8
SILICIDES			
Suessite (Fe_3Si)	*Impact suessite*	A frequent minor phase in urelites	9,10
Xifengite (Fe_5Si_3)	*Impact xifengite*	A rare phase in urelites, in association with suessite	10
PHOSPHIDES			
Allabogdanite [$(Fe,Ni)_2P$]	*Impact allabogdanite*	Occurs in shocked iron meteorites	11-13
SULFIDES			
Shenzhuangite ($NiFeS_2$)	*Impact shenzhuangite*	One occurrence in the Suizhou (L6) chondrite	14
PHOSPHATES			
Tuite [γ-$Ca_3(PO_4)_2$]	*Impact tuite*	One occurrence in the Suizhou (L6) chondrite	15
OXIDES			
Magnesiowüstite [(Mg,Fe)O]	*Impact magnesiowüstite*	In shocked chondrites in association with Mg-Fe-silicates	16,17
Wangdaodeite ($FeTiO_3$)	*Impact wangdaodeite*	One occurrence in the Suizhou (L6) chondrite	18
Liuite ($FeTiO_3$)	*Impact liuite*	From the shocked Tissint martian meteorite	19
Chenmingite ($FeCr_2O_4$)	*Impact chenmingite*	One occurrence in the Suizhou (L6) chondrite	20,21
Xieite ($FeCr_2O_4$)	*Impact xieite*	One occurrence in the Suizhou (L6) chondrite	22
Tschaunerite (Fe_2TiO_4)	*Impact tschaunerite*	From the shocked Tissint martian meteorite	23
Dmitryivanovite ($CaAl_2O_4$)	*Impact dmitryivanovite*	From the Northwest Africa 470 CH3 chondrite	24
Vestaite [$(Ti^{4+}Fe^{2+})Ti^{4+}{}_3O_9$]	*Impact vestaite*	Found in the eucrite NWA 8003	25
Feiite [$(Fe,Ti,Cr)_4O_5$]	*Impact feiite*	From the shocked Tissint martian meteorite	26
SILICATES			
Silica Polymorphs (SiO_2)			
Coesite (SiO_2)	*Impact coesite*	Identified in many meteorites	27-30
Stishovite (SiO_2)	*Impact stishovite*	Identified in many meteorites	6,29-32

Seifertite (SiO_2)	*Impact seifertite*	Found in shocked martian and lunar meteorites	33-36
Silica glass (SiO_2)	*Impact silica glass*	Found with other silica polymorphs in shocked meteorites	37,38
Olivine Polymorphs [$(Mg,Fe,Ca)_2SiO_4$]			
Wadsleyite [β-$(Mg,Fe)_2SiO_4$]			
& Asimowite [β-$(Fe,Mg)_2SiO_4$]	*Impact wadsleyite*	Found in varied shocked meteorites	30,39-42
Ringwoodite [γ-$(Mg,Fe)_2SiO_4$]			
& Ahrensite [γ-$(Fe,Mg)_2SiO_4$]	*Impact ringwoodite*	Found in varied shocked meteorites	30,43-47
Poirierite [$(Mg,Fe)_2SiO_4$]	*Impact poirierite*	One occurrence in the Suizhou (L6) chondrite	48
Pyroxene Polymorphs [$(Ca,Mg,Fe)_2Si_2O_6$]			
Clinoenstatite ($MgSiO_3$)	*Impact clinoenstatite*	From many meteorites by shock alteration of orthoenstatite	3,49-50
Majorite ($MgSiO_3$)	*Impact majorite*	From many shocked meteorites	30,44,51-58
Akimotoite [$(Mg,Fe)SiO_3$]			
& Hemleyite [$(Fe,Mg)SiO_3$]	*Impact akimotoite*	From many shocked meteorites	30,59-63
Bridgmanite [$(Mg,Fe)SiO_3$]			
& Hiroseite [$(Fe,Mg)SiO_3$]	*Impact bridgmanite*	From many shocked meteorites	17,30,64,65
Amorphous $CaSiO_3$	*Impact amorphous $CaSiO_3$*	Found as inversion of $CaSiO_3$ perovskite	57,66,67
Tissintite [$(Ca,Na,\square)AlSi_2O_6$]	*Impact tissinite*	From the shocked Tissint martian meteorite	66,67
Unnamed [$(Mg,Fe)SiO_3$]	*Impact unnamed [$(Mg,Fe)SiO_3$]*	From the Tenham (L6) chondrite	70
Feldspar Polymorphs [$(Ca,Na,K)Al(Al,Si)Si_2O_8$]			
Jadeite ($NaAlSi_2O_6$)	*Impact jadeite*	Formed by shock alteration of albite	30,71,72
Maskelynite [$(Ca,Na)Al(Al,Si)Si_2O_8$]	*Impact maskelynite*	Common form of impact glass	3,30,73-75
Lingunite [$(Na,Ca)AlSi_3O_8$]	*Impact lingunite*	From the shocked Sixiangkou (L6) chondrite meteorite	30,76
Liebermannite [$(K,Na)AlSi_3O_8$]	*Impact liebermannite*	From the shocked Zagami martian meteorite	77
Stöfflerite ($CaAl_2Si_2O_8$)	*Impact stöfflerite*	From the NWA 856 martian meteorite	78,79
Other Silicates			
Cordierite ($Mg_2Al_4Si_5O_{18}$)	*Impact cordierite*	From the Allende chondrite and Chaunskij mesosiderite	80,81
Zagamiite ($CaAl_2Si_{3.5}O_{11}$)	*Impact zagamiite*	Found in shocked martian meteorites	82,83
Unnamed [$(Fe,Mg,Cr,Ti,Ca,\square)_2(Si,Al)O_4$]	*Impact $(Fe,Mg,Cr,Ti,Ca,\square)_2(Si,Al)O_4$*	From the Tissint martian meteorite	84
Unnamed [$(Mg,Fe,Si)_2(Si,\square)O_4$]	*Impact $(Mg,Fe,Si)_2(Si,\square)O_4$*	Shock melt veins in Tenham and Suizhou chondrites	85

References: 1. Rubin & Keil (1983); 2. Mittlefehldt et al. (1998); 3. Rubin & Ma (2020); 4. Russell et al. (1992); 5. Rubin et al. (1997); 6. Garvie et al. (2011); 7. El Goresy & Donnay (1968); 8. Vdovykin (1970); 9. Keil et al. (1982); 10. Ross et al. (2019); 11. Britvin et al. (2002); 12. Britvin et al. (2019); 13. Litasov et al. (2019); 14. Bindi & Xie (2018); 15. Xie et al. (2003); 16. Chen et al. (1996); 17. Bindi et al. (2020); 18. Xie et al. (2020); 19. Ma & Tschauner (2018a); 20. Chen et al. (2003b); 21. Ma et al. (2019a); 22. Chen et al. (2008); 23. Ma & Prakapenka (2018); 24. Mikouchi et al. (2009); 25. Pang et al. (2018); 26. Ma & Tschauner (2018b); 27. Hollister et al. (2014); 28. Chao et al. (1960); 29. Ohtani et al. (2011); 30. Tomioka & Miyahara (2017); 31. Holtstam et al. (2003); 32. Kaneko et al. (2015); 33. Sharp et al. (1999); 34. Dera et al. (2002); 35. El Goresy et al. (2008); 36. Miyahara et al. (2013a); 37. Grieve et al. (1996); 38. Stöffler et al. (2018); 39. Price et al. (1983); 40. Malavergne et al. (2001); 41. Ozawa et al. (2009); 42. Bindi et al. (2019); 43. Binns et al. (1969); 44. Coleman (1977); 45. Feng et al. (2011); 46. Kimura et al. (2003); 47. Ma et al. (2016); 48. Tomioka et al. (2020); 49. Reid & Cohen (1967); 50. Tomioka & Fujino (1997); 51. Mason et al. (1968); 52. Smith & Mason (1970); 53. Walton (2013): 54. Kato et al. (2017); 55. Tomioka et al. (2002); 56. Ma & Tschauner (2016); 57. Xie & Sharp (2007); 58. Tomioka et al. (2016); 59. Sharp et al. (1997); 60. Tomioka & Fujino (1999); 61. Chen & Xie (2015); 62. Ferroir et al. (2008); 63. Bindi et al. (2017a); 64. Tschauner et al. (2014); 65. Vollmer et al. (2007); 66. Akaogi et al. (2004); 67. Tomioka & Kimura (2003); 68. Ma et al. (2015); 69. Rucks et al. (2018); 70. Xie et al. (2011); 71. Kimura et al. (2000); 72. Ozawa et al. (2014); 73. Stöffler et al. (1986); 74. Stöffler et al. (1991); 75. Rubin (2015b); 76. Gillet et al. (2000); 77. Langenhorst & Poirier (2000); 78. Spray & Boonsue (2016); 79. Tschauner & Ma (2017); 80. Fuchs (1969b); 81. Petaev et al. (2000); 82. Beck et al. (2004); ; 83. Ma et al. (2019b); 84. Ma et al. (2019c); 85. Ma et al. (2019d)